EXPLORING HYBRID NICKEL CATALYSTS ON DOPED-CERIA SUPPORTS FOR THE AUTOTHERMAL REFORMING OF SURROGATE LIQUID FUEL

LIU LEI

(*M. Eng. Zhejiang University, China*)

A THESIS SUBMITTED

FOR THE DEGREE OF DOCTOR PHILOSOPHY

DEPARTMENT OF CHEMICAL & BIOMOLECULAR ENGINEERING

NATIONAL UNIVERSITY OF SINGAPORE

2012

Acknowledgement

Foremost, I would like to express my sincere gratitude to my supervisor, Associate Professor Hong Liang for his continuous support of my PhD study, for his patience, invaluable guidance and immense knowledge. Professor Hong's knowledge and guidance helped me in all time of my research. His enthusiasm and persisting in principles of academic has a tremendous influence on me. I could not have expected a better mentor for my PhD study.

I would also like to express my gratitude to all my colleagues in our research group and also other friends for their supportive comments and cheerful assistance.

I am grateful for the Research Scholarship granted by National University that enables me to pursue my PhD degree. I would like to specially thank all the technical and clerical staff in the Department of Chemical & Biomolecular Engineering for their kindly assistance and research infrastructure support.

Last but not least, this thesis is dedicated to my beloved parents for their understanding and support throughout my 22 years' study.

TABLE OF CONTENTS

Summary

Nowadays, the world-wide diminishing petroleum oil resource has been becoming a critical challenge to mankind especially when increasing demand on energy from developing countries persists. Additionally petroleum usage has quickly built up significant environmental stress. To deal with these issues, it is of importance to explore clean and renewable fuels and promote energy efficiencies. Among the alternative fuels, hydrogen is considered to be the most promising energy source due to its high efficiency and clean emission. Reforming higher molecular weight hydrocarbons such as gasoline or diesel, whose main components are C_4 to C_{16} hydrocarbons, for producing reformate (H_2/COS) is the core of vehicle auxiliary power units (APUs) of fuel cells is. The APUs will make shipping and storage of hydrogen or syngas unnecessary and allow for continuous use of the well-established fossil oil delivery infrastructure. Hydrogen production using autothermal reforming (ATR) has attracted great attention due to its lower energy input than the traditional steam reforming process and also due to using a simple system design. However, development of a catalytically active but also stable reforming catalyst is the tough task for realizing commercial application of APUs because the presence of heavy and branched aliphatic hydrocarbons, aromatics and organosulfur compounds in the liquid hydrocarbon fuels produce complicated non-volatile carbonaceous species. Namely, these ingredients bring about carbon deposition, sulphur poisoning and sintering of catalytic sites that all ruin the performance of catalyst.

This PhD project studies ceria supported Ni-based catalysts for ATR of liquid hydrocarbons. The use of Ni as catalyst is of special interest due to its low cost and high catalytic activity. However, the Ni catalyst is very vulnerable to carbon

deposition and sulphur poisoning. The use of ceria or doped ceria as support of Ni has alleviated the deactivation trend due to the oxygen conducting trait of the doped ceria. On the basis of this recent progress, three types of ceria or doped ceria-supported nickel-based catalysts were prepared and evaluated in the ATR of proxy fuel in this thesis: (i) The ceria-supported nickel phosphide (Ni_xP_y), which was firstly prepared by electroless nickel deposition of nickel-phosphorous alloy grains on ceria. The NiP was then in-situ formed from the alloy in the initial stage of ATR. The catalyst was used to reform a surrogate gasoline and a surrogate diesel, and exhibited nil coking extent after reforming the surrogate fuel. The Ce^{3+} ions present at the surface of catalyst support act to sustain water-gas shift reaction as well as to enhance the stability of catalytic reactivity, which was verified in the ATR of a proxy fuel comprising of *n*-dodecane, 10 wt% naphthalene and 100 ppm S (thiophene). (ii) The metal oxide mixture ($La_xCe_{1-x}O_{2-\delta}$ and NiO) in nano-scale, synthesized from the metallo-organic gel (viz. the Pechini method) of the three metals, was developed as the precursor of ATR catalyst. The unique aspect the resulting catalyst lies in the reverse doping, viz. the supported NiO is doped by La^{3+} besides the major doping happening in ceria. In consequence, the reverse doping in the $La_xCe_{1-x}O_{2-\delta}$ (x = 0.1) supported Ni catalyst remarkably enhanced its catalytic activity in the ATR of the proxy fuel as defined above. iii) The third catalytic system combined doping the ceria support by Y^{3+} and hybridizing the Ni catalyst by boron species with the aim of improving resilience of the catalyst against deactivation effects. In this catalyst, the precursor of nickel metal was not the traditional NiO but nickel borate, $Ni_3(BO_3)_2$, instead. After Ni^{2+} was reduced to metal at high temperatures, the boron species still functioned to stabilize the Ni atomic clusters produced. Importantly, these Ni atomic clusters did not have bulk phase and hence the resulting catalyst manifested promising performance in 24 h

test (conversion>95%). Both XPS and XRD structural characterizations at ambient temperature indicated only nickel borate crystallites present in the used catalyst because the Ni atomic clusters and borate will resume nickel borate structure upon cooling. The XPS analysis also revealed that nickel borate induced generation of Ce^{3+} ions in the ceria support.

List of tables

List of figures

Nomenclature

ATR	Autothermal reforming
ENP	Electroless nickel plating
F	Flow rate
FESEM	Field emission scanning electron microscopy
GC	Gas chromatograph
GHSV	Gas hourly space velocity
H	Enthalpy
ICP-MS	Inductively coupled plasma-Mass spectrometry
POX	Partial oxidation
SOFC	Solid oxide fuel cell
SR	Steam reforming
TEM	Transmission electron microscopy
TGA	Thermogravimetric analyser
TPO	Temperature programmed oxidation
TPR	Temperature programmed reduction
XPS	X-ray photoelectron spectroscopy
XRD	X-ray diffraction
y	Yield

CHAPTER 1

INTRODUCTION

1.1 Background

It is now well established that the emission of carbon dioxide is responsible for the global warming. However, the most commonly used internal combustion engine in which combustion of fossil fuels occurs and would emit toxic pollutants and may result in global warming and other environmental problems. Therefore, it is necessary to develop alternative energy conversion systems which are clean and have higher efficiency. This results in ever-increasing attention on the usage of hydrogen-fed fuel cells, because hydrogen can be converted at a very high electrochemical efficiency and emits only water as a by-product. Although fuel cells are very attractive energy conversion systems of the future, they need hydrogen as the fuel, which is very difficult to store and to transport [1]. Thus on-board production of hydrogen by catalytic reforming of hydrocarbon fuels is a very promising technology to solve this problem [2-8]. The most practical way to produce hydrogen is by reforming of fossil fuels such as natural gas, gasoline, and diesel, because it has high-energy efficiency [9].

The rationale for doing catalytic reforming of diesel oil of which the main products are H_2, CO_2 and a smaller amount of CO lies in different energy efficiencies between the solid oxide fuel cell (SOFC) and the traditional internal combustion engine. Combining with other thermal cycles, energy efficiency of a SOFC system can reach up to 50% while the internal combustion engine has energy efficiency between 30-40%. To retain such advantage, the catalytic reforming should consume

as little energy as possible. As a result, autothermal reforming (ATR) is attractive since it is a thermal neutral catalytic reforming process. Besides this, compared to low-carbon-number hydrocarbons, for instance methane, liquid hydrocarbons are easy to store. Therefore a successful ATR catalytic system will make the on-board reforming of diesel oil become an auxiliary unit of SOFC that is powered by H_2 and CO, a clean fuel compared with hydrocarbons.

There are several approaches to reform the hydrocarbon fuels such as steam reforming (SR), partial oxidation (POX), and autothermal reforming (ATR) [10]. The last one is actually the combination of SR and POX. ATR takes the advantage of both such as: high hydrogen concentration in products, intermediate reaction temperature, and fast start up, etc. Therefore, it is believed to be the most suitable approach for hydrogen production by fuel cells used in smaller operation systems.

Fuel conversion, product selectivity, and their time-dependent stability are the criteria to assess a catalytic reforming system consisting of catalyst and reactor conditions. Deactivation is a major challenge in commercialization of this process. The reforming catalyst is usually in the form of metal oxide supported active metal particles. The active metals are mainly from the transition metals. Among those transition metals, noble metals (Pt, Pd, Rh, Ru, etc.) exhibit better activity and stability compared to those non-noble metals (Ni, Co, Cu, etc.). However, the noble metals are not feasible for commercial use due to their high cost and limited availability. The non-noble metals, especially Ni attracted great interest due to its low cost and high activity. Nevertheless, it can be easily deactivated. The catalyst deactivation comes from several aspects: sintering, carbon deposition, and sulphur poisoning, etc. Catalyst sintering is caused by the high temperatures used in the

reforming process, during which the active metals would sinter to form large aggregates and result the loss of active sites. Carbon deposition, or coking, rise from the decomposition of the hydrocarbon molecules. Especially the higher hydrocarbons and aromatics in the liquid fuels will cause more severe carbon deposition compared with simpler hydrocarbons. As for the sulphur poisoning, it is an even tougher problem compared with the above two. The hydrocarbon fuels, no matter gaseous or liquid, all contain sulphur compounds such as hydrogen sulphide and various organ sulphur compounds. Among these three deactivation reasons, carbon deposition and sulphur poisoning are considered to be the more difficult to be overcome. Sintering may just result gradually loss of active sites, but the other two will totally destroy the catalyst. In order to deal with carbon deposition and sulphur poisoning, it is necessary to figure out the mechanism involved in these processes. Researchers have done a lot of works in studying the deactivation process in detail and the mechanisms are quite reasonably proposed.

The deactivation mechanism for carbon deposition was proposed to include the following steps [11]: 1) firstly the hydrocarbon molecules would dissociative adsorb on the metal active sites and leave atomic carbon; 2) these atomic carbon then will polymerize to form amorphous carbon; 3) the polymerized carbon would bond with the metal atoms to form metal carbides; 4) the metal carbides will either diffuse through the metal particles and grow carbon whisker at the rear side which may lift the metal particles up at its tip, or stay at the metal surface and encapsulate the metal particles. The atomic carbon resulted from the dissociation of hydrocarbons are highly reactive and can be easily gasified by oxygen or steam. However, the reactivity of the polymerized carbon is much lower than the atomic carbons. Thus carbon deposition

can be regarded as the result of breaking the balance between atomic carbon gasification and polymerization.

As for sulphur poisoning, its mechanism is actually quite similar to that of carbon deposition. The sulphur compounds will also firstly dissociative adsorb on the metal active sites to form sulphur atoms [12]. Then these sulphur atoms will strongly bind with the metal atoms to from metal sulphides. Since sulphur is a highly electro negative element, the bonding between sulphur and the metal is so strong that it cannot be easily broken. The difference between sulphur poisoning and carbon deposition is that metal sulphides will not diffuse through the metal particles but just stay at the metal particle surface and occupy the active sites. However, sulphur poisoning will eventually result deposition of carbon. Thus sulphur poisoning is a much tougher problem.

Based on the mechanisms of carbon deposition and sulphur poisoning, researchers have developed many methods in designing catalysts resistant to deactivation. The basic ideas include: 1) avoid the bonding between carbon or sulphur and the metal atoms; 2) avoid the polymerization of the atomic carbon; 3) accelerate the gasification of the adsorbed carbon of sulphur species. In order to achieve the above goals, various catalyst compositions were tried out to find out an effective way to solve the problems. Although there are many different catalyst designs, they can be generally classified into three categories: 1) reducing the size of the active metal particles to nano size; 2) alloying the active metal with a second element; 3) modifying the support material to obtain a stronger interaction between the active metal and the support. Reducing the active metal particle size could probably prevent the polymerization of atomic carbon. This is because the polymerization process will

need enough carbon atoms in advance. If the number of active sites on one particle is small enough, less atomic carbon will be produced on this particle and the gasification rate would overwhelm the polymerization rate. Alloying the active metal could have several effects in promoting the catalysts. One is to lower down the affinity of the active metal to carbon and sulphur atoms by trimming its micro electron environmental. Another one is to sacrifice the second alloying element to protect the active metal. This second element would be more easily attacked by the carbon or sulphur atoms, thus the active metal will be left free from carbon and sulphur. As for the third category, it is believed that the interaction between the support and the active metal could enhance the performance of the catalyst. This metal-support interaction could probably result enhanced reducibility of the active metal and improve its dispersion. Currently, there is a great interest in employing ceria or doped-ceria as the catalyst support materials. The reason for this special interest lies in its superior oxygen storage capacity and oxygen conduction ability. It is believed that the oxygen species transferred from the ceria support to the active metal could effectively facilitate the gasification of the adsorbed surface carbon and sulphur species. The oxygen vacancies generated in the support could also enhance the associative adsorption and steam and thus facilitate the water-gas-shift reaction. By employing the above mentioned approaches, the researchers have developed many reforming catalysts which exhibit certain resistance to carbon deposition and sulphur poisoning. The experimental data obtained from these studies also helped to gain a further knowledge of the deactivation mechanism. However, the superior performance of these developed catalysts is still not good enough for commercialization. There is still much work need to be done.

For the purpose of catalyst preparation, carious approaches and techniques have developed so far. These approaches basically include: incipient wetness impregnation, precipitation, sol-gel, Pechini, etc. among these approaches, the impregnation is the most commonly used one. Sol-gel is a very method to prepare nanosized particles, but the expensive organmetallic compounds are needed as precursors. Instead, Pechini could be a good substitute since it only use metal salts as precursors. Nowadays, electroless nickel plating, which is usually used to deposit corrosion resistant coating, is also used in catalyst preparation. This method could generate highly uniform mixture of nickel atoms and phosphorous or boron atoms. Employing phosphorous or boron as the second alloying element could be good way to promote the nickel catalysts.

1.2 Research objectives and scope

The development of reforming catalysts which are resistant to carbon deposition and sulphur poisoning has always been a challenge for the fuel cell technology. The main objective of this research project is to develop stable Ni-based reforming catalysts for the reforming of surrogate liquid fuels. The poisoning effect of higher hydrocarbons, aromatics, and sulphur compound on the catalysts was examined. Also investigated was the surface chemistry on the catalysts involved in the catalytic process to explore the mechanisms behind it. The design of reforming catalysts can be concluded into mainly three categories:

1) Alloying the Ni metal with phosphorous atoms. This alloying was achieved by the electroless nickel plating (ENP) method. This method can simultaneously deposit Ni atoms and P atoms on the substrate material and an ideal mixture of these two elements could be obtained. By regulating

the variables in the ENP process, the NiP granular size and composition could be controlled.

2) Employing nickel borate as the active component in catalyst. Boron was reported to be able to promote the Ni catalysts. Here in this work, nickel borate instead of nickel boride was prepared via precipitation method as the active component in the catalyst.

3) Using ceria and doped-ceria as the support material. As mentioned above, ceria exhibits superior oxygen storage capacity and oxygen conduction ability. This property could promote the performance of the reforming catalysts by facilitating the gasification of the adsorbed species. Thus it is of great interest to employ ceria or doped-ceria as the support material in this work to combine with the above mentioned two types of active component.

By employing the above catalyst designs, the as prepared catalyst systems were evaluated in autothermal reforming of the formulated surrogate liquid hydrocarbon fuels. The results achieved can be divided into four parts as highlighted below:

1) The nickel phosphide catalyst was prepared by ENP process using a commercially purchased ceria as support material. This catalyst was evaluated in a surrogate gasoline fuel composed of *n*-octane and 6 wt% of naphthalene. The reaction conditions such as temperature, oxygen-to-carbon ratio, and steam-to-carbon ratio were optimized first. This catalyst showed superior resistance to carbon deposition while the two comparison catalysts both revealed carbon whiskers deposited on the catalyst. The

fresh and spent catalysts were characterized to explore the surface chemistry of the catalysts.

2) Another nickel phosphide catalyst system was developed using as in-house prepared ceria support. This ceria support was synthesised using Pechini method. This method results a much higher specific surface area compared with the commercial one and thus a higher nickel phosphide loading. This prepared nickel phosphide catalyst was then evaluated in the formulated surrogate diesel fuel composing *n*-dodecane, 10 wt% naphthalene, and 100 ppm sulphur (from thiophene). The more complicated fuel composition results a higher risk of catalyst deactivation. The fresh and spent catalysts were also characterized to examine the effect of phosphorous alloying the ceria support in the catalyst.

3) A ceria supported Ni catalyst was prepared by the Pechini method. Starting from the aqueous solutions of the precursors, this method could ensure a highly uniform distribution and dispersion of nickel in the ceria support. Furthermore, the effect of La doping on this catalyst was also studied. Effect of different La doping levels on this catalyst was investigated for this reaction as well. This catalyst was also evaluated in ATR of the surrogate diesel fuel same as above. The structures and properties of the fresh and used catalysts were examined to reveal how La doping on this catalyst could affect its catalytic performance.

4) The third catalyst system was the Y-doped ceria supported nickel borate catalyst. The Y-doped ceria was prepared by Pechini method. Then this material was used as the support in the precipitation process to prepare

nickel borate catalyst. The precipitation process used nickel nitrate as nickel source and sodium borohydride as a reducing agent. The as-prepared nickel borate catalyst was calcined in-situ during the reforming process to convert amorphous nickel borate to crystalline nickel borate. This catalyst was tested in the surrogate diesel fuel same as before. The promotion effect of borate and doped ceria support on the catalyst performance was investigated. Moreover, prolonged activity study was performed to explore the deactivation mechanism of this catalyst.

Finally, conclusions of this thesis work and recommendations for future work are given in Chapter 7.

CHAPTER 2

LITERATURE REVIEW

2.1 Hydrocarbon reforming

Hydrogen, which is considered to be the most promising fuel in future, has a much higher efficiency than the internal combustion engine and a totally clean emission. There are several approaches can be sued to produce hydrogen. Among these approaches, the catalytic reforming of hydrocarbon fuels is of great interest due to its energy efficiency and the potential for applications in smaller operation systems.

Basically there are three main reaction processes to catalytically convert hydrocarbon fuels to hydrogen: steam reforming (SR), partial oxidation (POX) and autothermal reforming (ATR) [10, 13-19]. These three reforming mechanism will be elucidated below in detail.

2.1.1 Steam reforming

Using steam reforming to produce hydrogen is a very mature technology in industry on a large scale for more than 80 years [20]. Steam reforming is the reaction of steam with hydrocarbon fuels at the presence of a catalyst at high temperatures (700 °C ~ 1100 °C) to produce H_2. This reaction is very endothermic. In industry, the reforming reaction is usually carried in a heated furnace at the presence of a supported nickel catalyst. The primary reactions involved in this process are shown below.

$$C_mH_n + mH_2O = (m+\tfrac{1}{2}n)H_2 + mCO \quad \Delta H^0_{298} > 0 \qquad (2.1)$$

$$CO + H_2O = H_2 + CO_2 \quad \Delta H^0_{298} = -41 \text{ kJ/mol} \qquad (2.2)$$

$$C_mH_n + 2mH_2O = (2m+½n)H_2 + mCO_2 \quad \Delta H^0_{298} > 0 \qquad (2.3)$$

Eq. 2.3 is the combination of Eq. 2.1 and Eq. 2.2. The reforming reaction (Eq. 2.1) and the water-gas-shift reaction (Eq. 2.2) are reversible and are usually in equilibrium since the reaction rates are very fast. Thus the products' composition could be controlled by thermodynamics. Beside the above reactions, there are also some other side reactions occur during steam reforming.

$$C_mH_n = mC + ½nH_2 \quad \Delta H^0_{298} > 0 \qquad (2.4)$$

$$2CO = C + CO_2 \quad \Delta H^0_{298} = -173 \text{ kJ/mol} \qquad (2.5)$$

$$C + H_2O = CO + H_2 \quad \Delta H^0_{298} = 175 \text{ kJ/mol} \qquad (2.6)$$

It can be seen that hydrocarbons could dissociate to form carbon which would adsorb on the active metals and deactivate the catalysts. Thus steam is usually added largely in excess so that the equilibrium of Eq. 2.2 moves towards more CO_2 production to yield more H_2. This could also avoid carbon deposition via the Boudouard reaction (Eq. 2.5) and carbon gasification reaction (Eq. 2.6). For the purpose of syngas production, the amount of steam is usually reduced to restrain the water-gas-shift reaction and avoid the production of CO_2. Otherwise steam will be supplied largely in excess to yield more hydrogen.

Currently methane steam reforming is the most widely practised technology for hydrogen or syngas production in industry. Commercial catalyst for this reaction is usually oxide supported Ni catalyst. The primary reactions involved in this process are shown in Eq. 2.7, Eq. 2.2 and Eq. 2.8. The water-gas-shift (Eq. 2.2) and reverse methanation (Eq. 2.8) reactions are usually associated with the steam reforming over a catalyst at high temperatures [21, 22]. The latter one is thermodynamically dependent

on methane steam reforming and water-gas-shift reaction, but is determined to be kinetically independent. For this process, low temperature is favoured because reaction Eq. 2.7 is endothermic, while low pressure is favoured since volume expansion occurs. The product gas is a mixture of hydrogen, carbon monoxide, carbon dioxide and unconverted methane and steam. The product gas composition could be governed by the reaction temperature, reactor pressure, the composition of the feed gas, and the steam-to-carbon ratio.

$$CH_4 + H_2O = 3H_2 + CO \quad \Delta H^0_{298} = 206 \text{ kJ/mol} \qquad (2.7)$$

$$CH_4 + 2H_2O = 4H_2 + CO_2 \quad \Delta H^0_{298} = 165 \text{ kJ/mol} \qquad (2.8)$$

Methane steam reforming is usually catalyzed by supported nickel catalyst in industry due to its high activity and low cost. Methane is firstly activated on the nickel surface. Then the resulting CH_x species will react with OH species adsorbed on the nickel or supports. Ronald Hughes and Kaihu Hou [23] studied methane steam reforming over a Ni/α-Al_2O_3 catalyst and proposed a kinetic mechanism for this process which can be described by:

$$H_2O + s = H_2 + O(s) \qquad (2.9)$$

$$CH_4 + 3s = CH_2(s) + 2H(s) \qquad (2.10)$$

$$CH_2(s) + O(s) = CHO(s) + H(s) \qquad (2.11)$$

$$CHO(s) + s = CO(s) + H(s) \qquad (2.12)$$

$$CO(s) + O(s) = CO_2(s) + s \qquad (2.13)$$

$$CHO(s) + O(s) = CO_2(s) + H(s) \qquad (2.14)$$

$$CO(s) = CO + s \qquad (2.15)$$

$$CO_2(s) = CO_2 + s \qquad (2.16)$$

$$2H(s) = H_2 + 2s \qquad (2.17)$$

where s denotes the active site on the catalyst.

This kinetic mechanism was made based on some assumptions such as: the reactants dissociative adsorbed on the surface nickel atoms; the adsorbed dissociates react to generate adsorbed hydrogen, carbon monoxide and carbon dioxide; these adsorbed gas then desorbed into the gas phase. Good agreement was obtained between the experimental data and the results predicted from the kinetic model which was derived from the proposed kinetic mechanism. This good agreement could strongly support the assumptions made for the kinetic mechanism. This dissociative adsorption of methane was also reported by other researchers. D.L. Trimm [24] reported that this dissociative adsorption of methane was structure sensitive. The activation energy on Ni(1 1 0) and Ni(1 1 1) was higher than that on Ni(1 0 0). Moreover, these assumptions could be a good fundamental knowledge for understanding the kinetic mechanism of higher hydrocarbon reforming.

When higher hydrocarbons such as gasoline or diesel are used as the fuel for steam reforming, the kinetic mechanism is much more complicated than that of methane. Many side reactions could occur due to its more complicated structure. Nevertheless, it is for sure that the fuel will crack into smaller molecules then the reforming reaction would take action. This is also why the study of methane steam reforming could help understanding of the mechanism for higher hydrocarbon reforming. However, since the fuel structure is more complicated, cranking of the

fuels would result severe carbon deposition and deactivate the reforming catalyst. Also, the liquid hydrocarbon fuels always contain large fractions of aromatics and sulphur compounds. These impurities would even make the catalyst deactivation more severe. Thus it is almost impossible to establish a kinetic model for such reactions. But researcher still did a lot of experimental work to explore the mechanism involved in this process. Patricia Irving [25], Francois Gitzhofer [26] and other researchers [27] carried out studies in steam reforming of liquid hydrocarbons and provided knowledge in catalyst design for such reactions.

Generally, steam reforming has the highest efficiency for hydrogen production and long-term stability at a steady state[28]. However, since steam reforming is an intense endothermic reaction, heat transfer is one of the main technical issues for a steam reforming reactor. Thus the reactors used in steam reforming process are usually in the form of a group reforming tubes in a row along the furnace. So it is difficult to start a steam reforming reactor quickly. As a result, steam reforming is only appropriate for large-scale productions.

2.1.2 Partial oxidation reforming

Partial oxidation is the reaction of oxygen and hydrocarbon fuels to produce syngas by using lower stoichiometric oxygen than that for total combustion (Eq. 2.18). This reaction is considered to be a potential alternative to the highly endothermic steam reforming process [29-35]. Partial oxidation is usually operated at a higher temperature compared with steam reforming and need external cooling since it is highly exothermic [36-38]. The high reaction temperatures used in partial oxidation reaction could minimize carbon deposition and sulphur poisoning. Moreover, no

storage and delivery system for water is required, which makes the reforming system simpler and reduces its cost.

$$C_mH_n + ½mO_2 = ½nH_2 + mCO \quad \Delta H^0_{298} < 0 \qquad (2.18)$$

Unlike steam reforming, it is easier to start a partial oxidation reactor quickly due to the characteristically exothermic reaction. Thus the reformer does not need to be optimized for heat transfer and can be lighter and more compact. This makes it suitable for small systems. When methane is used as the fuel, the moderate overall exothermicity of methane partial oxidation allows the use of an adiabatic reactor [37]. Especially this reaction is more suitable for solid oxide fuel cells (SOFCs) since it operates at a high temperature [39, 40]. This high temperature also makes the SOFCs immune of CO poisoning, thus both H_2 and CO can be used as fuel. Another advantage of partial oxidation reaction is that the stoichiometry of reaction (Eq. 2.7) has a product molar ratio $H_2/CO = 2$, which is favourable for Fisher-Tropsch and methanol synthesis.

Partial oxidation of methane (POM) is the mostly studied reaction in industry. Similar to methane steam reforming, nickel is also the most favourable catalyst for POM. So far, there are two types of mechanisms which have been proposed for POM process: two-steps mechanism and direct POM mechanism.

The two-steps mechanism basically involves three reactions shown in Eq. 2.19, Eq. 2.7 and Eq. 2.20. According to this mechanism, methane is firstly completely oxidized into carbon dioxide and steam (Eq. 2.19). Then the syngas will come from the methane steam reforming reaction (Eq. 2.7) and methane dry reforming (Eq. 2.20). Dissannayake and co-workers [41] provided experimental supports for this mechanism. They found an intense temperature increase near the entrance section of

the catalyst bed, which could be attributed to the highly exothermic methane complete combustion reaction as shown in Eq. 2.19.

$$CH_4 + 2O_2 = CO_2 + 2H_2O \quad \Delta H^0_{298} = -802 \text{ kJ/mol} \qquad (2.19)$$

$$CH_4 + CO_2 = 2CO + 2H_2 \quad \Delta H^0_{298} = 247 \text{ kJ/mol} \qquad (2.20)$$

The second mechanism, direct POM mechanism, was proposed by Hickman and co-workers [35]. This mechanism proposed that the reactants are directly dissociated into adsorbed species on the catalyst surface and syngas is produced by the reaction of the adsorbed surface species. The reaction steps involved in this mechanism are:

$$CH_4 + 5s = C(s) + 4H(s) \qquad (2.21)$$

$$O_2 + 2s = 2O(s) \qquad (2.22)$$

$$C(s) + O(s) = CO(s) + s = CO + 2s \qquad (2.23)$$

$$H(s) + H(s) = H_2 + 2s \qquad (2.24)$$

$$C(s) + 2O(s) = CO_2(s) + 2s = CO2 + 3s \qquad (2.25)$$

$$2H(s) + O(s) = H_2O(s) = H_2O + s \qquad (2.26)$$

where s denotes the active site on the catalyst.

It can be seen that the second mechanism is quite similar to that of the methane steam reforming described in previous section. They both proposed that the reactants dissociative adsorbed on the catalyst surface. This mechanism has been widely accepted and the first methane C-H cracking is considered to be the rate determination step.

The partial oxidation of higher hydrocarbons is much more complicated than that of methane just like steam reforming. L.D. Schmidt and co-workers [42] studied the partial oxidation of several higher hydrocarbon mixtures (*n*-octane + *i*-octane, *n*-decane + *n*-hexadecane, *n*-decane + naphthalene) and claimed that the mechanism of this process, which was the overall goal of this research, had not yet been established. However, they speculated that it should be qualitatively similar to methane partial oxidation. They proposed that the reaction was initiated near the entrance section of the catalyst bed by complete dissociation of the molecules through series of dehydrogenation and C-C cleavage reactions. The dissociated species then would react with the adsorbed oxygen to form hydrogen, carbon monoxide and carbon dioxide.

Although it is difficult to establish kinetic model for partial oxidation of higher hydrocarbons, there are still researchers did some work on it. O. Deutschmann and co-workers [43, 44] studied partial oxidation of iso-octane over Rh catalysts and carried out both experiment and modelling studies. The authors suggested that partial oxidation of iso-octane includes several reactions such as direct partial oxidation (Eq. 2.27), total oxidation (Eq. 2.28), steam reforming (Eq. 2.29), dry reforming (Eq. 2.30), water-gas-shift reaction (Eq. 2.2), methanation (Eq. 2.31) and carbon formation (Eq. 2.5). The reaction enthalpies are shown below:

$$i\text{-}C_8H_{18} + 2O_2 = 8CO + 9H_2 \quad \Delta H^0_{298} = -660 \text{ kJ/mol} \qquad (2.27)$$

$$i\text{-}C_8H_{18} + 12.5O_2 = 8CO_2 + 9H_2O \quad \Delta H^0_{298} = -5113 \text{ kJ/mol} \qquad (2.28)$$

$$i\text{-}C_8H_{18} + 8H_2O = 8CO + 17H_2 \quad \Delta H^0_{298} = 1261 \text{ kJ/mol} \qquad (2.29)$$

$$i\text{-}C_8H_{18} + 8CO_2 = 16CO + 9H_2 \quad \Delta H^0_{298} = 1590 \text{ kJ/mol} \qquad (2.30)$$

$$CO + 3H_2 = CH_4 + H_2O \quad \Delta H^0_{298} = -206 \text{ kJ/mol} \qquad (2.31)$$

The gas phase reactions were not considered to make the system as simple as possible and only surface reaction mechanism was applied in the model. This model used a detailed surface reaction scheme for partial oxidation of C_1-C_3 species and the assumption of rapid adsorption and destruction of the fuel molecules was made. The detailed surface reaction mechanism consisted of 56 reactions. This elementary-step-like reaction mechanism supported the understanding the reaction sequences helped to understand the experimental data. It can be seen that although the fuel is much more complicated than methane, the reaction mechanism is still quite similar to that of methane. This similarity made it possible for the researchers to explore the surface chemistry involved in the catalytic process, and provide basic knowledge for the design of reforming catalysts.

However, there is one main drawback of partial oxidation reaction compared with steam reforming reaction that the hydrogen concentration in products is lower. While steam reforming can extract hydrogen from water which is almost costless, partial oxidation can only extract it from the hydrocarbon fuels. Thus the overall energy efficiency and cost for partial oxidation could be not economically feasible. On the other hand, its high operating temperature creates difficulties in material selection and also result a higher possibility of coke formation[28]. Thus partial oxidation could be a good candidate got applications in fuel cell technology, but not the best.

2.1.3 Autothermal reforming

As mentioned above, steam reforming has higher hydrogen production efficiency but is not suitable for portable unit applications due to its highly exothermicity. Partial oxidation is suitable for small systems but its hydrogen production efficiency is too low, and the temperatures used in this reaction are too high for practical applications. Autothermal reforming is actually a combination of SR and POX (Eq. 2.19) [14, 45]. Thus this reforming process has higher energy efficiency than other processes as well as lower investment using a simple system design.

$$C_mH_n + xO_2 + (2m-2x)H_2O = (2m-2x + ½n)H_2 + mCO_2 ; \qquad (2.19)$$

The oxygen-to-fuel ratio x is a variable which can be used to control the total heat balance of an ATR process, either exothermic or endothermic. At a higher x value, the partial oxidation reaction will be dominant and the overall reaction would be more exothermic. On the other hand, steam reforming will be dominant and the overall reaction would be more endothermic. So there is a point where those two reactions will be in balance and the enthalpy change of the overall reaction could be zero. Usually the reaction is kept a little bit more exothermic to make possible self-sustenance of the reactor[28]. Thus, ATR requires no external heat source unlike SR and can be operated at lower temperature than that of POX. The steam-to-fuel ratio could also be controlled for different products composition. Higher steam-to-fuel ratio would favour the production of hydrogen via water-gas-shift reaction. If synthesis gas production is the purpose, this ratio should be lower to yield more CO.

A typical ATR setup system used in laboratory study is shown in Figure 2.1. The catalyst is usually placed at the centre of the tubular reactor. Fuel, water and air are delivered into the reactor after vaporized and mixed in the evaporator. The effluent gas was on-site analyzed by GC after going through the chiller and moister trap. This evaporator is applicable for those fuels whose boiling temperature is not very high. For the heavy fuels such as diesel, this may not be a good way to evaporate the fuel since it will experience severe thermal decomposition in the evaporator. Coking would occur and block the evaporator. Thus fuels like diesel is usually sprayed into the reactor using a spray injector. ATR takes advantages of both SR and POX [46]. Usually POX and SR are thought to proceed sequentially in ATR, where POX occurs first and then followed by SR. Thus it is possible to start the reaction quickly [47, 48]. Moreover, the presence of steam could facilitate water-gas-shift reaction and carbon gasification thus helps to enhance the production of hydrogen. And the presence of oxygen reduces the possibility of coke formation and facilitates a fast ATR reaction. The hydrogen concentration in products of ATR is in between of POX and SR. ATR is considered to be potentially more efficient than POX or SR alone and is able to reform higher hydrocarbons, which have higher energy density. The advantages of ATR make possible simple and small reactors with relatively high efficiency.

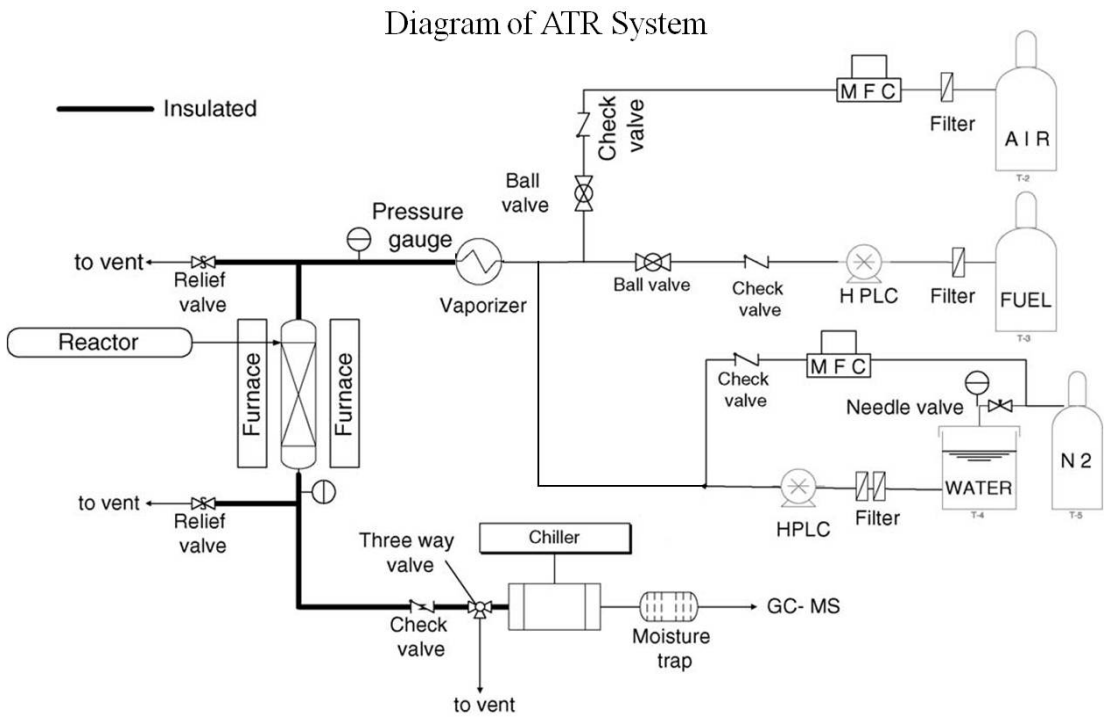

Figure 2. 1 Diagram of ATR system used in laboratory study

2.1.4 Hydrogen source

Producing hydrogen via reforming of hydrocarbon fuels is the most economic way. Various fuels have been studied for hydrogen production by reforming technologies for fuel cell systems. Basically hydrocarbons, gaseous hydrocarbons (methane, propane, butane…) and liquid hydrocarbons (gasoline, diesel…), are suitable for reforming process due to their high energy efficiency. The selection of hydrogen source depends on technical and economical factors. Table 2.1 shows the comparison of the commercially available hydrogen source for their volumetric hydrogen densities. It can be seen that the gaseous fuels such as methane, propane and butane have much smaller volumetric hydrogen densities compared with those liquid hydrocarbon fuels. The higher hydrocarbon fuels have the highest hydrogen density

both volumetric and gravimetric. Another advantage of the liquid fuels is that they are easier to store and transport. Thus they are more suitable for small systems.

Table 2. 1 Volumetric hydrogen density of fuel choices

Fuel	Volumetric Hydrogen density (kmol/m^3)
Methane	0.089
Methanol	49.4
Ethanol	51.4
Propane	0.182
Butane	0.213
Gasoline	≈ 55.4[a]
JP8	≈ 57.2[b]
Diesel	≈ 57.8[c]

a: Use *n*-octane as representative model.

b: Use *n*-dodecane as representative model.

c: Use *n*-hexadecane as representative model.

Currently the most commonly used fuel in industry for the production of hydrogen is methane. Methane steam reforming is an established process for large scale production of hydrogen [49-56]. Recently, steam reforming of methane also attracted interest as the fuel processing technology for fuel cells. However, this gaseous resource favours generation of hydrogen near the natural gas, otherwise high energy required compression process to liquefy methane, or costly pipeline infrastructure for easier transportation of methane is needed. Thus methane is actually not a good candidate as fuel for fuel cells.

Beside methane, ethanol is another fuel of great interest for fuel cell application. The rising concern about ethanol could be attributed to the development of biomass-derived fuels as hydrogen source regarding the shortage of fossil fuels [57-66]. Among those bio-fuels, bio-ethanol is considered to be the most promising one due to its abundant availability and renewable property. Compared with methane, it is easier to store, safer to handle and transport due to its lower toxicity and volatility [67-71].

Although ethanol is a good candidate as hydrogen source, the higher hydrocarbons such as gasoline, JP8 and diesel have the highest gravimetric and volumetric hydrogen density [18, 20, 28, 72]. They also have a well-established delivery infrastructure which makes them to be a more practical option for fuel cell application [73]. It is these advantages that make the higher hydrocarbon fuels one of the most attractive hydrocarbon fuels for fuel cell application. Thus higher hydrocarbon fuels will be used in this PhD study. However, although diesel is rich in hydrogen, it also contains some sulphur compounds and coke precursors which may cause catalyst deactivation by coking and sulphur poisoning [74-76]. Thus, it is necessary to develop a reliable reforming catalyst for such applications.

2.2 Catalysts for reforming process

Catalyst plays the most essential role in reforming process. The catalyst should exhibit high activity and good thermal and mechanical stability. For transportation fuel cell systems, the requirement for catalyst performance is even higher. Typically the catalyst should be able to process at a feed of 200,000 h^{-1} with a fuel conversion of >90% and hydrogen selectivity of >80%, and have a lifetime of 5000 h[77]. For this purpose, various catalysts have been investigated.

Reforming catalysts are typically in the form of metal oxide supported metals which serve as active sites. The metals are mostly transition metals which can be classified into two categories: noble metals such as Pt, Rh, Pd, Ru, etc., and non-noble metals such as Ni, Co, Cu, etc. Noble metals indeed display higher activity and stronger resistance to carbon deposition and sulphur poisoning. Either single or bimetallic noble metals have been thoroughly studied [78-81]. However, the superior performance of the noble metal itself is still quite limited, not mention its high cost which makes it economic unfeasible. Thus for practical considerations, non-noble metals especially Ni has attracted much interest. Although Ni has a relatively high activity and good stability, it is prone to be deactivated by coking and sulphur poisoning. To overcome this problem, it is usually promoted with other elements, such as noble metals [82, 83], Mn[84], K[85], etc. These elements are believed to be able to trim the chemical environment of the Ni atoms, which would enhance its performance toward coking and sulphur poisoning.

Another important part of a catalyst is the support material selected. Active metals are typically deposited or incorporated into carefully engineered oxide supports. Various metal oxides have been investigated. Alumina is the most commonly used support material[86]. It is highly thermal and mechanical stable and usually has a high specific surface area. Other oxides such as MgO [48, 87], CeO_2[29], or ZrO2[88], etc, are also quite commonly used. In order to enhance the catalyst performance, two or more oxides are usually mixed as the support material. For example, YSZ [89, 90], CeO_2-ZrO_2[36, 46], MgO-Al2O3[91], etc[47, 92, 93]. Particular attention is currently focused on oxygen-ion conducting materials, especially doped-ceria. Ceria is known to be an oxygen-ion conducting material due to its oxygen vacancies in lattice. This oxygen vacancy could be further enhanced by

doping with other metals, such as Gd[94], Zr[95], etc. This high oxygen-ion conductivity could facilitate the removing of deposited coke. The Gd doped ceria is of special importance due to its significantly improved thermal stability. Besides doped-ceria, the oxygen-ion conducting perovskite materials are also of special interest as support materials [47, 96].

Since the reforming catalysts are prone to be deactivated by carbon deposition and sulphur poisoning, it is important to clarify the mechanism of the catalyst deactivation process. The following subsections will discuss the mechanism of carbon deposition and sulphur poisoning.

2.2.1 Catalyst deactivation

No matter the active metals or the support materials, the only target is to prevent catalyst deactivation. The catalyst must be active, selective, durable, and tolerant to coking and sulphur poisoning. This is one of the most significant challenges in developing of fuel processing catalysts.

2.2.1.1 Carbon deposition

Alkanes and aromatics present in the fuel would crack and form deposited carbon during the reforming process. Sometimes there is a difference between coke and carbon. Usually carbon is considered to be the product of Boudouard reaction (Eq. 2.5) while coke is attributed to the result of fuel cracking or condensation of hydrocarbons. However, this distinction is arbitrary and carbon will be used to denote both in this study for convenience. The non-noble metals especially Ni is easier to be deactivated compared with the noble metals due to carbon deposition. This can be considered as the most difficult challenge in the commercialization of fuel cell

applications. Researchers have done a lot of works on exploring the mechanism of carbon deposition and developing reforming catalysts which are resistant to it. The most studied fuel is methane due to its simplest molecule structure and the widely application in industry. The higher hydrocarbon fuels such as gasoline and diesel would cause much severe carbon deposition than methane due to their more complicated molecule structure and fuel compositions. These liquid fuels usually contains large fraction of aromatics.

In this section, the mechanism of carbon formation during the hydrocarbon reforming processes will be summarized to provide a basic understanding of this issue. As suggested in the previous section about reforming mechanism, the study of the mechanism for methane reforming is very substantial for the study of mechanism for higher hydrocarbon reforming. The study of mechanism of carbon deposition is also similar to that, because researchers always start from the simplest case.

Kiyoshi Otsuka and others [97, 98] proposed the mechanism for carbon formation in methane reforming: 1) methane decomposes to hydrogen and carbon on the metal active sites; 2) the carbon atoms dissolve and diffuse into the metal bulk phase; 3) the carbon atoms segregate to form a grapheme layer; 4) carbon whiskers grow at the metal particles by stacking the grapheme layers.

The carbon deposition process for reforming of higher hydrocarbons is also similar to that of methane. The mechanism of carbon deposition was also proposed by other researchers. Just like methane decomposition, it is believed that the higher hydrocarbons also dissociative adsorb on the active sites. This dissociative adsorption will lead to the production of highly active atomic carbon (C_α) [99]. This highly reactive atomic carbon could be easily gasified to form carbon monoxide. However,

an excess amount of C_α could convert to amorphous C_β which is much less reactive. Consequently, C_β may accumulate on the metal particle surface or dissolve into the metal.

There are mainly two kinds of carbon observed for the reforming process: encapsulated-like carbon and whisker-like carbon. Carbon whisker is the most commonly seen carbon species from SEM analysis. It is usually formed by the dissolved carbon [11]. This process is believed to begin from the formation of metal carbide. Once the metal carbide formed, diffusion through the metal particle to grain boundary would occur. As a result, carbon precipitates and forms carbon whiskers. The metal particle would be lift up at the tip of a growing carbon whisker. The metal particle could remain as an active catalyst, but the growing carbon whiskers could block the catalyst bed and increase the pressure drop inside the reactor to unacceptable levels [100].

The other kind of carbon is the encapsulated-like carbon. In this case, carbon will not diffuse through the metal particle but remain at the surface and encapsulate the metal particle. Once formed, this kind of carbon could deactivate the catalyst and is difficult to be gasified. Generally speaking, catalyst deactivation is the result of encapsulation. The whisker carbon could block the catalyst bed and cause pressure drop, but does not affect greatly the activity of the catalyst.

2.2.1.2 Sulphur poisoning

Sulphur compounds are common impurities present in the fossil fuels [101]. Hydrogen sulphide is the most commonly seen in natural gas. For the higher hydrocarbon fuels such as gasoline or diesel, more complicated organ sulphur

compounds are present. The level of sulphur contamination in these hydrocarbon fuels is typically in between 3000-10000 ppmw [102]. The presence of sulphur compounds is a great challenge for the catalysts currently used in the hydrocarbon reforming process in oil refineries, which resulted millions of dollars lost every year [103, 104]. In industry, there are two ways to deal with this problem. One is direct reforming of the hydrocarbon fuels. The other is to carry out desulphurization of the hydrocarbon fuels prior to the reforming process. The first method is very critical for the reforming catalysts since they could be very easily deactivated by the sulphur compounds. As for the second choice, the only problem is that the cost for the desulphurization step is quite high and this way is not economically feasible. Thus the first method is still preferred due to its low cost and convenience. For this purpose, researchers have done vast of work on developing reforming catalysts which are resistant to sulphur poisoning. In this section, the mechanism of sulphur poisoning will firstly be discussed, since it is very helpful in designing reforming catalysts.

Sulphur poisoning refers to the loss of catalyst activity due to strong chemisorption of the sulphur compounds on the active sites. Since very strong interaction exists between sulphur and the active sites, sulphur will be continuously accumulated on the catalyst surface and result rapid loss of active sites. Therefore, sulphur poisoning could be effective at a very low level.

The behavior of hydrogen sulphide (H_2S) and sulphur dioxide (SO_2) metal catalysts have been studied a lot [105, 106]. It was suggested that these molecules chemisorbed dissociative on the metal surfaces either spontaneously or be thermal activation. This dissociative chemisorption leaves sulphur atoms which form sulphides with the metals. Sulphur, which is a highly electronegative element, could

form stable compounds with all transition metals [12, 105]. Among these metals, the noble metals especially Au has a weaker bonding with sulphur compared with the non-noble metals such as Ni and Cu. This is because the electro negativity of noble metals is higher than that of the non-noble metals and is closer to that of sulphur. Martin A. Abraham and co-workers proposed a deactivation mechanism for steam reforming of sulphur-doped hexadecane on an Rh-Ni bimetallic catalyst [107]. This catalyst showed good performance in steam reforming of the fuel without sulphur. However, significant deactivation occurred at the presence of sulphur and the extent of deactivation was dependant on the amount of Rh. They found that the sulphur compound decomposition mainly occurred on the surface of Ni particles, and possibly the sulphur adsorbed on the Rh particles might migrate to nearby Ni sites. They attributed this to the different electro negativity of these two elements. Thus the Rh-S bond is weaker than the Ni-S bond. This migration of sulphur could help to retain the activity of Rh. This is also one of the reasons that researchers use bimetallic catalysts to resist sulphur poisoning.

The metal sulphides basically show two main types of spatial orders: isotropic sulphides for the Group VIII sulphides and layered sulphides for the Group IV to VII sulphides. In both cases, sulphur would withdraw charges from the metals and induces perturbations in the electronic properties of the metals. This perturbation in electronic state could lead the significant changes in the catalytic properties of these metals [108, 109]. For example, it was found that sulphur could inhibit the chemisorption of small molecules (H_2, CO, CO_2, etc.), alkane hydrogenolysis, and water-gas-shift reaction [104].

Praveen K. Cheekatamarla and co-workers studied autothermal reforming of diesel over a ceria supported Pt catalyst and proposed a reaction/sulphur poisoning mechanism based on experimental data and surface characterization results [20, 110]. In this case, the support material was also involved in the reaction/poisoning process. Sulphur compounds in diesel would decompose to form SO_2 in reaction. SO_2 adsorbed on the ceria surface which is close to Pt sites would be easily oxidized to SO_3 and form ceria sulphate species. Then the ceria sulphate will diffuse into the bulk ceria in the presence of excess SO_3 which is favoured by Pt. Although the interaction between ceria support and SO_3 could protect Pt sites, it will still decrease the reaction rate. This is because sulphate will not be removed even under reducing environment, and will result a permanent loss of partial activity due to impeding of oxygen mobility which is helpful in removing adsorbed surface carbon species. Even when sulphur source is removed from the feed stream, SO_3 would desorb from the ceria support and spill onto the Pt sites, which continue the suppression of catalyst activity.

2.2.2 Reforming catalysts resistant to carbon deposition

It is believed that carbon deposition could be controlled to certain extent by employing proper reforming catalysts and appropriate conditions. In this section, only the reforming catalyst related aspects will be discussed. Based on the coking mechanism mentioned above, researchers have tried various methods to develop reforming catalysts which are resistant to carbon deposition. Basically there are two ways to deal with this problem.

The first one is to prevent the formation of amorphous carbon (C_β). As mentioned in the above carbon deposition mechanism, the hydrocarbons dissociative adsorb on the active sites which will lead to the production of highly active atomic

carbon (C_α). This highly reactive atomic carbon could be easily gasified to form carbon monoxide. However, an excess amount of C_α could convert to C_β which is much less reactive. Consequently, C_β may accumulate on the metal particle surface or dissolve into the metal. It can be seen that the formation of C_β is a necessary step for carbon deposition. Thus it makes sense to find a method to prevent C_α from converting to C_β. The production of C_β is actually a process of C_α polymerization. This polymerization process would require more C_α atoms to be produced, which consequently require active sites in an ensemble. This could be also classified into two aspects.

1) It is possible that the production of C_β could be reduced by minimizing the number of active sites in an ensemble, namely the metal particle size [111-113].

Obtaining small metal particles is usually achieved by employing proper catalyst preparation method or by addition of other component to enhance the dispersion of the metal particles. Dong Jin Suh and co-workers [86] studied the Ni-alumina aero gel catalysts for CO_2 reforming of methane and revealed the relation between Ni particle size and carbon deposition. The TEM studies showed that the formation of whisker carbon was significantly affected by the Ni particle size and occurred mostly on the metal particles larger than 7 nm. Similar results were also obtained by A. Holmen and his co-workers [114]. They studied the alumina supported Ni catalysts for methane steam reforming and discovered higher resistance to carbon deposition over the catalyst with a smaller metal particle size. It was suggested that smaller particles had a larger saturation concentration level of whisker carbon than larger ones, which would result in smaller driving force for carbon diffusion and thus higher resistance to carbon deposition. Elisabete Moreira Assaf et al reported a La

promoted Ni catalyst for methane partial oxidation reaction [38]. It was found that the addition of La could largely enhance the dispersion of Ni particles and the catalyst showed good carbon resistance. Another side of obtaining small metal particles is to prevent sintering. Sintering is also an important factor which may result catalyst deactivation, though it was not introduced in this chapter. Masahiro Kishida and co-workers reported a Ni catalyst covered with silica layers for propane steam reforming [115]. They found this catalyst to be highly resistant to carbon deposition and attributed it to the catalyst design which prevented sintering of Ni particles. Andrew T. Hsu et al also reported a Fe promoted Ni/Al_2O_3 catalyst which showed good carbon resistance in autothermal reforming of ethanol [116]. They attributed this to the synergistic effect of $NiAl_2O_4$-$FeAl_2O_4$ mixed crystals which were resistant to sintering.

2) It is also possible to accelerate surface carbon (C_α) gasification. The forming of C_β is the result of slow C_α gasification rate compared with fast C_α polymerization rate. Thus if the C_α gasification rate could be largely enhanced, the C_α polymerization rate would for sure be reduced. Thus carbon deposition over the catalyst could be minimized.

One approach to enhance carbon gasification is to induce second element to the active metal. Suljo Linic et al reported a Sn promoted Ni catalyst for catalytic reforming of hydrocarbons [117]. This catalyst showed high resistance to carbon deposition and the authors attributed it to the promotion effect of Sn, which enables the catalyst to oxidize carbon atoms instead of forming C-C bonds. Calles, A.J. Vizcaíno et al studied the promotion effect of Mg and Ca on the $Cu-Ni/SiO_2$ catalyst for ethanol steam reforming [118]. Two promotion effects were found for these two promoting elements: they were found to be able to reduce the Cu-Ni particle size, and

more importantly they could favour the formation of defective carbon which has a higher gasification rate. These promotional effect resulted obvious reduction in carbon deposition. Keiichi Tomishige et al reported a Fe promoted Ni catalyst for steam reforming of tar from biomass [119]. It was found that Fe tended to be enriched on the surface and could supply oxygen species to accelerate gasification of carbon species. Besides accelerating carbon gasification, it is also possible to prevent the adsorption of carbon on the active sites. Mark Saeys et al reported a B promoted Ni catalyst for methane steam reforming which showed good resistance to carbon deposition [51]. The DFT studies indicated that boron and carbon showed similar chemisorption preferences on the Ni catalyst. Therefore, boron could be used to block carbon from adsorption on Ni.

Another approach to accelerate carbon gasification is to modify the support materials. Currently the use of ceria or doped-ceria as support materials for reforming catalysts has attracted great interest. Ceria is well known due to its high oxygen storage capacity and mobility [120, 121]. This property of ceria could be further enhanced by doping with other rare earth elements such as Gd, Pr, Sm, etc. by creating oxygen vacancies [122]. The oxygen species transferred from ceria support to the surface active sites could facilitate the gasification of the adsorbed carbon species [123, 124]. The ceria support would also facilitate the adsorption of steam molecules, thus promoting water-gas-shift reaction and steam gasification of the adsorbed carbon species [125].

Wenjie Shen et al studied the Rh/CeO_2 catalyst for ethanol steam reforming [126]. It was found that ceria prevented the sintering of Rh and thus maintained sufficient metal-support interfacial areas, which facilitated carbon gasification via the

high oxygen storage-release capacity. Martin Schmal et al studied the Pt/CeO_2-Al_2O_3 catalyst which showed good performance for autothermal reforming of propane [127]. It was suggested that ceria was responsible for the decreasing carbon monoxide concentration and promoting the water-gas-shift reaction. Shudong Wang et al reported a Rh/CeZrO catalyst which showed good carbon resistant for autothermal reforming of methane [128]. This good carbon resistant was attributed to the oxygen storage capacity of the catalyst. Shik Chi Tsang et al also suggested that ceria could offer a kinetic resistance to carbon deposition for hydrocarbon reforming reactions due to its facilitated redox activity [129]. In order to increase the interaction between the active metal and ceria, they designed a Ni catalyst in which Ni was coated with ceria to obtain an intimate contact. This design ensured the catalyst a stable activity in methane steam reforming. S. Assabumrungrat et al studied the doping effect of La, Gd, Nb and Sm on Ce-ZrO_2 toward partial oxidation of liquefied petroleum gas [130]. It was found that the impact of doping element is strongly related to the extent of oxygen storage capacity and amount of lattice oxygen. Thus different catalytic performance was observed for different doping elements, among which La showed the best promotional effect. Fábio B. Noronha et al reported a Rh/CeO_2 catalyst for ethanol steam reforming and proposed a reaction scheme [131]. As proposed, ethanol dissociative adsorbed on the catalyst and resulted ethoxy species and bridging OH groups. Then the ceria support extracted oxygen from the bridging OH groups and transferred it to the active site to oxidize the ethoxy species.

The second way for preventing carbon deposition is to prevent the formation of metal carbide. As indicated in the above mechanism, forming metal carbide is an essential step prior to diffusion through the metal particle. Once the metal carbide formed, diffusion through the metal particle would occur and carbon precipitates and

forms carbon whiskers. The metal particle would be lift up at the tip of a growing carbon whisker. Carbon is a highly electronegative element (χ=2.55) just like sulphur (χ=2.58). This is higher than all those transition metals which can be used as active metals in reforming catalysts. Thus carbon can easily withdraw charge from these metals and form metal carbides. Thus it is possible to trim the micro electron environment of the transition metals, making them less affinity to carbon and prevent the formation of metal carbides. The mostly used method to achieve this purpose is to introduce a second element into the active sites.

Zongping Shao and co-workers reported a Li and La promoted Ni/Al_2O_3 catalyst for methane reforming [132]. After the modification of Ni/Al_2O_3 catalyst with Li and La, carbon deposition greatly reduced under pure methane condition. Kazunari Domen et al also reported a La promoted Ni/Al_2O_3 catalyst for steam reforming of *n*-dodecane [133]. The addition of La to the catalyst was found to completely suppressed carbon deposition under the reaction conditions. Stylianos G. Neophytides et al studied the Au promoted Ni/YSZ catalyst for methane steam reforming [134, 135]. It was found that only 1% Au addition with respect to Ni made the catalyst to be highly carbon tolerant. Sometimes, the catalyst design could have multi effects in promoting the catalyst performance. Luwei Chen et al studied the effect of Ca addition on a Ni/Al_2O_3 catalyst for ethanol steam reforming [136, 137]. In this work, Ca was found to have several functions such as: proper doping level of Ca could reduce the Ni particle size; increase the density of Ni 3d band valence electrons which could promote dissociation of methane; effective carbon removal by steam gasification.

In general, the researchers have developed many kind of catalyst toward preventing carbon deposition during catalytic reforming of hydrocarbons. The study of reaction/deactivation mechanism could help the researchers in designing catalysts, while the experiment data could also provide further knowledge of the mechanism. However, characterization of the surface chemistry involve in the catalytic process is a tough job though various equipments have been employed. Thus it is kind of impossible to clarify all the phenomena during the reaction. For instance, sometimes researchers developed a catalyst which showed good activity but cannot explain the reason for it. In any case, a lot of works in developing carbon resistant catalysts still need to be done to solve this problem.

2.2.3 Reforming catalysts resistant to sulphur poisoning

Sulphur poisoning is an even tougher problem compared with carbon deposition [138, 139]. This is because poisoned catalyst can hardly be regenerated. The bonding between sulphur and the active metal is very strong and it is quite difficult to break it [140, 141]. Levi T. Thompson et al [142] studied the effect of sulphur on Pt/Mo_2C and indicated that sulphur selectively poisoned just small part of the Mo_2C support but irreversibly poisoned the Pt sites. Unlike metal carbide, metal sulphide will not diffuse through the metal particle but just stay at the surface and cover the active sites. This makes the catalysts to be very sensitive to the concentration of sulphur. Usually a few ppm of sulphur could result severe catalyst deactivation, not mention the much higher sulphur content in the fossil fuels. Sulphur poisoning will for sure result carbon deposition after a while of reaction which makes the reforming catalysts eventually face both of the deactivation mechanisms at the

same time. Thus dealing with sulphur poisoning is a much tougher job compared with carbon deposition.

Based on the mechanism of sulphur poisoning, there are basically two ways to resist it: either by preventing adsorption of sulphur or by accelerating removal of adsorbed sulphur species. This is actually similar to that of preventing carbon deposition, because they have a similar deactivation mechanism.

Preventing the adsorption of sulphur could be achieved by either alloying a second element to the active metal or by ensemble size control. One purpose of alloying the active metal is actually to sacrifice one of the elements which adsorb sulphur preferentially. Thus the other active metal would be protected from sulphur adsorption and remain high activity. On the other hand, the bimetallic catalysts could exhibit very special properties toward reaction with sulphur [143, 144]. It is believed that the bimetallic bonding could redistribute the charge around the bonded metals. This electronic perturbation could affect the reactivity of the bonded metals toward sulphur. As for the mechanism of ensemble size control, its mechanism is similar to that of preventing carbon deposition. This point was reported by Alstrup and Andersen [145]. They studied the sulphur adsorption on nickel and found the dependent reaction rate on the particle size. The second way, which is accelerating the removal of adsorbed sulphur species, is also similar to accelerating carbon gasification as mentioned in previous section. The most commonly used method nowadays is employing the ceria or doped-ceria as catalyst supports. The reason for using this material is still due to its high oxygen storage capacity and oxygen mobility. Just like carbon, the transferred oxygen species is also very essential for removal of adsorbed sulphur.

Johannes W. Schwank et al studied the effect of metal particle size on sulphur tolerance of Ni catalyst for autothermal reforming of isooctane [146]. It was found that larger Ni particles were more vulnerable to sulphur poisoning but increasing the amount of highly amount of dispersed Ni particles will not enhance sulphur tolerance further. Abdul-Majeed Azad et al developed supported Pd catalysts for steam reforming of logistic fuels such as JP8, Jet-A and diesel [102]. The active metal was prepared with a highly dispersion and a high sulphur tolerance was obtained for it. This performance enhancement was attributed to the high dispersion of Pd. Moreover, CuO was used as additive into the catalyst. The addition of CuO further enhanced the sulphur tolerance of the catalyst. It was suggested that this was due to the further increased metal dispersion and the oxide acted as a sacrificial sulphidation site, which took the sulphur species away from the active metal. J. William Medlin et al carried out experimental and computational studies of sulphur resistant bimetallic catalysts for reforming of biomass gasification products [147]. The results revealed that the Ni-Ru catalyst showed a high level of sulphur resistance compared to Ni. This was attributed to the different sulphur and ethylene binding energy at different types of active sites across the bimetallic surface.

Xanthias Karatzas et al studied the CeO_2-ZrO_2 supported bimetallic RhPt catalyst for autothermal reforming of low-sulphur diesel[148]. The TEM analysis showed highly dispersion of the Rh_iO_x and Pt particles. Moreover, the doped-ceria support was believed to enhance water-gas-shift reaction and reduce carbon deposition on the catalyst. All these effects enabled the catalyst to be highly active in autothermal reforming of this low-sulphur diesel. Yong Lu et al studied the addition of CeO_2-Gd_2O_3 into the Pt/Al_2O_3 catalyst for autothermal reforming of retail gasoline [149]. It was found that the addition of CeO_2-Gd_2O_3 into Al_2O_3 greatly suppressed Pt

sintering and improved Pt-CeO_2 interaction. This enhanced metal-support interaction promoted oxygen ion conductivity in bulk ceria and facilitated the removal of surface sulphur and carbon species. Mingyuan He et al reported a highly sulphur tolerant $Pt/Ce_{0.8}Gd_{0.2}O_{1.9}$ catalyst for steam reforming of liquid hydrocarbons [150]. This catalyst was proved to be resistant to >300 μg/g sulphur in steam reforming of isooctane. It was found that strongly electron-deficient Pt sites were immune to sulphur poisoning. Moreover, the sulphur compound was completely converted to hydrogen sulphide under the redox mechanism of the Pt-ceria interaction. The authors suggested that this catalyst could provide some insight into the nature of Pt sites and conversion-pathway of sulphur compounds and thus aid further improvement in catalyst design.

As suggested earlier, sulphur poisoning is a much tougher problem compared with carbon deposition. The mechanism of this process is not studied as clear as that for carbon deposition. Thus it seems that the only way to go is just trying different types of catalysts and see which can work out, then try to find out the mechanism that why this catalyst could show good performance. Noble metals are still the favourite candidates as active metals. However, the high cost prevents them from application in industries. Ni is cheap and its reactivity is high, but it is so vulnerable to sulphur poisoning and also carbon deposition. In recent years of studies, ceria became a hotspot due to its prominent oxygen storage capacity and oxygen conduction ability. This could have provided a good solution to the weak Ni catalyst. But vast of works still need to be done to solve this problem.

2.4 Electroless nickel plating (ENP)

The electroless nickel plating, which was used as one of the reforming catalyst preparation methods, will be discussed in this section. It is known that the development of catalysts is of great industrial importance. To date, various catalyst synthesis methods have been developed: incipient wetness impregnation, precipitation, Pechini, Sol-gel, etc. Among these methods, impregnation is the most commonly used one. Sol-gel has the advantage of producing nano-sized particles. But the cost for this process is quite high since organmetallic compounds are used. Instead, Pechini was used as a good alternative method since it just uses metal nitrates. In this section, brief introduction of these two methods, impregnation and Pechini, will firstly be discussed.

The impregnation method is a commonly used technique for preparation of heterogeneous catalysts. Typically, the active metal precursor (usually as metal salts) is dissolved in an aqueous solution. Then the selected catalyst support material is added to the prepared solution. The catalyst support usually contains some pore volume that draws the solution into the pores through capillary action. Then the catalyst is dried and calcined to remove the volatile components in the solution, depositing the metal on the catalyst surface [151, 152]. The impregnation method is widely used in catalytic studies due to its simplicity in preparation. However, this method cannot give good control of the metal particle size and usually result in poor active metal distribution. For the bimetallic catalysts, the metal particle distribution is even poorer.

The Pechini method, based on the metal-ion-containing hydro gel, can be used to prepare heterogeneous catalysts and permits good stoichiometric control and reproducibility [153, 154]. In this approach, an aqueous solution containing suitable

metal salts is mixed with a chelating ligand system (citric acid/glycine). Then chelation, or the formation of complex ring-shaped compounds around the metal cations, takes place in the solution. After adding a polyhydroxy alcohol (like ethylene glycol), the liquid is heated under around 200 °C to allow the chelates to polymerize and a gel is formed. The resulting gel is then calcined to execute pyrolysis and ensure the growth of crystal phases in the oxides. The Pechini method could ensure a very high extent of compositional uniformity in a multicomponent metal oxide. This is because the distributional uniformity of the metal ions in the hydrogel precursor is very close to that in the homogeneous aqueous solution.

Electroless nickel plating (ENP) process, firstly discovered by Brenner and Riddell in 1946 [155], is an auto-catalytic reaction used to deposit a coating of nickel-phosphorous (Ni-P) or nickel-boron (Ni-B) on a substrate [156, 157]. The process relies on the presence of a reducing agent which reacts with the metal ions to deposit metal alloy. This technique has many advantages such as high hardness, resistance to corrosion, and wear resistance. Thus it is usually used to prevent corrosion and wear [158, 159]. Nevertheless, the ENP process is also used to prepare heterogeneous catalysts nowadays. The reaction for using this technique to prepare catalysts is that it can give uniform alloying of nickel with phosphorous or boron. As mentioned above, alloying the active metal with a second element is an effective approach to prepare catalysts resistant to deactivation. Phosphorous and boron are among those candidate elements. Through the ENP process, phosphorous or boron could be highly uniformly dispersed in the active nickel sites. Thus a highly intimate contact of nickel with phosphorous or boron could be obtained.

2.4.1 Basic composition of ENP process

The unique properties of the deposited nickel alloy by the ENP process mainly depend on the formula of the ENP bath. The primary components for an ENP bath include: nickel source, reducing agent, complexing agent, stabilizer and surfactant.

Several nickel salts could be used as nickel source in the ENP process: nickel nitrate, nickel sulphate, nickel chloride or nickel acetate. The preferred nickel source is nickel nitrate or nickel sulphate, while the other two are usually used for very limited applications. The chloride anion could act deleteriously when alumina or ferrous alloy is used as the substrate for ENP process [156]; while the use of nickel acetate can bring no improvement to the bath performance but a higher cost. The concentration of nickel of en ENP solution is about 6.5g/L for most industrial applications, and the plating reaction is zero order to this concentration.

Reducing agent is the most important component except for the nickel source. There are four reducing agents used in electroless plating bath: sodium hypophosphite, sodium borohydride, dimethylamine borane and hydrazine [160]. Nickel reduction during the electroless plating process is said to result from the catalytic dehydrogenation of the reducing agent. As said before, the deposit produced in this process is a nickel alloy. This other alloying element, phosphorous, boron, or nitrogen, is just from the different reducing agent. The Ni-P alloy is the most important one due to its unique physical and chemical properties and the low cost of sodium hypophosphite [161]. Sodium borohydride is widely used to reduce nickel ion in basic ENP solution where its decomposition releases eight electrons for the reduction reaction. The Ni-B deposit generated using this reducing agent exhibits similar

characteristics as Ni-P alloy, but is especially suitable for application in electronic devices [162].

During the ENP process, the free nickel ions which are loosely bonded to a number of water molecules may precipitate as nickel phosphate or nickel hydroxide. This precipitate would result the loss of nickel ions and give rise to several problem such as affect the quality of the deposits and initiate spontaneous bath decomposition. Therefore, complexing agents are usually employed to control the availability of free nickel ions. The commonly used complexing agents in ENP process include: ammonia, monocarboxylic acids, alkanolamines, hydrocarboxylic acids and their salts [163]. There are mainly three principal functions of complexing agents: 1) act as buffering agent to maintain pH value of the solution in an acceptable range; 2) prevent the precipitation of nickel salts; 3) reduce the number of free nickel ions on the ENP solution. Additionally, the complexing agents could also influence the nickel deposit.

Another problem of the ENP process is that tiny hydrogen bubbles would adsorb on the surface of the deposit and cause micropitting. The pinholes resulted from micropitting could decrease the resistance of the deposit to corrosion [164]. This problem actually could be solved by adding surfactant with proper structures to the ENP bath. The surfactants could significantly reduce micropitting on the deposit and improve the resistance to corrosion. In addition, it can also reduce water evaporation and maintain the bath temperature. Several types of surfactants could be used in the ENP process: non-ionic (e.g. Tween 80), cationic (e.g. dodecyltimethylammonium chloride) and anionic (e.g. sodium dodecylbenzenesulfonate).

2.4.2 Reaction mechanisms of ENP in acidic hypophosphite bath

Though there are several different ENP processes, only the ENP in acid hypophosphite bath which produce a Ni-P deposit will be discussed here. Understanding the mechanism of this process is very essential for improving this technique for application in different environments. The ENP process is a heterogeneous reaction in a liquid-solid system, where the solid metallic surface acts as a catalyst. Without this catalyst, the process can hardly proceed. This would indicate that more than one agent are adsorbed on the active sites of the catalytic surface in this reaction. Thus many mechanisms could be deduced for describing the reaction rates. To date, there are several mechanisms have been proposed for the ENP process, such as atomic hydrogen mechanism, electrochemical mechanism, hydride transfer mechanism, and mixed potential theory [163, 165-167]. However, no one could explain all the experimental phenomena found in the ENP process.

Although none of them is an ideal mechanism for the ENP process, the atomic hydrogen mechanism will be briefly discussed to get a rough understanding of this process. According to this mechanism, nickel in the ENP process is actually reduced by the adsorbed atomic hydrogen released by the reaction of water with hypophosphite at the catalytic surface:

$$H_2PO_2^- + H_2O = H_2PO_3^- + 2H_{ad} \qquad (2.20)$$

This adsorbed atomic hydrogen then reduce the nickel ions at the catalytic surface:

$$Ni^{2+} + 2H_{ad} = Ni^0 + 2H^+ \qquad (2.21)$$

The two atomic hydrogen atoms would also combine to form hydrogen gas:

$2H_{ad} = H_2$ (2.22)

In addition, a secondary reaction between hypophosphite and the atomic hydrogen would occur to produce the elementary phosphorous:

$H_2PO_2^- + H = P + OH^- + H_2O$ (2.23)

However, this mechanism cannot explain why the stoichiometric utilization of hypophosphite is less than 50% and is not consistent with the simultaneous reduction of hydrogen and nickel.

Beside the above mentioned mechanisms, researchers sometimes propose new mechanisms using their own experimental data. A. Micek-Ilnicka and A. Małecki [168] proposed the following mechanism after testing all reasonable possibilities:

$Ni^{2+}_{ads} + H_2PO^{2-}_{ads} + H_2O = Ni^0 + 3H^+ + HPO_3^{2-}$ (2.24)

$H_2PO_2^-{}_{ads} + H_2O = HPO_3^{2-} + H^+ + 2H_{ads}$ (2.25)

$H_2PO_2^-{}_{ads} + H_{ads} = P^0 + H_2O + OH^-$ (2.26)

$2H_{ads} = H2$ (2.27)

In this model, it was assumed that nickel ions, hypophosphite ions, hydrogen ions, and atomic hydrogen were adsorbed on the same kind of the catalytic site. The catalytic reduction of adsorbed nickel ions by adsorbed hypophosphite ions was assumed to proceed simultaneously with the reduction of adsorbed hypophosphite ions by adsorbed atomic hydrogen. The kinetic equation derived based on this mechanism was consistent with the experiment results.

2.4.3 Process of ENP

The ENP process is a very complicated heterogeneous reaction whose mechanism is still not completely understood. There are many variables that could affect the proceeding of this reaction and the quality of the metal alloy deposit. Thus the processing of ENP needs to be handled carefully.

The pretreatment of the substrate has significant effects on the ENP process. It is known that the ENP process cannot proceed without a catalyst. Usually the metal substrate would serve as catalyst to initiate the reaction. These metals are typically Group VII metals: Co, Ni, Ru, Rh, Pd, Ir, and Pt [162]. The nickel alloy could be directly deposited on these metal substrates. However, sometimes the substrate materials cannot serve as catalyst. For example, the metal oxides, carbides, PTFE and PI materials are all not catalytically active in nature [169-171]. In this case, it is necessary to deposit nuclei of an intrinsically active metal on their surface to initiate the catalytic process. After the reaction was initiated, the produced nickel alloy will cover the nuclei. But the newly produced nickel atom would serve as the new catalyst in this process. Thus it is actually a self-catalytic process once after initiated [163]. Typically the employed intrinsically active metals include Cu, Ag, Pd, and Au.

After pretreatment of the substrate material, it can be used in the ENP process. During this process, there are several factors that could influence the reaction: bath temperature, pH value, nickel and hypophosphite ion concentration, phosphite anion, complexing agents, agitation, and bath loading. Here they will be selectively discussed.

The bath temperature is an important variable determining the reaction rate [163]. The reaction rate is in proportion to the reaction temperature. But a too high temperature would cause decomposition of the plating solution. Thus the optimal temperature for acidic hypophosphite ENP solution is in between 80-90 °C, while that for the basic ENP bath is in between 60-70 °C. It should be noted that phosphorous content in the nickel alloy is in reverse proportion to temperature. Thus proper reaction temperature should be selected to obtain a desired alloy composition.

Hydrogen ion is an intermediate product during the ENP process, which may lower the pH value of the solution. No matter for acidic or basic bath, lowering pH value would decrease the deposition rate and eventually cease the reaction. Thus complexing agents are usually added in the plating bath as buggering agents to avoid drastic pH value change. Sometimes, the reaction is so intense that even these buffering agents are helpless. Then additional diluted basic solutions like ammonia solution need to be added to the plating bath to moderate the pH value.

The nickel concentration of the ENP bath needs to be controlled at certain range. Lower nickel concentration would result low deposition rate while higher nickel concentration will not increase the rate any further but is wasteful. On the other hand, increasing the concentration of hypophosphite will increase the deposition rate and result a higher phosphorous content in the nickel alloy [168]. At last, agitation is very useful for the ENP process. Since lots of hydrogen gas will be produced during the reaction, agitation could help to release it and facilitate the reaction equilibrium to proceed to desired direction. It may also facilitate mass transport of the reactants, thus improves the deposition rate and result more uniform distribution of the deposit.

2.4.4 Catalysts prepared by ENP method

Although the ENP process is mostly used in production o corrosion resistant deposit, it can also be used in synthesis of catalysts. The advantage of this process is that it can obtain very uniform mixture of nickel and the other alloying element like phosphorous or boron. The key point in this application of ENP process is controlling the size of the alloy deposit. Unlike the uniformly deposited film that favoured in the corrosion resistant materials, nano sized alloy particles are favoured in catalyst preparation.

Zhi-Jie Wu et al reported a supported nickel borate catalyst prepared by electroless nickel plating for sulfolene hydrogenation and acetophenone reactions [172, 173]. In this work, MgO supported Ni-B catalyst was synthesised using Ag nuclei as the initial catalyst in a basic ENP bath. By regulating the reaction variables, nano sized Ni-B particles were deposited on the MgO support. According to the TEM images of the prepared catalysts, it can be seen that the deposit size is below 50 nm, and could be controlled by varying the pH value. The composition of the Ni-B alloy could also be altered by changing the reaction variables such as molar ratio of starting materials, pH value, and other additives. The optimal catalyst showed good catalytic performance in the sulfolene hydrogenation and acetophenone reactions. It was also found that the catalyst activity was independent on the composition of the Ni-N alloy.

Zhijie Wu et al reported a strategy of size-controlled synthesis of supported nickel nanoparticles via electroless nickel plating process [174]. The reaction variables were optimized for production of nano sized metal particles, and a 9 nm diameter and narrow size distribution were obtained. Ag nuclei were also used as the initial catalyst. The reducing agent used in this work was N2H4, thus there was no

alloying element in the nickel particle. This catalyst showed high activity, selectivity, and stability in the selective hydrogenation of p-nitrophenol to p-aminophenol.

The above catalysts were all used in hydrogenation reactions, while the catalyst prepared using this technique could also be used in other applications. H.B. Hassan and Z. Abdel Hamid reported a carbon supported Ni-B electrode prepared by electroless plating for direct alcohol fuel cell applications [175]. In this work, an acidic plating bath using nickel chloride as nickel source and dimethylamine borane as reducing agent was used to prepare Ni-B coating. This as-prepared Ni-B/C electrode showed enhanced electro-catalytic activity for electro-oxidation of methanol and ethanol. They also tried the Ni-P/C electrode prepared via the same deposition technique, but its performance was worse than the Ni-B/C electrode. The superior performance of the electrode for alcohol oxidation was attributed to the alloying B with both structural effect and electronic effect.

Except for the production of nickel alloys, the ENP process also could be modified to prepare other types of alloys by altering the metal source. KwangSup Eom et al reported a Co-P catalyst prepared by electroless plating with a high hydrogen generation rate in sodium borohydride solution [176]. Moreover, Melanie T. Schaal et al reported an Ag-Pt/SiO_2 catalyst prepared by electroless plating for hydrogenation of 3, 4-epoxy-1-butene and showed good catalytic activity.

It can be seen that the electroless nickel plating technique could be used for synthesis of heterogeneous catalysts for certain reactions. The alloying effect was found to be the main cause for the elevated catalytic performance. This is just the advantage of the ENP process that highly uniform mixing of the alloying elements

could be achieved by this technique. However, there are still more work need to be done to further explore this technique for wider applications.

CHAPTER 3

NICKEL PHOSPHIDE CATALYST FOR AUTOTHERMAL REFORMING OF SURROGATE GASOLINE FUEL

3.1 Introduction

Fuel cells powered by hydrogen or syngas (H_2/CO) possess advantages of high energy efficiency and clean emission over internal combustion engines. Conducting reforming of gasoline or diesel whose main component comprises C_4 to C_{16} hydrocarbons for the production of hydrogen on board is of special interest. This route could avoid shipping and storage of hydrogen or syngas and allow for continuous use of the existing fossil oil delivery infrastructure [9, 28]. Hence, development of a Ni-based catalyst possessing adequate chemical stability in the reforming of larger molecular weight hydrocarbons, such as gasoline or diesel, is crucial to the evolution of this clean energy source. A combination of the existing catalytic reforming techniques, i.e. steam reforming (SR) and partial oxidation (POX), generates autothermal reforming (ATR). As a result, the exothermic POX could cover the heat the endothermic SR reaction demands[20]. A typical ATR is (taking *n*-octane for example):

$$C_8H_{18} + xO_2 + (16\text{-}2x)H_2O \xrightarrow[\text{Cat}]{} 8CO_2 + (25\text{-}2x)H_2 \qquad (3.1)$$

where x is the oxygen-to-fuel molar ratio. The degree of the exothermic (POX) or the endothermic (SR) of the overall reaction can be controlled by the x value.

The chemical stability of the Ni-based catalyst is about its capability to avert the deactivating actions of sulphur-containing compounds and coke deposited. Deposition of carbon at Ni catalyst during the reforming of hydrocarbons is a hazard to POX and ATR because coking causes jam in a packed-bed reactor and deactivation of catalyst [177]. The mechanism of carbon deposition at the Ni catalyst has been extensively investigated [178, 179]. Nevertheless, most of them focused on the POX of methane in which impregnated Ni catalysts were used. Furthermore, compared to methane, it would be more difficult to reform liquid hydrocarbons due to a heavier coke deposition extent. To tackle this problem, the precious metal-modified Ni catalysts and the supported-precious metal catalysts have been explored to reform long chain alkanes under the autothermal condition [59, 107, 180-182]. Despite displaying stronger resistance to carbon deposition than nickel, noble metals are in general too costly to suit industrial applications. Hence, the supported-Ni catalyst system still remains practically attractive. Modification of the refractory oxides supports has been an effective way to improve coking resistance at the Ni crystallites supported on them. Recently, the doped cerium oxides have become a novel type of support mainly because they contain oxygen vacancies. Lattice oxygen ions in the doped ceria could contribute to removing of carbon filaments from the Ni catalyst at the reforming temperatures [29, 36, 46, 50].

Different from using the impregnated Ni catalyst, we synthesized nano sized NiP alloy nodules on micron-sized particles of ceria by means of the electroless nickel plating (ENP). Despite being an amorphous alloy, the as-deposited Ni(P) (P ≈ 12 wt.%) nodules were converted to nickel phosphide crystallites, Ni_xP_y, at the reaction temperature of ATR. In the following sections we denote the CeO_2-supported Ni_xP_y catalyst as NiP/Ce for the sake of simplicity. In principle, the nickel phosphide

crystallite is formed by polar covalent bonding. It has been reported recently that the Ni_xP_y catalyst, obtained from a different ENP procedure, was used to catalyze dechlorination of an organic chloride[183]. The present work focuses on understanding how the designated catalytic conditions affect the conversion of the surrogate hydrocarbon fuel and the yields of H_2, CO, CO_2 and CH_4. It has been also confirmed that the NiP/Ce catalyst remained carbon-free after the ATR of the fuel consisting of *n*-octane and naphthalene. Fundamental aspects for this improvement have also been explored experimentally.

3.2 Experimental

3.2.1 Materials

Cerium (IV) oxide (CeO_2) powder with average particle size of less than 5.0 μm was purchased from Sigma Aldrich. Cerium nitrate hexahydrate (Sigma Aldrich, >98%), nickel nitrate hexahydrate (Sigma Aldrich, >98%), ammonium solution (Merck, 25%), stannous chloride (Sigma Aldrich, >98%), palladium chloride (Sigma Aldrich, >98%), hydrochloric acid (Merck, 37%), sodium hypophosphite (Merck, >98%), DL-malic acid (Merck, >98%), Sodium acetate (Merck, >98%), lactic acid (Merck, >98%), borax (Merck, >98%), lead acetate (Sigma Aldrich, >98%), *n*-dodecane (Sigma Aldrich, >99%), and naphthalene (Sigma Aldrich, >99%) were all used as received. A nickel-based SR commercial catalyst (Alfa Aesar, HiFUEL^{TM} R-110) was used as benchmark.

3.2.2 Catalyst preparation via ENP process

The catalyst was initially prepared by depositing Ni(P) nano nodules to ceria particles in an acidic electroless nickel plating bath [184]. Before plating, the ceria particles were modified by the following surface roughening procedure. Firstly, 5 g ceria was added into 100 mL solution of cerium nitrate hexahydrate [$Ce(NO)_3 \cdot 6H_2O$, 2.52 g] under stirring. The pH value of the slurry formulated was adjusted to about 10.0 by dropping 2.5% ammonia solution into the slurry. The slurry was then stirred for 1 h and aged subsequently for 4 h. During this treatment, most of $Ce(OH)_4$ precipitate first attached to the CeO_2 particles and then formed a gel layer. The solid was collected by filtration, followed by drying overnight at 80 °C and calcining at 600 °C for 1 h. This step enhanced the surface roughness, which was confirmed by both the increase in specific surface area from 7 $m^2\ g^{-1}$ to 17 $m^2\ g^{-1}$ and micrograph image of the CeO_2 particles (Figure 3.1). The modified oxide powder was then sensitized in an aqueous solution containing stannous chloride ($SnCl_2 \cdot 2H_2O$, 20 g L^{-1}) and hydrochloric acid (0.24 M) under stirring for 10 min at room temperature. The sensitized oxide was rinsed with deionized (DI) water subsequently. Then the oxide was activated in an aqueous solution containing palladium chloride ($PdCl_2 \cdot 2H_2O$, 0.3 g L^{-1}) and hydrochloric acid (0.12 M) under stirring for 5 min at room temperature. After that, the oxide was fully washed using DI water and dried at 50 °C in vacuum. A certain amount of the activated ceria was transferred into the nickel plating solution with pH=5 and 60 °C for 10 min with constant stirring. The recipe of the nickel plating solution is listed in Table 3.1. After plating, the powder was washed thoroughly with DI water and dried at 50 °C in vacuum. After that, the Ni(P) deposited ceria, Ni(P)/Ce, obtained has a Ni loading of 5.6 wt. % and a ratio of Ni to

P by weight of about 7. Finally it is worthy of note that such extent of plating cannot be attained without enhancing surface roughness of CeO_2 particles.

One of the two control catalysts used in this study was prepared by the impregnation method as reported everywhere. An appropriate amount of $Ni(NO_3)\cdot 6H_2O$ was dissolved in 50 ml DI water, then the ceria powder was added into this solution. After stirring under room temperature for about 3 hrs, the mixture was heated at 60 °C overnight under stirring to evaporate water. The obtained solid was calcined in air at 600 °C for 3 hrs to obtain a NiO/Ce powder. It would be then reduced to Ni/Ce under ATR conditions. The Ni loading in this control catalyst was about the same as the Ni(P)/Ce. Finally, a nickel-based SR commercial catalyst (Ni loading: 15-40 wt. % denoted by CC) was adopted as another control catalyst to benchmark the performance of the NiP/Ce catalyst.

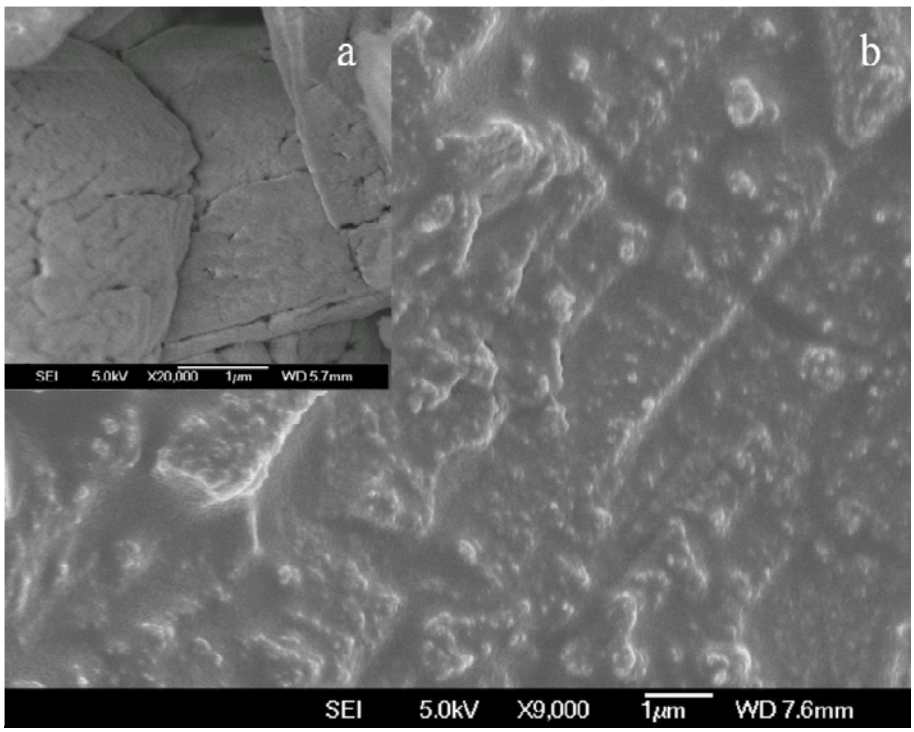

Figure 3. 1 FE-SEM images of the surface morphology of the ceria particles adopted as support (a) and that of the modified ceria particles (b)

Table 3. 1 Compositions of electroless nickel plating bath

Chemical	Concentration
Nickel nitrate hexahydrate	22.4 g L^{-1}
Sodium hypophosphite	25 g L^{-1}
DL-malic acid	4 g L^{-1}
Sodium acetate	8.5 g L^{-1}
Lactic acid	21 ml L^{-1}
Borax	6 g L^{-1}
Lead acetate	3 mg L^{-1}

3.2.3 Catalyst characterization

The composition of the catalyst precursor Ni(P)/Ce was determined by Inductively Coupled Plasma-Mass Spectrometry (ICP-MS, Agilent 7500 Series). The total nickel loading was about 5.6 wt. %, whereas the Ni(P) alloy comprised 87.5 wt. % of Ni and 12.5 wt. % of P. The content of palladium is about 0.3 wt. %. The specific surface area of the precursor was gauged on an Autosorb-1 (Quantachrome) by applying the multi-point BET method after degassing at 300 °C for 3 h under N_2 purging. Its magnitude is about 30m^2 g^{-1}. The temperature-programmed reduction (TPR) was conducted on the same instrument using a sample of 100 mg and a gas (5% H_2 in N_2) flow rate of 80 mL min^{-1}. The heating rate was set as 10 °C min^{-1}. The morphologies of the different catalysts were observed and recorded on a field-emission scanning electron spectroscope instrument (JEOL, JSM-6700F). Crystalline structures of the catalysts were determined on an X-ray diffractometer (XRD, SHIMADZU XRD-6000, Cu Kα radiation) using a scanning rate of 5 ^{o} min^{-1}. The

oxidation states of Ni, P and Ce in the NiP/Ce and Ni/Ce catalysts were characterized on an instrument of X-ray photoelectron spectroscopy (XPS, Kratos Axis HiS System) equipped with Al *Kα* X-ray source (1486.6 eV) and the take-off angle of 90° with pass energy of 40 eV. C1s (284.6 eV) was used as the internal reference to calibrate the spectra obtained. To double confirm the carbon filament deposited on the Ni/Ce catalyst but not on the NiP/Ce catalyst during ATR of the *n*-octane, two temperature-programmed oxidation profiles of the two catalysts were obtained respectively from the measurement on a (Quantachrome ChemBET 3000). Typically, ca. 50 mg sample was placed in a U-tube holder and subsequently degassed at 300 °C for 1 hr by flushing the sample with N_2 gas at a flow rate of 80 mL/min. After degassing, the probe gas consisting of 5% O_2 and N_2 was allowed to pass through the sample at a flow rate of 55 ml/min, and then the sample was heated from ambient temperature to 1000 °C, over which a TPO profile was recorded.

3.2.4 Experimental setup and reaction conditions

Approximately 1g catalyst powder was packed between two plugs of quartz wool in the centre of a quartz tube reactor (1.2 cm o.d., 1 cm i.d., 40 cm long). The micro plug flow reactor was then placed in a thermostat-controlled vertical tube furnace. The air and nitrogen mixture into the reactor was metered by Alicat mass flow controller. The fuel (*n*-octane or *n*-octane containing 6 wt. % naphthalene) and water streams were regulated respectively by ISO-2000 isocratic pumps and sent to joining with the air/N_2 stream. The tri-components (fuel, air/N_2 and water) stream was then directed into a mixer wrapped up by a heating band to carry out vaporization and mixing before being connected to the catalytic bed. The temperature of the mixer was set at 250 °C and a blank run indicated that the fuel was not pyrolyzed in the mixer.

Before the reaction starts, the catalyst was exposed to a flow of air (30 ml min^{-1}) for about 30 min at 900 °C to convert the amorphous Ni(P) alloy to Ni_xP_y crystallite (or NiP as denoted). The optimal reforming conditions comprised the following parameters: fuel-supply rate = 0.04 ml min^{-1}, oxygen and steam supply rates: O_2/C=0.5 and H_2O/C=1.7, reforming temperature 900 °C, and GHSV=9000 ml hr^{-1} g_{cat}^{-1}. It may be noted that although identical amounts of the CC catalyst and the Ni(P)/Ce catalyst were loaded in order to satisfy the same GHSV, the former one contained a higher Ni content by several times. The outlet stream was connected to a Shimadzu GC after passing a cold trap to knock out any condensable components. The performance of the catalyst was assessed by fuel conversion, distribution of gaseous products and their yields, which were evaluated using the following equations where nitrogen was used as internal standard:

$$\text{Conversion} = \frac{F_{total}(y_{CO} + y_{CO_2} + y_{CH_4})}{F_C \text{ in fuel}} \qquad (3.2)$$

$$\text{Yield} = \frac{F_{total} y_p}{F_p \text{ in fuel}} \qquad (3.3)$$

$$F_{total} = \frac{F_{N_2} \text{ in feed}}{y_{N_2}} \qquad (3.4)$$

where F stands for molar flow rate in mol s^{-1} and y the mole fraction of a component *p* (subscript) in the gas outlet stream. F_p stands for the mass flow rate of component p in the feed (for hydrogen, H_2 is used as the basic unit for calculation). Theoretically the conversion should be determined from the amount of octane at the exit of the reactor with respect to that used in the feed. However, the fuel conversion is determined using

Eq. 2 here due to some practical reasons, such as limitation of gas analysis and the removal of fuel in the water condensation process.

3.3 Results and discussion

3.3.1 Determination of the ATR conditions

Prepared by the electroless plating, the amorphous Ni(P)/Ce displays a complete different TPR profile from the NiO/Ce prepared by the impregnation method (Figure 3.2). The TPR diagram of Ni(P)/Ce presents only a sharp peak at 150 °C and a broad peak centred at 290 °C with a shoulder peak at 363 °C, while NiO/Ce revealed the normal exothermic reduction peak of NiO at about 380 °C. The sharp peak at 150 °C represents reduction of superficial passivation layer on the Ni(P) nodules. The broad peak at 290 °C can be ascribed to the reduction of Ce^{4+} ions of the ceria support by referencing the reported work [110], while the broad peak at 480 °C on the TPR of the NiO/Ce catalyst is known to be the normal reduction peak of ceria. As can be found, the two ceria supports exhibit discrepant reduction temperatures and peak intensities, viz. the reducibility, just because of the presence of the two different catalysts on them. According to the previous studies [110, 185], the supported noble metal catalysts (Pt, Rh) reveal unique capability to facilitate reduction of the ceria support underneath. This facilitation leads to generation of oxygen vacancies in ceria and thus enhances the oxygen conductivity of the support, helping clean up in-situ carbon filaments formed during the reforming reaction.

The conversion of *n*-octane (to CH_4, CO, and CO_2) increases with the increase in temperature (Figure 3.3). However, the concentration of H_2 is basically not affected by reaction temperature while the concentration of CO slightly increased. Compared

with the two control catalysts, viz. CC and Ni/Ce, NiP/Ce shows lower conversions at temperatures below 900 °C but finally presents a comparable activity at 900 °C. Therefore, the subsequent investigations were undertaken at this temperature.

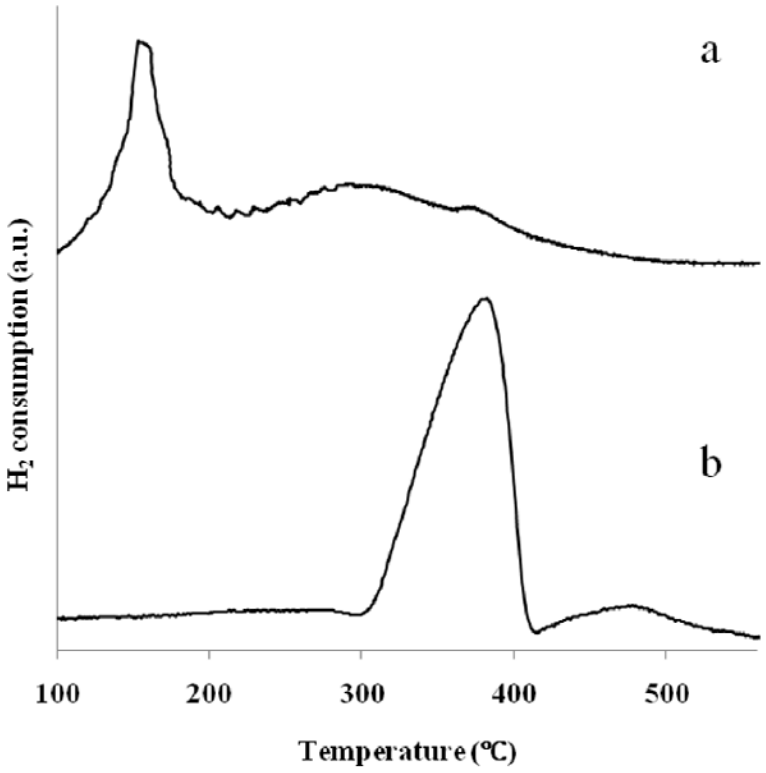

Figure 3. 2 TPR profiles of (a) fresh Ni(P)/Ce and (b) NiO/Ce

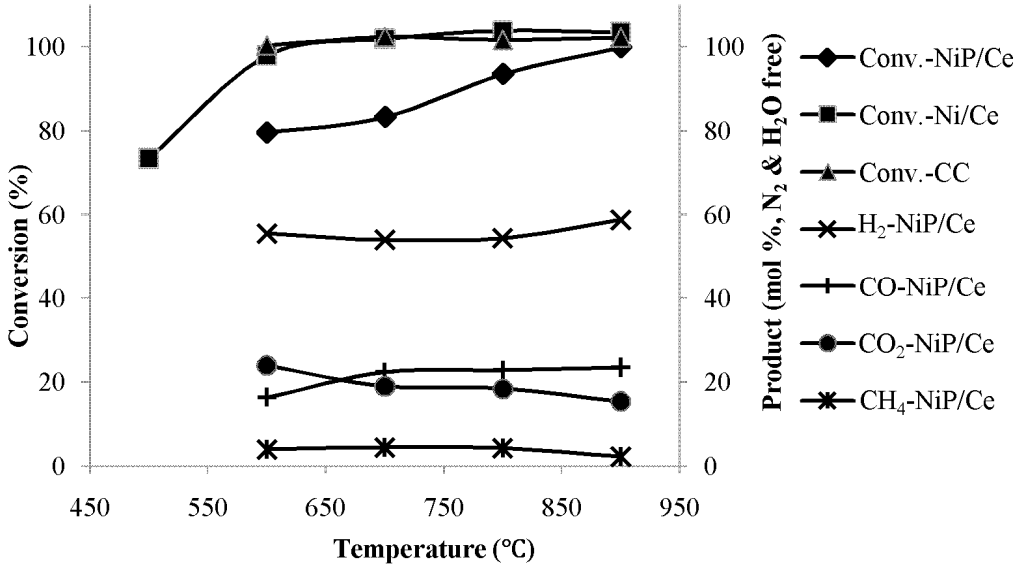

Figure 3. 3 Variation of *n*-octane conversions (wrt. the three catalysts) and the concentrations of the four species in the product stream (from the NiP/Ce system) with reaction temperature (C_8H_{18}=0.04 ml min^{-1}, O_2/C=0.5, H_2O/C=1.7, GHSV=9000 ml hr^{-1} g_{cat}^{-1})

As indicated in Eq. 3.1, the O_2/C ratio affects the extents of SR and POX, the sign of reaction heat and the concentration of H_2 in the product stream. The effect of O_2/C ratio on the composition of the product stream is reflected in Figure 3.4, where the conversion of *n*-octane is independent of the O_2/C ratios. With the increase in O_2/C ratio, the H_2/CO ratio decreases due to an increase in the production of CO. To approximately estimate the O_2/C ratio that leads to the thermal balance between POX and SR and results in thermoneutrality of the reaction, the reaction heat at 298 K and the standard state, i.e. $\Delta H^0_{r,298} = 1674.8 - 571.6x$ ($0 \le x \le 8$), is used, which is acceptable because enthalpy is a state function. The overall reaction shifts to exothermic direction with the increase in the *x* value. As a result, when *x* equals 2.93, namely the O_2/C ratio is about 0.37, the reaction reaches thermoneutral ($\Delta H^0_{r,298} = 0$). An O_2/C ratio slightly above 0.37 is desirable to assure the reaction be weak exothermic so that the decrease in H_2% can be minimized. Based on this consideration, the O_2/C ratio of

0.5 was selected to undertake the rest studies. With this ratio, the concentrations of H_2 and CO in the product stream are 60 mol % and 20 mol %, respectively (Figure 3.4). In addition, the conversion became slightly above 100% with use of the high O_2/C ratios, which is likely due to the effect of cleaning the carbonaceous residues in the mixer prior to reactor.

With respect to the effect of H_2O/C ratio on the product composition, the H_2O/C ratio of 1 was figured out on the basis of the O_2/C ratio of 0.5 (or $x = 4$ in Eq. 3.1). We also notice that an increase in the H_2O/C ratio from 1.1 to 1.4 brings about a slight increase in the concentrations of H_2 and CO_2 and a decrease in CO in the outlet stream (Figure 3.5). This variation marks a minor extent of water gas shift reaction (WGSR, $CO + H_2O \rightarrow CO_2 + H_2$). After that, no further shift toward the CO_2 and H_2 side was observed with the increase in H_2O/C ratio. Such a weak degree of WGSR could be due to the exothermic nature of the reaction when the equilibrium is reached at 900 °C.

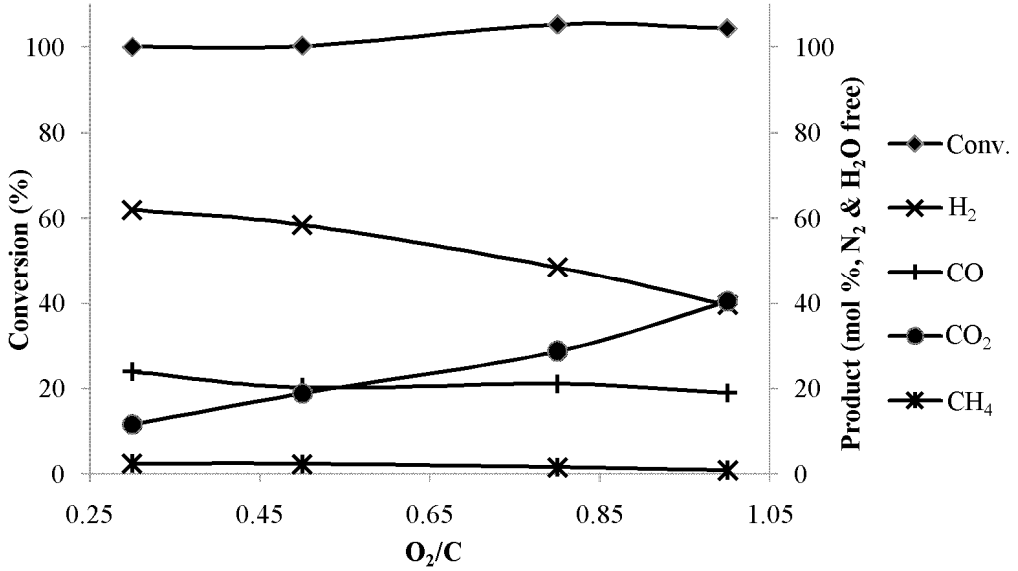

Figure 3. 4 Variation of n-octane conversion and the composition of product stream with O_2/C ratio in the NiP/Ce catalytic system (C_8H_{18}=0.04 ml min^{-1}, H_2O/C=1.7, 900 °C, and GHSV=9000 ml hr^{-1} g_{cat}^{-1})

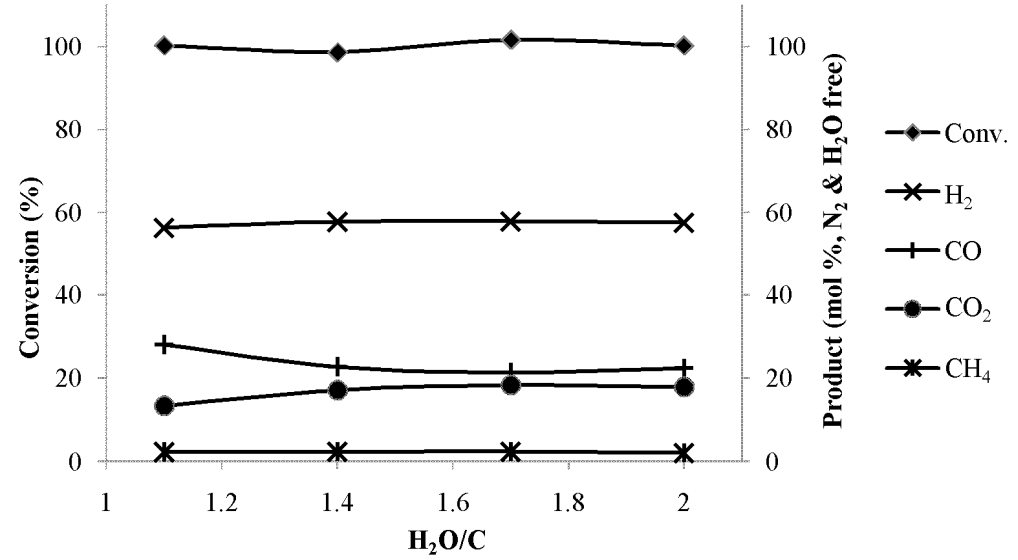

Figure 3. 5 Conversion and composition of the gas product as a function of H_2O/C ratio (C_8H_{18}=0.04 ml min^{-1}, O_2/C=0.5, 900 °C, GHSV=9000 ml hr^{-1} g_{cat}^{-1})

3.3.2 Evaluation of the catalysts in ATR of *n*-octane

The three catalysts all manifest a conversion of near 100% (Table 3.2) under the conditions of O_2/C=0.5, H_2O/C=1 and 900 °C. The yields of CO and CO_2 are similar in these three catalysts (Figure 3.6), while the yield of H_2 produced from the NiP/Ce catalytic system is slightly lower than those from the other two catalytic systems. The yields of H_2 in the three systems are above 1, which suggests the occurring of SR under the reaction conditions adopted. It can also be noted that there is still 2% methane in the product stream from the NiP/Ce catalytic system over the entire evaluation process. This can be attributed to a feeble deactivating effect of phosphorous atoms in the nickel phosphide cluster.

Table 3. 2 Average conversions of the three catalytic systems during 8-h ATR of *n*-octane and *n*-octane with naphthalene

Catalyst	ATR of *n*-octane		ATR of *n*-octane with naphthalene (6 wt. %)	
	Average	Error	Average conversion	Error
NiP/Ce	98%	±2%	98%	±3%
Ni/Ce	98%	±3%	98%	±3%
CC	99%	±3%	98%	±2%

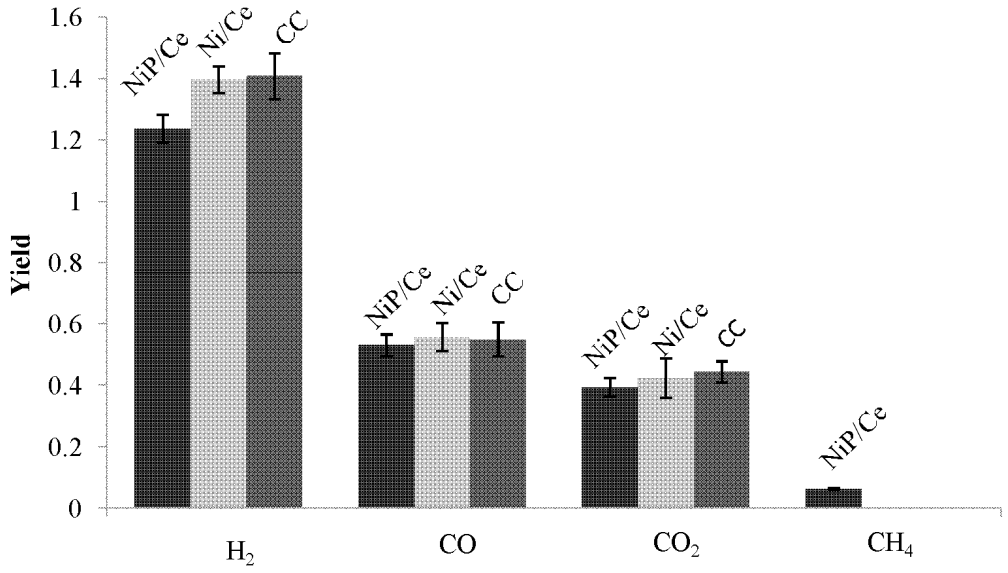

Figure 3. 6 Comparison of the average product yields during 8-hr ATR of *n*-octane in the three catalytic systems (C_8H_{18}=0.04 ml min^{-1}, O_2/C=0.5, H_2O/C=1.7, 900 °C, GHSV=9000 ml hr^{-1} g_{cat}^{-1})

The Ni(P) nodules, deposited by electroless plating on the ceria support, do not display a XRD pattern due to their amorphous identity. Nevertheless, the true catalyst is the crystalline NiP cluster, which is generated from the Ni(P) under the ATR conditions. This can be proved by the XRD diagram of the used catalyst (Figure 3.7). A peak at 44.2 ° is present on the background of CeO_2 pattern (28.6°, 33.1°, 47.5° and 56.4°) [185]. This peak is the strongest one in the XRD pattern of NiP [186]. As for the Ni/Ce catalyst downloaded from the micro reactor, a small peak at 44.5 ° for Ni (111) is found as expected [187]. On the contrary, the amorphous Ni(P) deposit is converted to crystalline NiP grains (~100 nm) with clear periphery after 8 h ATR (Figure 3.8). These NiP grains are also confirmed by EDX. It is worthy of note that there were nil carbon filaments grown on the NiP/Ce catalyst after 8h ATR. On the contrary, short carbon whiskers are found on Ni/Ce catalyst after it is used for ATR under the same conditions (Figure 3.9). The above identification of carbon filaments is further checked by TPO (Figure 3.10). A small oxygen uptake peak arises at about

413 °C on the TPO profile of Ni/Ce catalyst, which can be assigned to the oxidation of carbon. A similar test based on less sensitive thermogravimetric analysis has reported that carbon oxidation takes place at 665K [27]. In contrast to this, the used NiP/Ce catalyst does not show such a TPO peak at the temperature nearby but rather a very weak peak at 303 °C, which is known to be due to oxidation of a part of Ni on the NiP/Ce catalyst according to XPS study. Similarly, Ni/Ce catalyst shows a relatively apparent Ni oxidation peak at 330 °C. The CC catalyst after ATR is also scrutinized by FE-SEM and it demonstrates better carbon deposition resistance than the Ni/Ce catalyst.

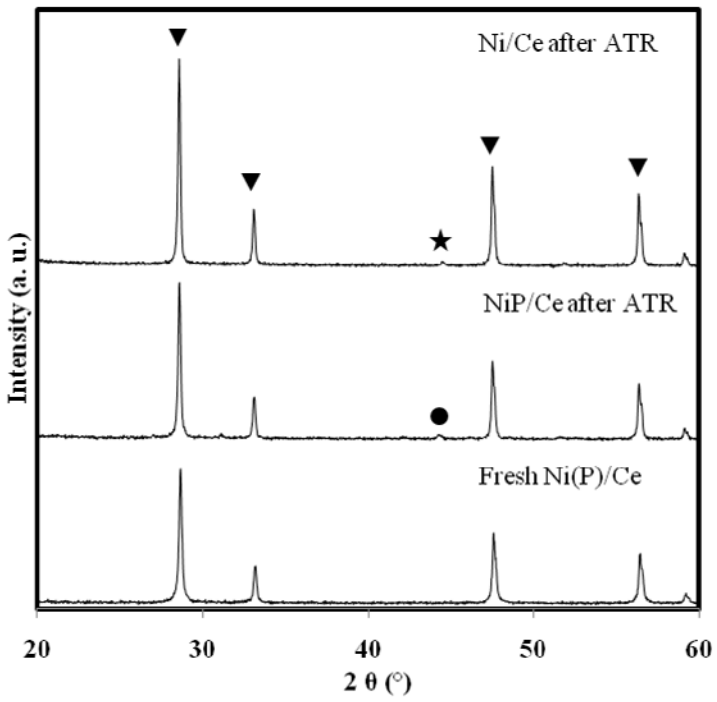

Figure 3. 7 XRD patterns of NiP/Ce before and after ATR, Ni/Ce after ATR ((▼) CeO_2, (●) NiP, (★) Ni)

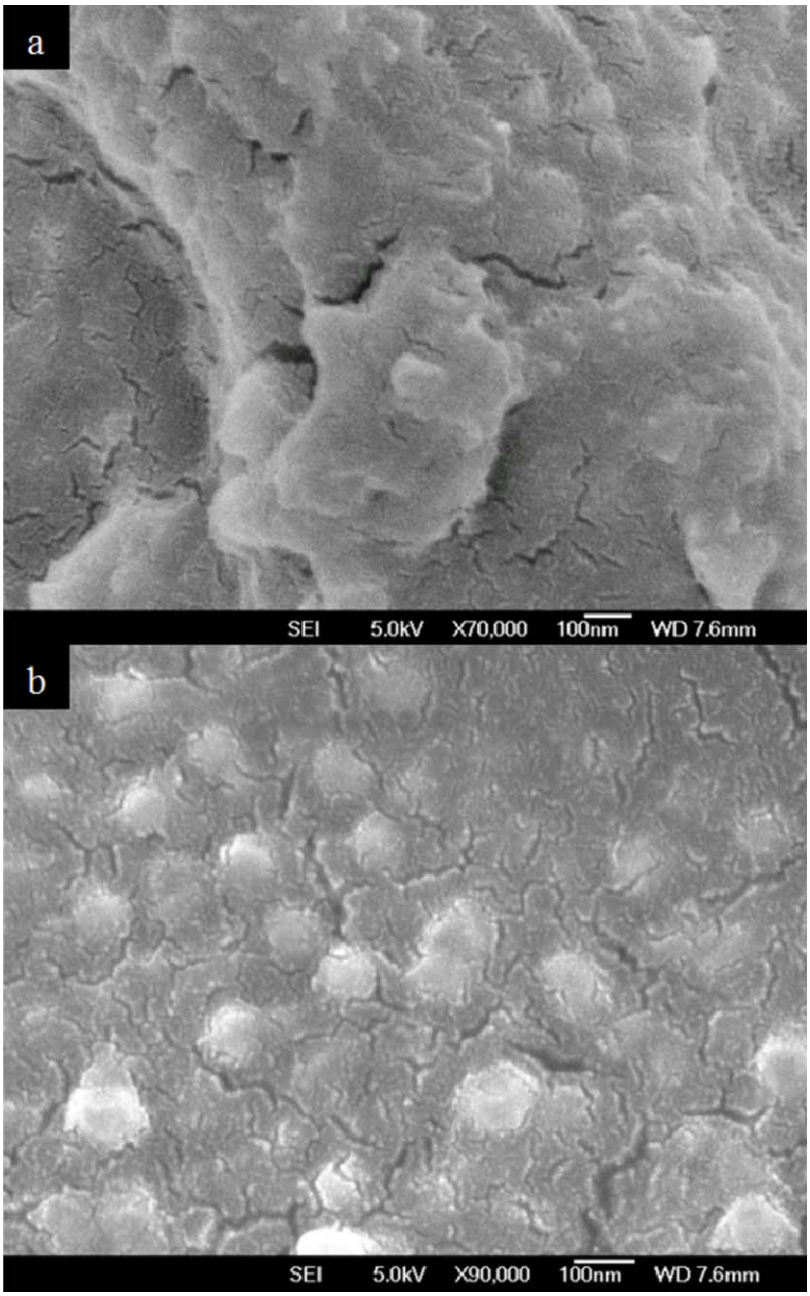

Figure 3. 8 FE-SEM images of (a) the Ni(P)/Ce as electroless deposited and (b) the NiP/Ce after 8-hr ATR of *n*-octane

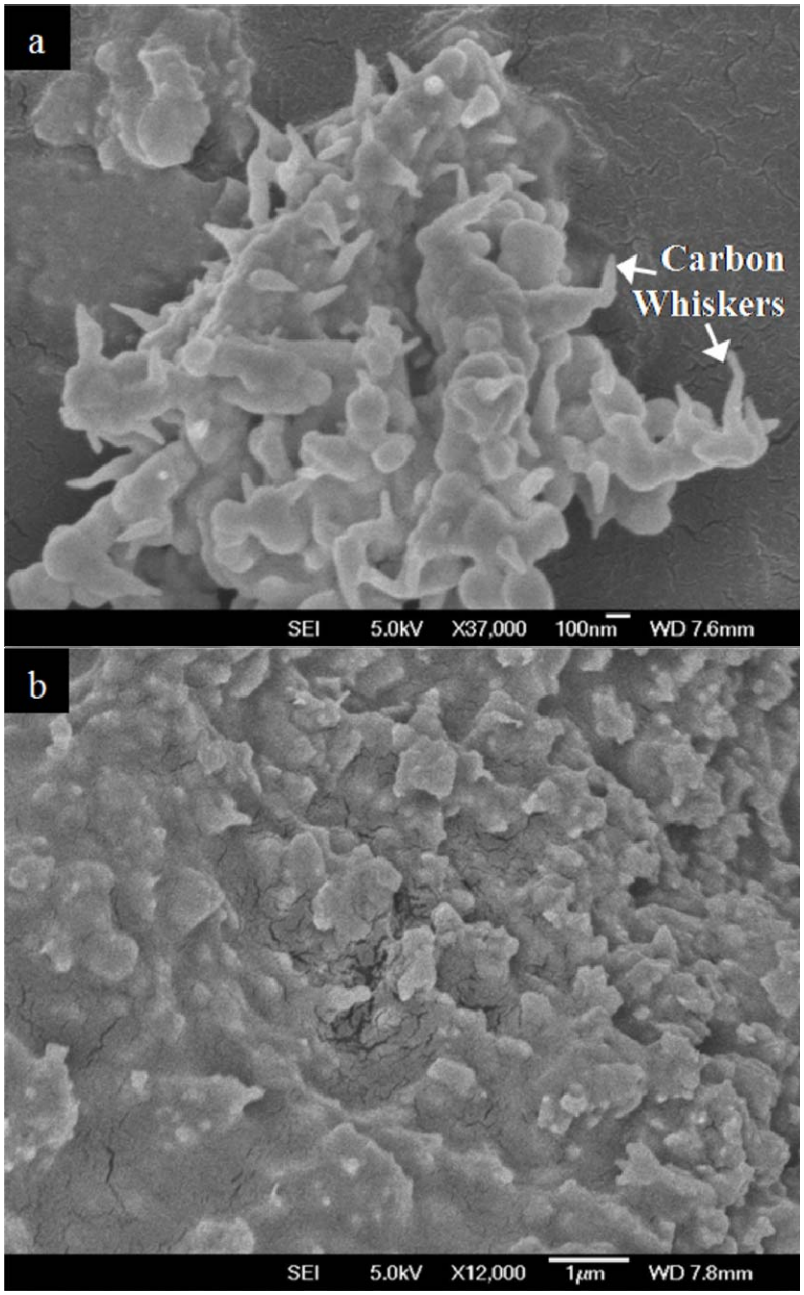

Figure 3. 9 FE-SEM images of the used catalysts: (a) Ni/Ce and (b) CC after 8-hr ATR of *n*-octane as shown in Figure 3.5

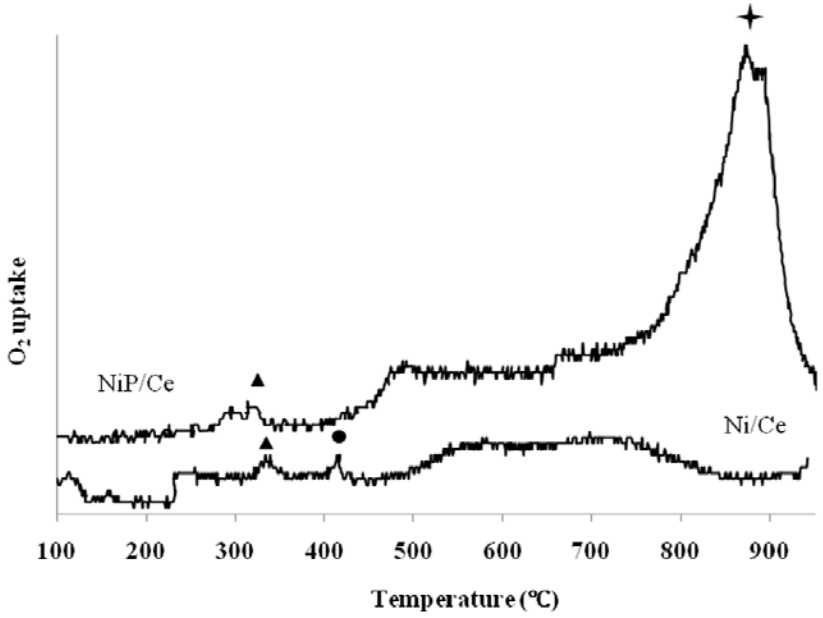

Figure 3. 10 TPO profiles of NiP/Ce and Ni/Ce after 8-hr ATR of *n*-octane

To understand how the P component affects the charge density at Ni before and after ATR, XPS spectra of Ni 2*p* and P 2*p* of the catalyst are investigated (Figure 3.11). The precursor of catalyst, Ni(P)/Ce, shows the Ni 2*p* doublet: ($2p_{3/2}$) peaks at 855.0 eV and 852.6 eV. The former peak is the characteristic peak of Ni^{2+} species, while the latter is the characteristic peak of Ni^0 species. Similarly, the P 2*p* spectrum could be described by the 2*p* doublet: ($2p_{3/2}$) peaks at 133.0 eV and 129.3 eV. The former peak can be assigned to P^{5+} of PO_4^{3-} ions, which are the counterion of Ni^{2+}, presumably due to the presence of the $Ni_3(PO_4)_2$ superficial passivation layer that is left behind by the electroless nickel plating [188, 189]. On the other hand, the $2p_{3/2}$ component at 129.3 eV characterizes P^0 in the Ni(P) amorphous phase [190-192] where the Ni^0 species has been identified by Ni ($2p_{3/2}$) at 852.6 eV.

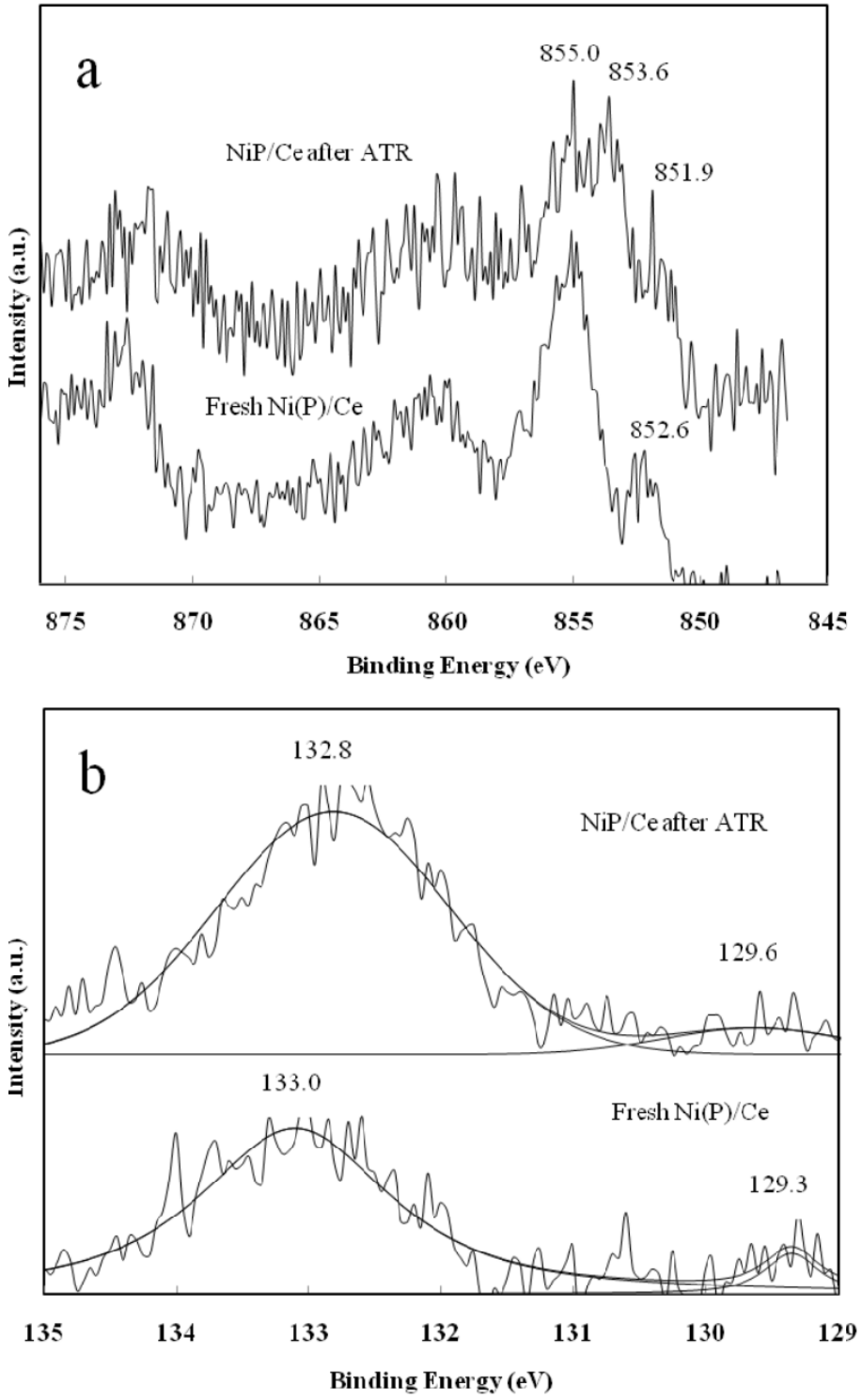

Figure 3. 11 (a) The Ni XPS 2*p* core level spectra and (b) the P XPS 2*p* core level spectra of the NiP/Ce catalyst before and after 8-h ATR respectively

After ATR of *n*-octane at 900 °C for 8h, a new peak at 853.6 eV is found in the Ni $2p_{3/2}$ spectrum. It reflects a Ni species carrying the charge between +2 (855.0 eV) and 0 (852.6 eV) as found above. This Ni species is likely those Ni atoms on NiP crystallites that are partially oxidized. It also deserves to note that the Ni^0 ($2p_{3/2}$) component shifts down by about 0.7 eV to 851.9 eV, which is apparently below the range the reported binding energy of Ni^0 (852.5-852.9 eV) [193]. Correspondingly, the P^0 ($2p_{3/2}$) shifts up by about 0.3 eV to 129.6 eV. This result proposes that the P-Ni bonding in the nickel phosphide cause a slight increase in the electron density at the Ni atom and a slight decrease in electron density at the P atom. It is known that carbon deposition at Ni atoms takes place through thermal cracking of hydrocarbon species. The pristine Ni^0 atomic sites provide suitable Lewis acidity to accept carbon species, leading to the growth of carbon filaments. A slight increase in the electron density at Ni^0 could weaken Lewis acidity of Ni^0.

As far as the effect of ceria support is concerned, we examine the Ce XPS 3*d* spectrum of the used NiP/Ce catalyst (Figure 3.12). The peaks between 875-895 eV correspond to Ce $3d_{5/2}$, between 895-910 eV correspond to Ce $3d_{3/2}$ and the peak at 916 eV is the characteristic satellite peak corresponding to + 4 states [194]. The peak of Ce^{4+} ions at 888.2 eV displayed by the catalyst precursor shifts to 884.9 eV, known as the characteristic peak of Ce^{3+} [194]. This reduction in the valence of Ce induces generation of oxygen vacancies in the ceria support in order to maintain the electrical neutrality in its lattice. Namely, the support is converted to O^{2-}conducting phase from CeO_2. Besides the NiP/Ce catalyst, the oxidation states of Ce in the Ni/Ce catalyst and in a particular control catalyst as well, prepared as an activated ceria, are also checked. This control catalyst is prepared by soaking the ceria, obtained from the sensitization and activation treatment, in the electroless plating solution without nickel nitrate

under the same ENP conditions (temperature and treatment duration) as used to make Ni(P)/Ce. In contrast to the NiP/Ce catalyst, none of Ce^{3+} species is present in the used Ni/Ce catalyst recovered from ATR under the same condition according to its Ce XPS 3*d* spectrum. Xu and co-workers [195] reported that $CePO_4$ is formed in the automotive exhaust catalyst through the reaction of ceria with gaseous H_3PO_4 and other phosphorous compounds. On the contrary, NiP/Ce is a different system, where P forms covalent bond with Ni and hence the P component is unlikely to reduce Ce^{4+} ions, which has been justified by the XPS study. Meanwhile, the control catalyst developed by the blank ENP shows no any phosphorous compound residue as well as Ce^{3+} species. This means that the generation of Ce^{3+} species in the support is not caused by the reduction in the ENP system. It also indicates that Pd is not responsible to the enhanced reducibility of ceria since the preparation of this control catalyst went through the sensitization and activation treatment prior to the test. In the TPR examination of NiP/Ce (Figure 3.2b), the phenomenon of enhancing reducibility of Ce^{4+} by NiP has been verified. Although the true root cause for why the Ce^{3+} species is generated only in the support on which NiP particles but rather Ni particles are overlaid is still not clear, the presence of NiP phase is surely responsible to the reduction of partial Ce^{4+} ions in ceria to Ce^{3+} ions during ATR. In this context, the NiP phase is presumed to mediate the reduction of surface Ce^{4+} ions by the deposited carbon. The O^{2-} ion conducting $Ce^{III}Ce^{IV}_{1-n}O_{2-y}$ phase generated could in turn facilitate gasification of the deposited carbon [120]. Consequently, the fact that NiP/Ce catalyst reveals resistance to coke deposition can be attributed to the two complementary factors: a slight increase in charge density at the Ni atoms and the presence of oxygen vacancies in the ceria support. The presence of Ce^{3+} ions in the ceria support of NiP can be also verified by TPO experiment (Figure 3.10). A rather strong peak happening

at about 870 °C on the TPO diagram of the used NiP/Ce catalyst reflects oxidation of Ce^{3+} ions [196].

Finally it may need to bring up that the Pd colloids employed to initiate electroless nickel plating do not contributes to the reforming. Although only a trace amount of Pd in the NiP/Ce (namely less than 0.3 wt. % Pd of NiP) could be found by ICP-MS, which was performed by dissolving the sample in a nitric acid solution, none of the Pd species can be detected by XPS on NiP/Ce. This is expected since Pd colloids function as seeds for the growth of Ni-P alloy, hence they are quickly covered up by the Ni(P) alloy soon after plating. As a result, these Pd sites are inaccessible despite being catalytically reactive.

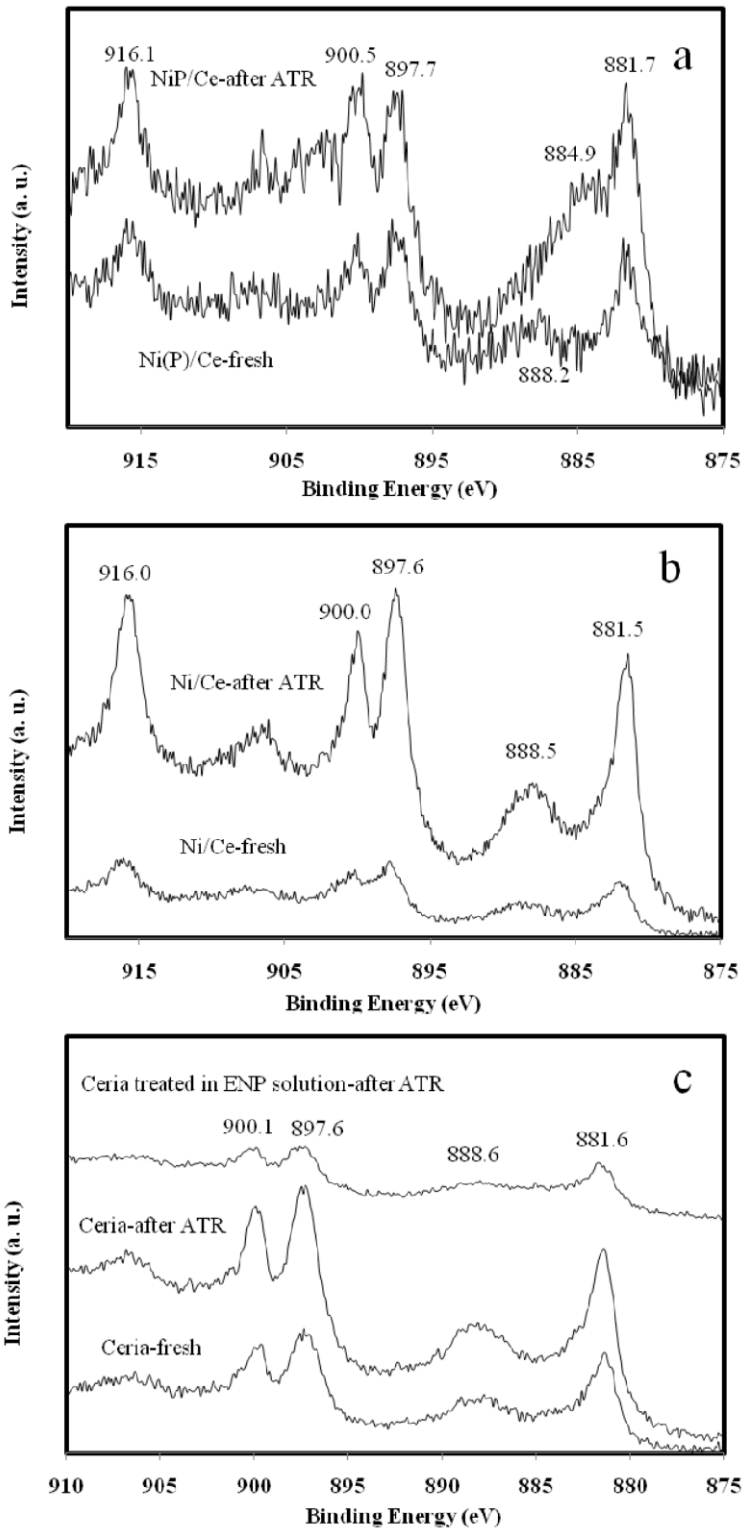

Figure 3. 12 The Ce XPS 3*d* core level spectra of (a) NiP/Ce (b) Ni/Ce catalysts and (c) ceria before and after 8-h ATR of *n*-octane respectively

3.3.3 Evaluation of the catalysts in ATR of n-octane containing naphthalene

Fossil fuels usually contain a certain amount of aromatic compounds which are much more stagnant than alkanes to be reformed and will worsen the coking extent therefore. In this study we selected naphthalene because it is present in gasoline or diesel for improving octane rating [197]. The feed stream of hydrocarbon was made up of 94 wt. % *n*-octane and 6wt. % naphthalene. It has been noted in the preceding discussion that the NiP/Ce and CC catalysts possess better coking resistance than the Ni/Ce catalyst. The inclusion of naphthalene in *n*-octane could thus strengthen the test standard for coking resistance of the NiP/Ce and the CC catalysts.

The conversions of the hydrocarbon stream exhibit insignificant difference over the 8h reaction duration (Table 3.2). In addition, the yields of the four compounds in the product stream over the 8h reaction (Figure 3.13) are slightly different from those presented in Figure 3.6. The CC catalyst still presents a slightly higher H_2 yield than the NiP/Ce catalyst within this reaction period of time, while the Ni/Ce catalyst presents about the same H_2 yield as the NiP/Ce catalyst because the Ni/Ce produces a small amount of CH_4 in this system in contrast to the absence of naphthalene. As estimated, the FE-SEM examination of the spent catalysts (Figure 3.14) reveals carbon filaments deposition not only on Ni/Ce catalyst but also on the CC catalyst in this case. Clearly, the CC catalyst becomes vulnerable to reform naphthalene. Unlike the two references, the NiP/Ce catalyst still remained free of coking under the same ATR conditions.

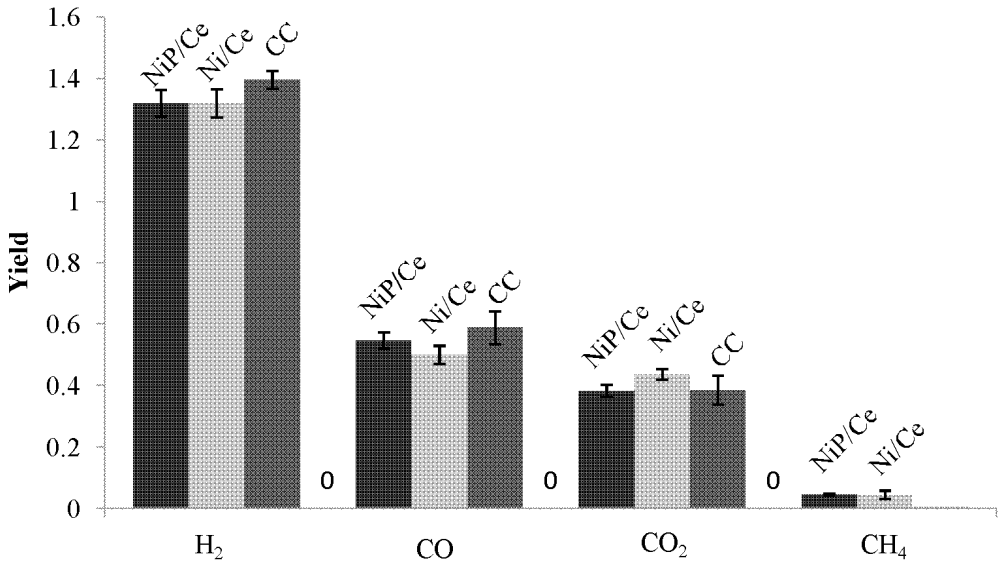

Figure 3. 13 Comparison of the average product yields during 8-h ATR of *n*-octane containing 6 wt. % naphthalene in three catalytic systems (C_8H_{18}=0.04 ml min^{-1}, O_2/C=0.5, H_2O/C=1.7, 900 °C, GHSV=9000 ml hr^{-1} g_{cat}^{-1})

The Ni 2*p*, P 2*p* and Ce 3*d* XPS spectra of NiP/Ce and Ni/Ce catalysts down loaded from this relatively tougher reforming system were examined as well. Similar to the previous finding, an enhancement of electron density at Ni and the occurrence of Ce^{3+} species are also found in the used NiP/Ce catalyst. Especially in the Ce 3*d* spectra, the peak at 885.0 eV for Ce^{3+} is stronger than that in Figure 3.12; and another strong peak at 903.4 eV which is also characteristic for Ce^{3+} species can be found. In line with the rationale described above, we are inclined to deem that a stronger coking extent due to the presence of naphthalene enhanced reduction of Ce^{4+} ions under the mediation role of the NiP catalytic sites.

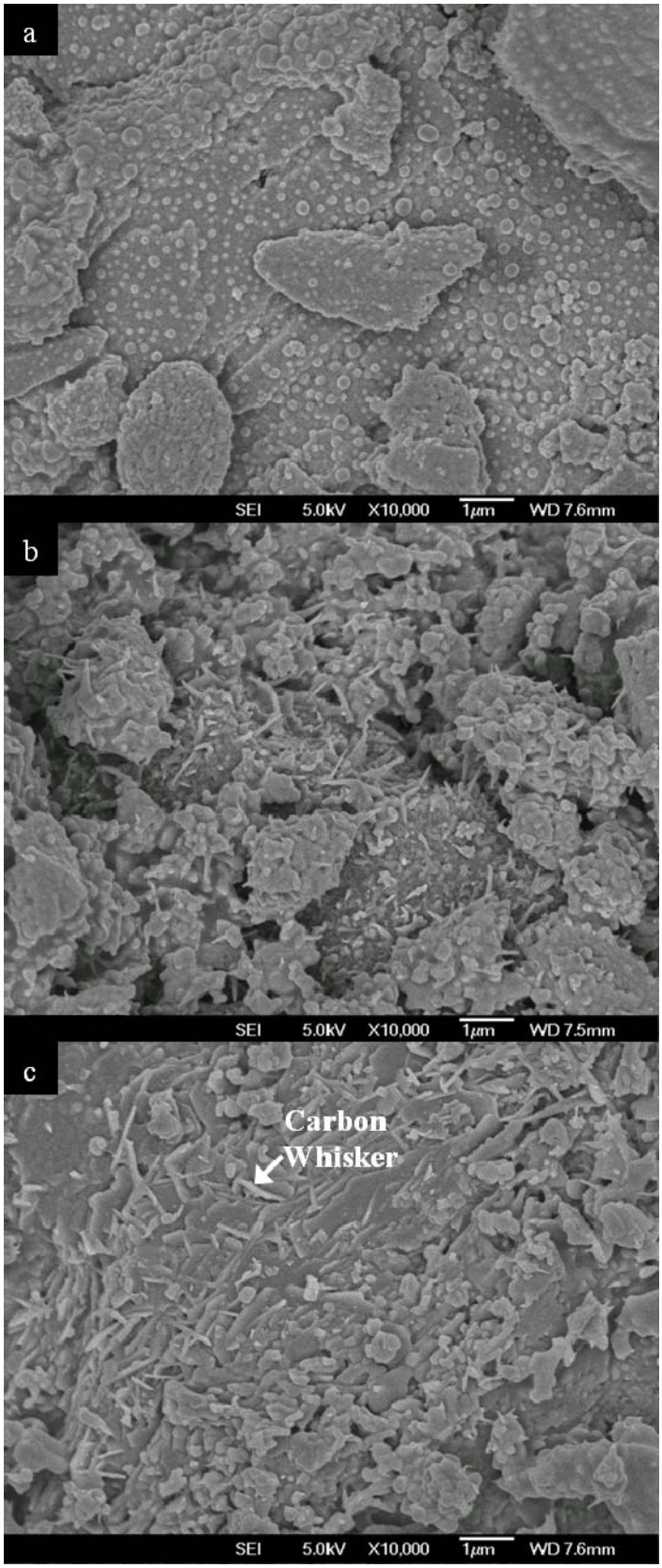

Figure 3. 14 FE-SEM images of (a) NiP/Ce, (b) Ni/Ce, and (c) CC catalysts after 8-h ATR of *n*-octane with 6 wt. % naphthalene

3.4 Conclusions

The electroless deposition of nickel phosphorus alloy, Ni(P), nodules (~100nm) on ceria particles of several microns in size is achieved. The ceria-supported Ni(P) is used to catalyze the autothermal reforming (ATR) of *n*-octane and *n*-octane-naphthalene (6 wt. %) mixture, respectively. The impregnated Ni/Ce catalyst and a nickel-based commercial steam reforming catalyst (CC) are employed as the control catalysts. The ATR is carried out under the conditions comprising O_2/C ratio (=0.5), H_2O/C ratio (=1.7), GHSV=9000 ml hr^{-1} g_{cat}^{-1}, hydrocarbon= 0.04 ml min^{-1}, and at the reaction temperature of 900 °C. The amorphous Ni(P) alloy was converted to the crystalline nickel phosphide Ni_xP_y (x/y ≈ 3.7 by mole) in-situ under the ATR conditions, which is named as NiP/Ce for simplicity. The XPS analysis shows that there is a slight increase in charge density at the Ni atoms in NiP/Ce compared to that in Ni/Ce. Besides this, the surface of ceria support is changed to an O^{2-}-conducting $Ce^{III}Ce^{IV}_{1-n}O_{2-y}$ phase by ATR, but it does not happen in the Ni/Ce catalyst. The enhanced reducibility of ceria in NiP/Ce catalyst is supported by the TPR test. Such variations in charge allocation and doping state render the NiP/Ce catalyst resistance against coking, but the two control catalysts are prone to coking, especially in the ATR of the *n*-octane-naphthalene (6 wt. %) mixture, over an arbitrarily set reaction duration of 8h. It is supposed that the NiP nano grains, the catalytic sites, facilitate the reduction of those Ce^{4+} ions located over the surface of support by the deposited coke to form Ce^{3+} ions. Accompanying the formation of Ce^{3+}, the oxygen vacancies are induced in the ceria support.

CHAPTER 4

INTERACTIONS BETWEEN CeO_2 AND Ni_XP_Y FOR ENHANCING COKING AND SULFUR RESISTANCE IN AUTOTHERMAL REFORMING OF LIQUID HYDROCARBONS

4.1 Introduction

Performing catalytic reforming of diesel oil on board is an effective way to explore hydrogen energy source. It has been known that presence of heavy hydrocarbons, aromatics and sulfur (H_2S and organosulfides or thiols) in diesel fuel is to deteriorate the reforming catalyst, such as the commercial SR catalysts designed for partial oxidation of natural gas will be unable to sustain the desired fuel conversion and hydrogen selectivity over a long run. This is because the catalysts lack adequate resistance against carbon deposition and sulfur adsorption. Therefore deactivation of catalyst becomes the major obstacle to the realization of ATR of diesel fuel on a large scale [14, 177, 198, 199].

To date this problem has been tackled by chemical modifying the catalyst support or the Ni active sites. The former way is often attained through introduction of alkaline earth metal oxides and rare earth oxides into the alumina support or substitution of alumina by these two groups of oxide [40, 47, 93, 200]. Of the several popular rare earth oxides, ceria demonstrates unique performance because it is an oxygen electrolyte when doped and can hence supply lattice oxygen ions to participate in the reforming. Gd-doped ceria is usually preferred since it shows

significantly improved thermal stability compared with the pristine ceria [150]. The second way stated above has been often realized through incorporation of a low dose of precious metal into the Ni^0 active site [27, 59, 82, 107]. With the exception of noble metals, other metal elements like Co, Cr, Cu or Mo are also used to promote both activity and stability of the supported Ni catalysts [196, 201-203].

To advance the concept of intermetallic catalyst, we focused on exploring nickel phosphide (Ni_xP_y) crystallite as catalyst. It was synthesized through calcining amorphous nickel phosphorous alloy Ni(P) obtained from electroless nickel plating [186]. As Ni_xP_y crystallite is formed by polar covalent bonding, it must have different chemical properties from Ni^0 crystallite in the catalytic reforming of hydrocarbons. This viewpoint has been verified in the ATR of a mixture of *n*-octane and naphthalene (6 wt%) [204]. The Ni_xP_y/CeO_2 catalyst will be expressed by the short form NiP/Ce in the following sections. The catalyst possesses two special structural characteristics: Ni atom carries a small amount of negative charge in contrast to the pristine Ni^0 and the presence of stable Ce^{3+} species in the CeO_2 support. It has been known that although CeO_2 can be reduced to Ce_2O_3, the reversed process readily happens in the presence of oxygen. Hence, the nickel phosphide species is deemed to play a role in stabilizing Ce^{3+} species. The two structural characteristics described above contribute to not only catalytic activity and H_2 selectivity of the ATR of liquid hydrocarbons but also to coking resistance as indicated by the experimental data. In this work, we examined the two supported NiP catalysts, NiP/Ce and NiP/CGO (Gd:Ce =1:9 by mole), by using the ATR of a heavier surrogate fuel oil comprising of *n*-dodecane, naphthalene (10 wt%) and thiophene (100 ppm S). The loss of the conversion of fuel and the yield of reformates caused by introducing naphthalene and thiophene into *n*-dodecane was studied. These two catalysts displayed limited difference in fuel conversion and

hydrogen selectivity within the given duration of ATR, but the NiP/CGO catalyst displayed obviously vulnerable coking resistance than the NiP/Ce catalyst. The superiority of NiP/Ce is attributed to a higher Ce^{3+} concentration in its support detected by experiment. The Ni-based commercial SR catalyst was adopted as benchmark for the investigation.

4.2 Experimental

4.2.1 Materials

Cerium nitrate hexahydrate (Sigma Aldrich, >98%), gadolinium nitrate hexahydrate (Sigma Aldrich, >98%), nickel nitrate hexahydrate (Sigma Aldrich, >98%), glycine (Sigma Aldrich, >99%), citric acid (Sigma Aldrich, >99%), ethylene glycol (Merck, >98%), stannous chloride (Sigma Aldrich, >98%), palladium chloride (Sigma Aldrich, >98%), hydrochloric acid (Merck, 37%), sodium hypophosphite (Merck, >98%), DL-malic acid (Merck, >98%), Sodium acetate (Merck, >98%), lactic acid (Merck, >98%), borax (Merck, >98%), lead acetate (Sigma Aldrich, >98%), *n*-dodecane (Sigma Aldrich, >99%), thiophene (Merck, >99%), and naphthalene (Sigma Aldrich, >99%) were all used as received. A nickel-based SR commercial catalyst (Alfa Aesar, HiFUEL^{TM} R-110) was used as benchmark.

4.2.2 Catalyst preparation

4.2.2.1 Preparation of support via Pechini method

Both ceria supports were synthesized using the Pechini method [205]. All chemicals used here were AR grade. Firstly, an aqueous solution containing $Ce(NO)_3 \cdot 6H_2O$, glycine and citric acid was prepared, in which the molar ratio of metal ions to all the functional groups (-NH_2 and –COOH) was maintained at 0.154 and the ratio of citric acid to glycine by mass was 0.129. The concentration of the solutes was approximately 20 % by mass. As to the preparation of Gd-doped ceria, the required amount of $Gd(NO_3)_3 \cdot 6H_2O$ was introduced into the above solution. The resulting aqueous solution was then mixed with 0.8 portion of ethylene glycol by volume. The mixture was thickened on a hot plate at 200 °C under stirring and a gel was obtained in the end of evaporation. The gel was then subjected to pyrolysis at 400 °C for 2 h and calcination at 600 °C for another 2 h to remove carbon residues and to allow for the growth of crystal phase.

4.2.2.2 Preparation of catalysts via ENP process

The cerium (IV) oxide powder obtained was then sensitized in an aqueous solution containing 20 g L^{-1} stannous chloride ($SnCl_2 \cdot 2H_2O$) and 20 mL L^{-1} hydrochloric acid (37 wt%) under stirring for 30 min at room temperature. The sensitized oxide was rinsed with deionized (DI) water subsequently. Then the oxide was activated through soaking in an aqueous solution containing 0.3 g L^{-1} palladium chloride ($PdCl_2 \cdot 2H_2O$) and 10 mL L^{-1} hydrochloric acid (37%) under stirring for 10 min at room temperature. After that, the oxide was washed in DI water by agitation and filtrated for several times, which was followed by vacuum drying the oxide

powder at 50 °C. A certain amount of the activated ceria was dispersed in a pre-formulated nickel plating solution at 80 °C for 30 min under stirring. After plating, the powder was washed thoroughly with DI water and dried at 50 °C in vacuum. The resulting pre-catalyst powder was pressed into pellets and then crushed and sieved. Particles with 0.5-1 mm sizes were used. The two supported Ni-P alloy pre-catalysts obtained through this preparation are denoted as Ni(P)/Ce and Ni(P)/CGO respectively.

A nickel-based SR commercial catalyst (Ni loading: 15-40 wt%; denoted by CC) was also adopted as benchmark. The catalyst was designed to obtain H_2 from reforming fuel for fuel cell application. The commercial catalyst was also crushed to 0.5-1 mm granules for evaluation.

4.2.3 Catalyst characterization

The compositions of the synthesized catalysts were determined by Inductively Coupled Plasma-Mass Spectrometry (ICP-MS, Agilent 7500 Series). The content of palladium was less than 0.3 wt%. The specific surface areas of the samples were gauged on a surface area and pore size analyzer (Autosorb-1 Quantachrome) by applying the multi-point BET method after degassing at 300 °C for 3 h under N_2 purging. The temperature-programmed reduction (TPR) was conducted on the same instrument using a sample of 50 mg and a gas (5% H_2 in N_2) flow rate of 80 mL min^{-1}. The heating rate was set at 10 °C min^{-1}. The crystalline structures of catalysts were determined by X-ray diffractometry (XRD, SHIMADZU XRD-6000, Cu Kα radiation) using a scanning rate of 5 ° min^{-1}. The coking degree on the used catalysts was determined using thermogravimetric analysis (TGA) on a thermal analyzer (DTG-60AH, Shimadzu) over a temperature range from 50 to 800 °C with a heating rate of

10 °C min^{-1} and under air purge of 100 ml min^{-1}. The oxidation states of Ce ions in the ceria support were determined by X-ray photoelectron spectroscopy (XPS, Kratos Axis HiS System equipped with Al *Kα* X-ray source, 1486.6 eV). A take-off angle of 90° with pass energy of 40 eV was set and C1s (284.6 eV) used as the internal reference to determine biding energies of different peaks.

4.2.4 Experimental setup and reaction conditions

Approximately 1g catalyst (0.5-1 mm particles) was packed between two plugs of quartz wool in the centre of a quartz tube reactor (1.2 cm o.d., 1 cm i.d. and 40 cm long). The micro plug flow reactor (PFR) was then placed in a thermostat-controlled vertical tube furnace. The synthetic air (O_2/N_2) and nitrogen mixture were metered into the reactor by a mass flow controller (Alicat). The fuel (*n*-dodecane) and water streams were regulated respectively by ISO-2000 isocratic pumps and sent to combine with the synthetic air stream. The feed stream (air, fuel, and water) was led to a mixer to carry out vaporization and then to the PFR. The temperature of the mixer was set at 250 °C and a dry run in the absence of catalyst indicated that the fuel was not pyrolyzed in the mixer. The optimal reforming conditions comprising of the following parameters: fuel-supply rate = 0.02 ml min^{-1}, oxygen and steam supply rates: $O_2/C=0.5$ and $H_2O/C=3$, to reforming temperature 750 °C, and GHSV = 10,000 h^{-1}. Specifically, the PFR loaded with catalyst was heated to 750 °C under a N_2 flow, which was then switched to a flow of super heated steam passing through the mixer with the aim of fixing particle packing of catalyst bed. The PFR was held under this condition for 1 h before the fuel was directed to the reactor. The outlet stream was connected to Shimadzu GC after passing a cold trap to knock out condensable components if any. After reaction, the inlet stream was switched to nitrogen to protect

the catalyst under N_2 until the PFR was cooled down to room temperature. The performance of the catalyst was assessed by fuel conversion, distribution of product gases and their yields, which were computed using the following equations where nitrogen in the synthetic air was used as internal standard:

$$\text{Conversion} = \frac{F_{total}(y_{CO} + y_{CO_2} + y_{CH_4})}{F_C \text{ in fuel}} \qquad (4.1)$$

$$\text{Yield} = \frac{F_{total} y_p}{F_p \text{ in fuel}} \qquad (4.2)$$

$$F_{total} = \frac{F_{N_2} \text{ in feed}}{y_{N_2}} \qquad (4.3)$$

where F stands for molar flow rate in mol s^{-1} and *y* the mole fraction of a component p (subscript) in the gas outlet stream. Theoretically, the conversion should be determined from the amount of dodecane at the exit of reactor with respect to that at the entry of reactor. However, the fuel conversion is determined using Eq. 1 due to the limitation of analyzing the trace amounts of gaseous hydrocarbons such as methane and ethylene as well as the difficulty of quantifying a small amount of fuel trapped in the water condensation process [28]. In addition to the use of pure *n*-dodecane, the surrogate fuel containing 90 wt % *n*-dodecane, 10wt% naphthalene and 100 ppm S was also formulated to test the coke and sulfur tolerance of the catalysts.

4.3 Results and discussion

4.3.1 Surface area and crystalline structural features of the catalysts

Both Ce (the short form of CeO_2) and CGO synthesized in-house were calcined at 600 °C despite being below the ATR temperature because the resulting oxides must reserve a large enough surface area (Table 4.1) for the subsequent electroless deposition. The successive electroless deposition produced Ni(P) alloy grains on both supports and caused decreases in surface area. The CGO support experienced a greater reduction in surface area than the Ce support after deposition of Ni(P). This can be ascribed to the CGO support as it exhibits a lower energy surface than the Ce support. Such difference was observed when we did the pre-activation treatment for the electroless deposition of Ni(P). A longer activation time or the use of a more concentrated activation solution was required for treating CGO in order to achieve a similar loading of Ni(P) to those that were attained on the Ce support. Doping ceria by Gd(III) results in smaller crystallites [206] which likely constitute a close-packed surface microstructure. Our study also observed different microstructures on the CGO and Ce supports, respectively (Figure 4.1). In addition, the microstructures of the two Ni(P)–deposited particles (Figure 4.2) showed rather different topologies: the Ni(P) alloy grains on the Ce support are more extensively spread, which was the result of the attainment of a higher concentration and more uniform distribution of Pd clusters introduced from the activation step. Whereas poorer wetting of Ni(P) on CGO, relative to that on the Ce support, is responsible to the deposition of agglomerated Ni(P) nodules because tiny Ni(P) particles would dropped off CGO during plating [155] and redeposit back to CGO after growth in the plating solution through aggregation. This random attachment of Ni(P) nodules and

the afterward electroless metal deposition on them brought about a larger decrease in BET surface area from the magnitude CGO owned originally.

Table 4. 1 BET specific surface area and compositions of the supports and fresh catalysts

Sample	BET surface area (m^2/g)		Composition	
	fresh	used	Ni (wt %)	P (wt %)
CeO_2	88	/	/	/
$Gd_{0.1}Ce_{0.9}O_x$ (CGO)	90	/	/	/
NiP/Ce	80	34	15	2
NiP/CGO	65	25	15	2

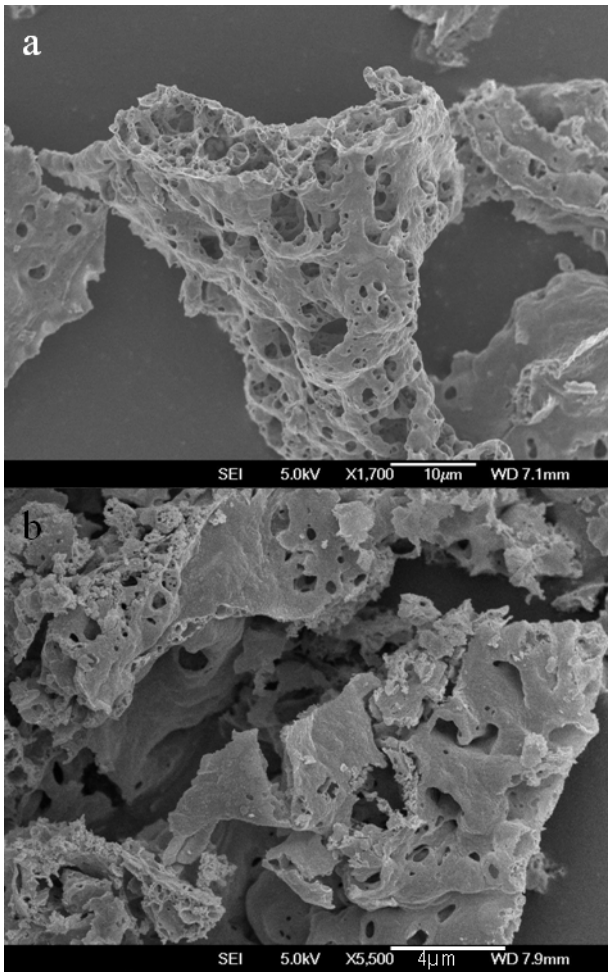

Figure 4. 1 FE-SEM images of (a) ceria support and (b) CGO support after calcination at 600 °C for 2 h

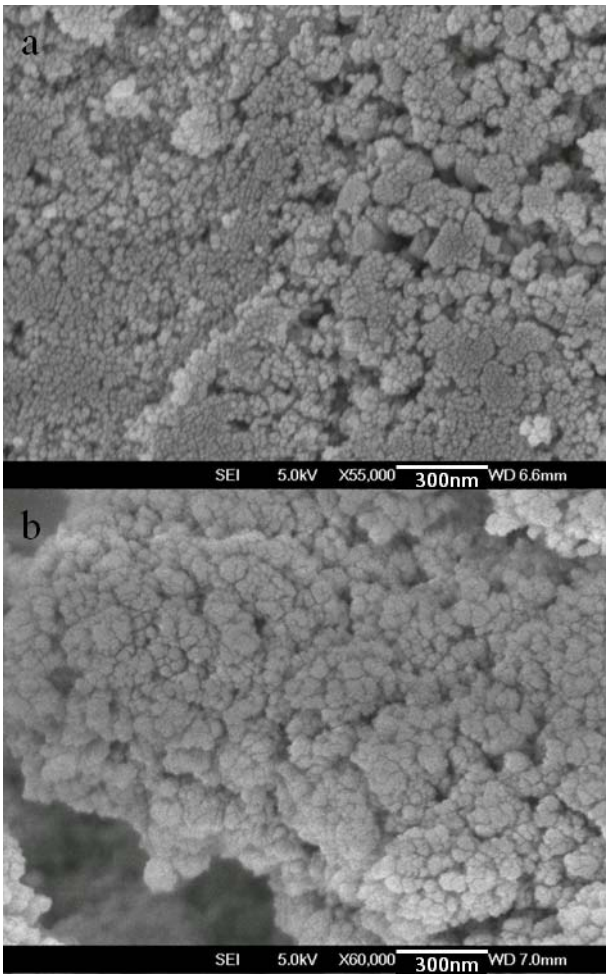

Figure 4. 2 FE-SEM images of (a) Ni(P)/Ce and (b) Ni(P)/CGO

The Ni(P) formed on both CGO and Ce have amorphous phase (*a* and *c* in Figure 4.3) on the background of CeO_2 crystal that possesses a fluorite-like structure (with $2\theta = 28.6°$, 33.1°, 47.5° and 56.4°) [94]. The ratio of Ni to P by weight is ca. 7.5 according to ICP analysis. The amorphous Ni(P) can be in situ converted to crystalline Ni_xP_y (i.e. NiP in short form), the active catalytic site, under the ATR conditions. The used catalysts, NiP/Ce and NiP/CGO, were down loaded from the micro-PFR after 24 h ATR of the fuel (comprising of 90 wt% *n*-dodecane, 10 wt% naphthalene and 100 ppm sulfur). They displayed characteristic XRD peak of NiP at 44.2° (b and d in Figure 4.3) [207]. A small peak appearing at 31.2 ° in these two diagrams can be attributed to $Ni(PO_3)_2$ generated from partial oxidation of NiP [188].

In addition, a drastic decrease in surface area in either used catalyst was also observed (Table 4.1) indicating further sintering of the supports at the ATP temperature higher than the calcination temperature used to prepare the two supports.

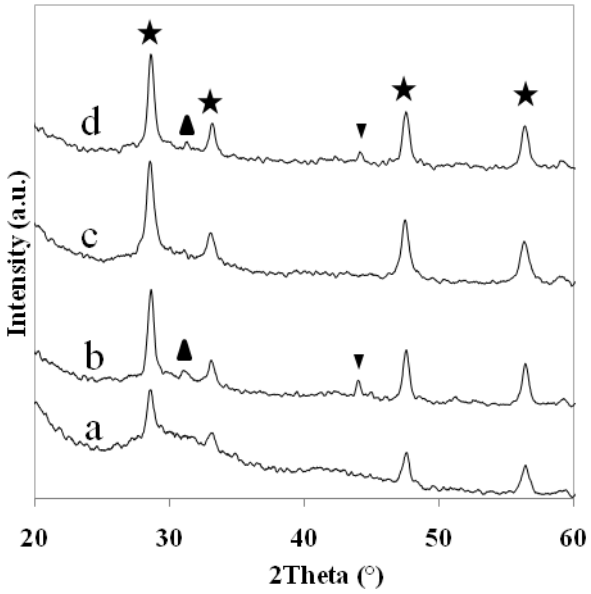

Figure 4. 3 XRD patterns of (a) Ni(P)/Ce, (b) the used NiP/Ce catalyst, (c) Ni(P)/CGO and (d) the used NiP/CGO catalyst (▼: NiP; ★: CeO_2; ♟: $Ni(PO_3)_2$)

4.3.2 H_2-TPR of the supports and catalyst precursors

The H_2-TPR profiles of the supports and catalyst precursors are shown in Figure 4.4. The TPR profile of the Ce support shows two small reduction peaks centered at around 480 °C and 780 °C respectively due to the reduction of surface and lattice Ce^{4+} ions [129]. Compared with the TPR of Ce, the first reduction peak of CGO displays at a slight higher temperature and the second reduction peak becomes weaker. This difference suggests that Gd(III) doping makes the reduction of Ce^{4+} more difficult. Regarding the precursor for the NiP/Ce catalyst, its TPR profile consists of four peaks. The first two peaks centered at 200 °C and at 300 °C could be assigned to the reduction of Ni^{2+} ions in the passivation layer on Ni(P) granules. The Ni(P) bulk is irreducible as the oxidation states of both types of atoms are close to

zero. The rest two peaks emerging at ca. 460 °C and 720 °C are known to come from reduction of the ceria support. However, it is noteworthy that the surface Ce^{4+} reduction peak shifts downward by ca. 30 °C, indicating an enhanced reducibility of ceria owing to the presence of the overlaid nickel phosphide. Similarly, the TPR profile of the precursor of the NiP/CGO catalyst shows four corresponding reduction peaks as well but the amount of surface Ni^{2+} species is apparently less than its counterpart on Ce. This suggests a dense external surface area of the Ni(P) grains, which is in accord with the dense aggregate structure the Ni(P) granules revealed on CGO. In addition, the reduction of surface Ce^{4+} becomes very feeble, implying that the Gd^{3+} ions in CGO lattice might retard chemical reduction of Ce^{4+}.

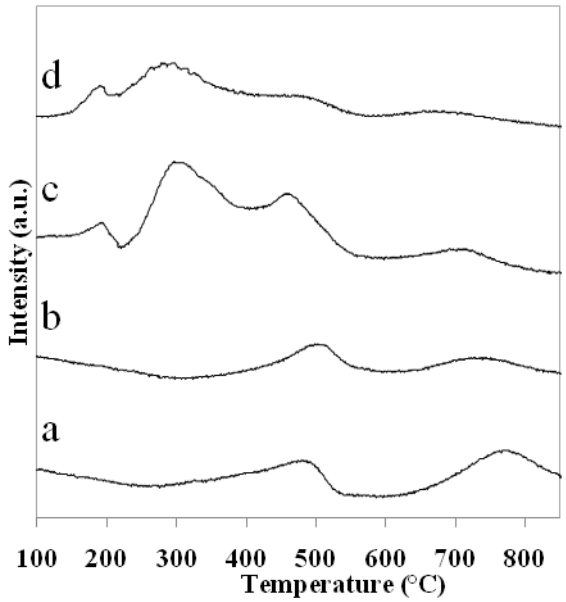

Figure 4. 4 TPR profiles of (a) CeO_2, (b) CGO, (c) Ni(P)/Ce and (d) Ni(P)/CGO

4.3.3 The XPS evidence of surface Ce^{3+}species in NiP catalysts

From the above H_2-TPR investigation, the Ce support displayed different degrees of surface reducibility. To verify this result, the Ce 3*d* XPS spectra of the catalysts NiP/Ce and NiP/CGO before and after use were examined. Indeed, both the used catalysts showed different surface concentrations of Ce^{3+} ions (Figure 4.5). It is known that the peaks from 875-895 eV correspond to Ce $3d_{5/2}$, from 895-910 eV correspond to Ce $3d_{3/2}$, and the peak at 916 eV is the characteristic satellite peak corresponding to +4 state [194]. For the two precursors, i.e. Ni(P)/Ce and Ni(P)/CGO, only the characteristic peaks of Ce $^{4+}$ ions are present. On the contrary, two new shoulder peaks at 885.2 eV and 903.8 eV that characterize Ce^{3+} ions arise in the spectra of the used catalysts NiP/Ce and NiP/CGO, which are in situ generated under the ATR conditions from their respective precursors. Furthermore, the Ce^{3+} peak is obviously stronger in the spectrum of NiP/Ce than in that of NiP/CGO, which follows the same order as those exhibited by the H_2-TPR profiles (Figure 4.4). It is worthy of note that the Pd(0) nuclei, initially deposited to these two supports for initiating electroless plating, did not contribute to catalyzing ATR of the fuel since they were covered by Ni(P) and then NiP according to the mechanism of electroless nickel plating. The XPS spectra of the catalysts also showed no fingerprint of Pd species.

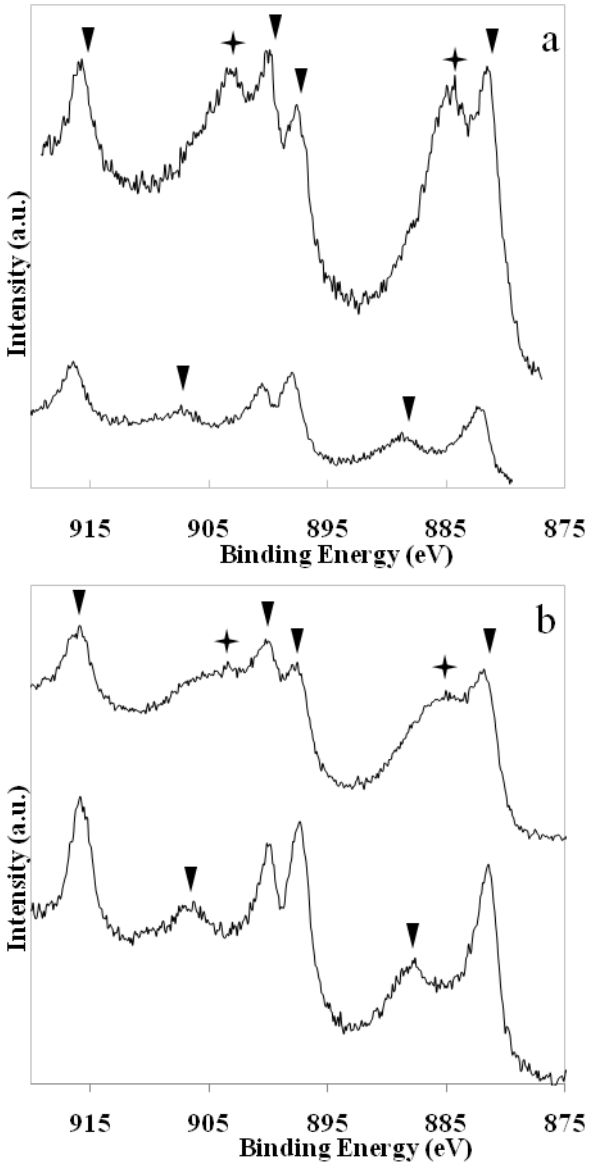

Figure 4. 5 The Ce XPS 3*d* core level spectra of (a) the used NiP/Ce (top) and Ni(P)/Ce (bottom), (b) the used NiP/CGO (top) and Ni(P)/CGO (bottom) (▾: Ce^{4+}; +: Ce^{3+})

4.3.4 Investigation of the tolerance of catalyst to aromatic compounds

The two synthesized nickel phosphide catalysts and the control catalyst (CC) were assessed for ATR activity of *n*-dodecane (fuel) with time (Figure 4.6). The CC shows an almost quantitative fuel conversion whereas both NiP/Ce and NiP/CGO present slightly lower and similar values. With respect to the yields of ATR products, the CC achieves about a higher H_2 yield by 20% and a higher CO yield by 5% than the two

NiP-supported catalysts. This is deemed to be the stronger SR tendency of the CC. The three product streams also contain CO_2 that comes from mainly the water-gas shift (WGS) because a sub-stoichiometric amount of oxygen (O_2/C=0.5) cannot support combustion at a large extent. Figure 6c reveals very similar CO_2 yields from the three catalysts. It is conceivable that the CeO_2 in the two synthesized catalysts promotes WGS despite the relatively lower fuel conversion of them compared with the CC in which the support contains alumina as the main ingredient. It has been checked that either CeO_2 or CGO support alone contributes about 50% conversion of fuel. This conversion was reported to go through a mixture of POX, combustion, and hydrocarbon cracking that produce mainly CO and CO_2 gases and C1-C4 species but low H_2 yields [208]. The presence of NiP on the two supports largely boosts the conversion of fuel since NiP acts as the reactive site for both POX and SR.

As aromatic compounds are much more stable than normal alkanes to thermal cracking on Ni(0) reactive site, the above three catalysts were further evaluated in the ATR of a fuel composed of *n*-dodecane and naphthalene (Figure 4.7). The CC exhibits the lowest catalytic activity of the three catalysts notably after 20 h. Compared with the above system, this inversion of catalytic activity sequence reflects the role of CeO_2 that supplies smaller hydrocarbon fragments (C1-C4) for ATR on the NiP catalytic site. Hence both NiP/Ce and NiP/CGO present not only higher conversions but also higher yields of H_2 than the CC system. On the other hand, the CC presented a CO yield not only greater than the other two catalysts but also higher than even the catalyst itself when the fuel was *n*-dodecane alone as shown in Figure 4.6d. This phenomenon can be attributed to reforming of CO_2 by carbon produced from thermal cracking because the CO_2 yield showed a decreasing slope correspondingly with proceeding of ATR in the CC system. This means a severe

coking happened on the CC and the coke further reformed CO_2 produced from combustion of the hydrocarbons and WSR. It can be noted that the CC lost activity clearly since the 20th hour of reaction and so did the H_2 and CO yields. This coincidence supports deactivation of the CC due to coking, which covers Ni(0) reactive sites, represses thermal cracking, and in turn weakens POX and SR. In contrast to the CC, the NiP/Ce and NiP/CGO catalysts showed milder loss of activity over the 30 h evaluation period. Correspondingly, the H_2 yields obtained from them decreased much less than that from the CC.

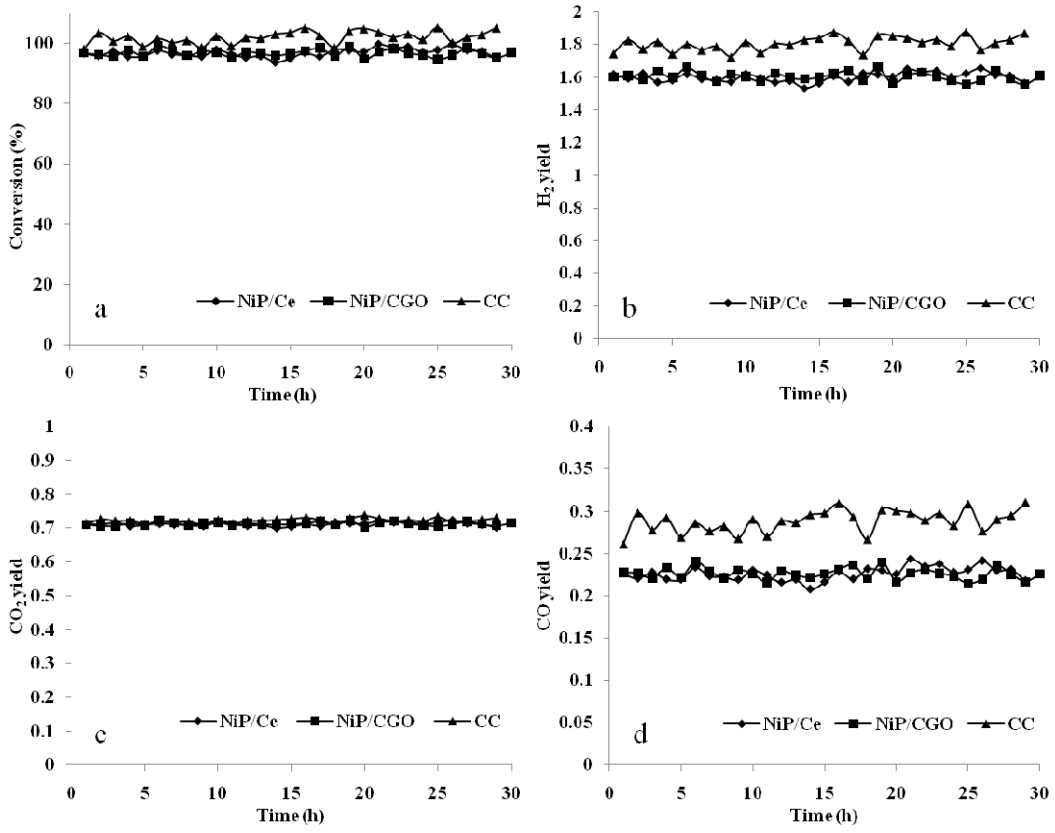

Figure 4. 6 Conversions and product yields vs time on stream of *n*-dodecane autothermal reforming over carious catalysts ($C_{12}H_{26}$=0.02 ml min^{-1}, O_2/C=0.5, H_2O/C=3, 750 °C, GHSV=10 000 ml hr^{-1} g_{cat}^{-1})

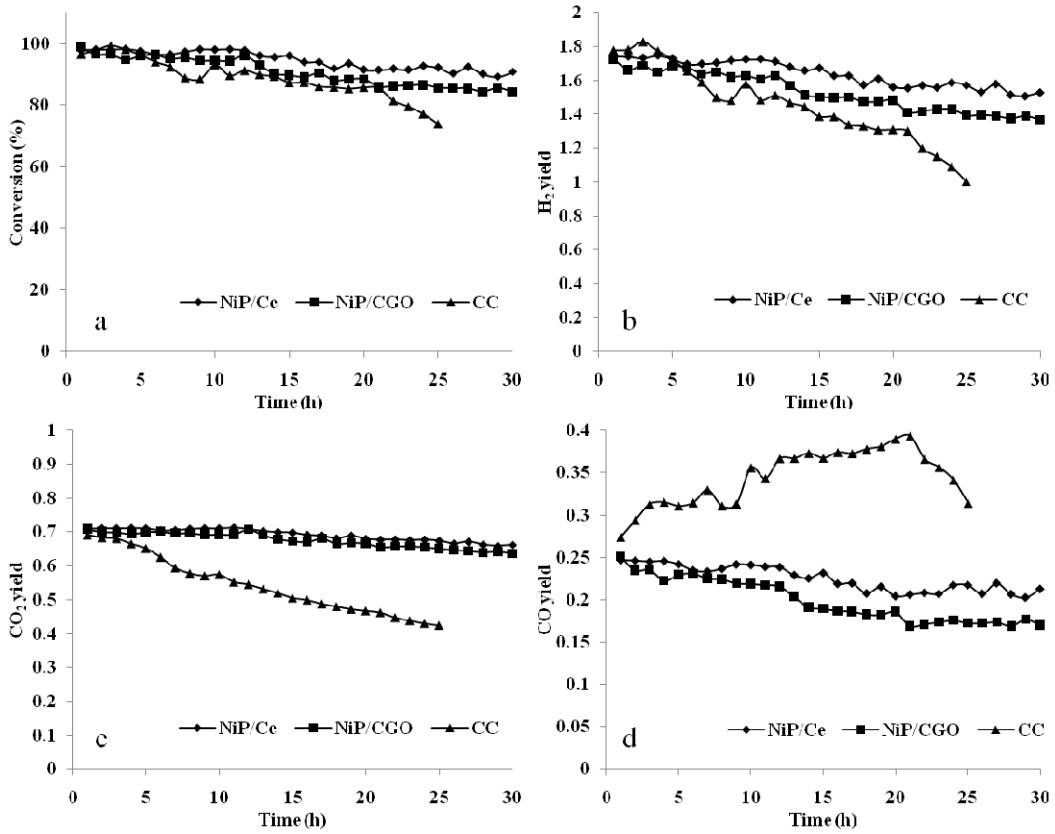

Figure 4. 7 Conversions and product yields vs time on stream of *n*-dodecane containing 10 wt% naphthalene autothermal reforming over carious catalysts ($C_{12}H_{26}$=0.02 ml min^{-1}, O_2/C=0.5, H_2O/C=3, 750 °C, GHSV=10 000 ml hr^{-1} g_{cat}^{-1})

It is also noted the presence of naphthalene in the fuel of ATR also caused more pronounced discrepancies between the two NiP catalysts in terms of fuel conversion and the H_2 and CO yields. Of them the NiP/Ce is superior and this can be related to its smaller NiP grain sizes as well as a larger surface concentration of Ce^{3+} ions on the basis of the structural characterizations described above. The effect of the former factor is straightforward while the latter one relies on the oxygen vacancies and the dissociative adsorption of steam at Ce^{3+} ions. The resulting O· or OH· radicals could be transferred to nickel reactive sites and remove surface carbon species to form CO, CO_2 and H_2 [181].

4.3.5 Investigation of the tolerance of catalyst to sulfur

Besides aromatics, organic sulfur compounds (thiophene, benzothiophene and dibenzothiophene) often existing at the level of 0.1% by weight in real fuels will also cause severe deactivation of an ATR catalysts. They undergo thermal cracking at high temperatures to primarily form H_2S [209], which is decomposed to form sulfur upon chemisorptions on Ni catalyst [107],[106]. Sulfur would form stable binding to metallic sites with all transition metals [105], leading to sulfur poisoning. First, the three catalysts were evaluated in ATR of *n*-dodecane containing 50 ppm thiophene (Figure 4.8). They presented rather similar catalytic activity despite exhibiting a slow decrease in fuel conversion over 30 h ATR course. However, the H_2 yield of the CC catalytic system underwent a quick decrease in the second 10 h and this was accompanied by a fast increase in the CO yield and a fast drop in the CO_2 yield. Such trends can be correlated by the reforming $CO_2 + C \rightarrow 2CO$, which helps cleaning coke formed due to thermal cracking on the CC and prevents noticeable loss of fuel conversion. It is also considered that WGS on the CC was severely impeded during the same period of time since the decrease in the H_2 yield and the increase in the CO yield took place concurrently. In contrast to the CC, both NiP catalysts lead to slight decreases in the H_2 and CO yields in the first10 h, which then basically stayed there in the rest of examining course. From this comparison, the CC catalytic system exposes its susceptibility due to the presence of 50 ppm thiophene that causes both coking and S poisoning. The two NiP catalysts presented stronger capabilities of buffering these deactivation effects. The similar effect of hydrodesulphurization by nickel phosphide was reported previously [193].

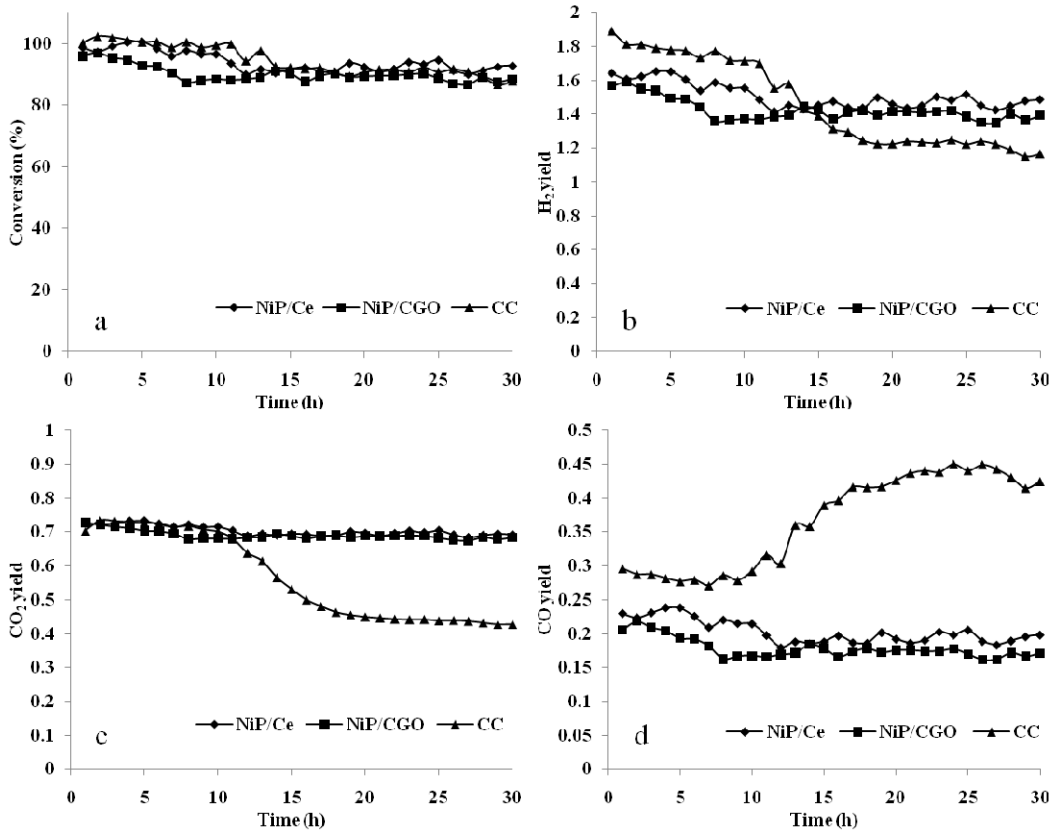

Figure 4. 8 Conversions and product yields vs time on stream of *n*-dodecane containing 50 ppm S autothermal reforming over carious catalysts ($C_{12}H_{26}$=0.02 ml min^{-1}, O_2/C=0.5, H_2O/C=3, 750 °C, GHSV=10 000 ml hr^{-1} g_{cat}^{-1})

When the sulfur content was increased to 100 ppm, its deactivating role became more intense (Figure 4.9). The fuel conversions in the two NiP catalytic systems dropped from about quantitative level to 80% in the first 8 h and maintained stable in the rest of assessing course. On the contrary the CC catalytic system could hardly retain the fuel conversion before it dropped to about 70% during the first 20 h reaction and the conversion then returned back slightly. Regarding the H_2 yield, it dropped in the first 8 h and stabilized at 1.2 afterwards in the two NiP catalytic systems. Looking at the CC catalytic system, the changes in the yields of H_2, CO and CO_2 follow the same pattern as what was observed when 50 ppm thiophene was introduced in *n*-dodecane. As expected, the lower yields of these three products were obtained due to the heavy deactivation effect. These yields were stabilized at certain

levels respectively as a result of the balance over the reforming of CO_2 by coke and WGS in the CC catalytic system. The increase in thiophene concentration also brought about swapping of catalytic activities and yields of the three products between the two NiP catalysts, namely, NiP/CGO performed somewhat superior over NiP/Ce. It implies that Gd-doped CeO_2 has a stronger intrinsic capability of sustaining WGS reaction than CeO_2 under the poisoning attack of thiophene.

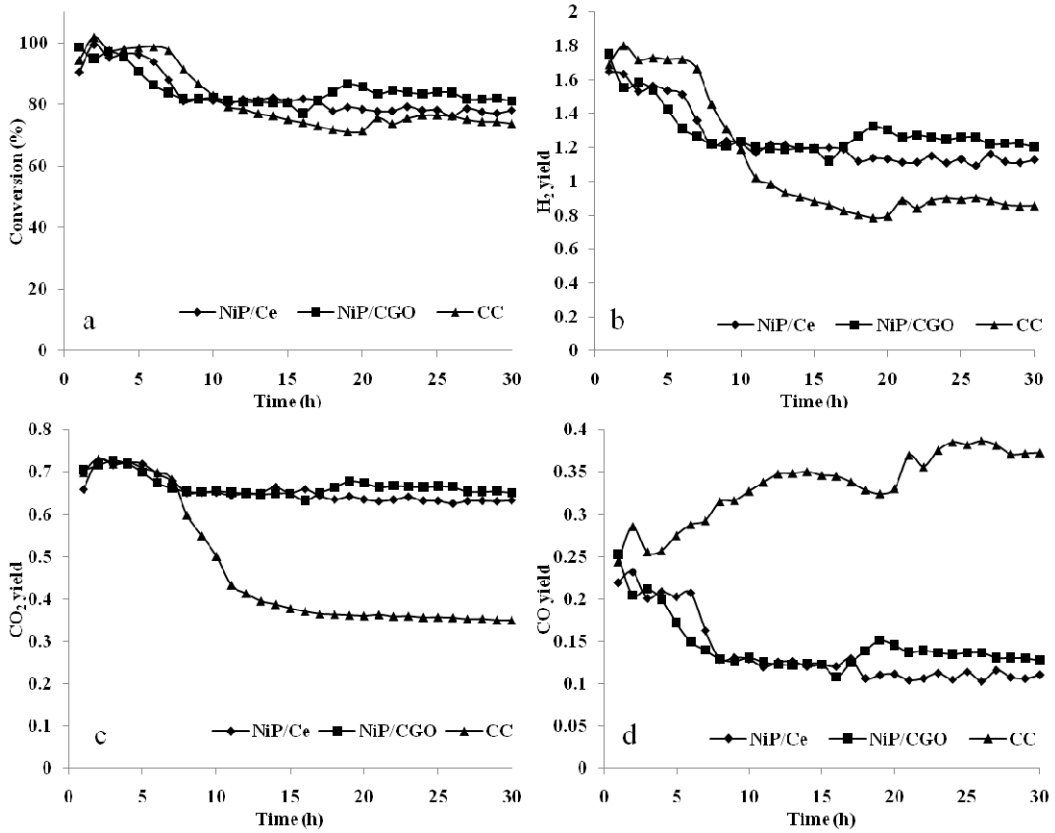

Figure 4. 9 Conversions and product yields vs time on stream of *n*-dodecane containing 100 ppm S autothermal reforming over carious catalysts ($C_{12}H_{26}$=0.02 ml min^{-1}, O_2/C=0.5, H_2O/C=3, 750 °C, GHSV=10 000 ml hr^{-1} g_{cat}^{-1})

4.3.6 Investigation of the aromatic and sulfur tolerance of the three ATR catalysts

A mixture of *n*-dodecane, naphthalene (10 wt%) and thiophene (100 ppm S) was formulated as the surrogate fuel compared with pure *n*-dodecane tested above

(Figure 4.10). Although the conversions of this fuel were lower in the three catalytic systems compared to that of pure *n*-dodecane, the conversions sustained by the two NiP catalysts were greater than that by the CC catalyst over 24 h duration. It is noteworthy that the CC presented a H_2 yield well below the two NiP catalytic systems, which is not in proportional to the discrepancy of the fuel conversions as found in Figure 4.10a. It can also be perceived that the CC gave rise to obviously lower CO_2 and CO yields. It is presumed that WGS on the CC was severely impeded during the same period of time since the decrease in the H_2 yield and the increase in the CO yield took place concurrently. Hence when POX and SR paths were blocked by coking and strong sulfur adsorption, the hydrogen production was tightened. To verify coking extents happening on the NiP/Ce and the control catalyst during the 24h ATR of the tri-component fuel, the catalysts downloaded from the reactor were scrutinized by thermogravimetric analysis (Figure 4.11). The TGA test showed that the used CC contained about 4 wt% coke while the used NiP/Ce contained almost no coke. As for the NiP/CGO catalyst, it was observed that coking started to happen at the upper layer of the catalyst bed near the inlet after 24h ATR. The micrographs of the used NiP/CGO particles from upper layer and lower layer of the catalytic bed verify this deliberation (Figure 4.12).

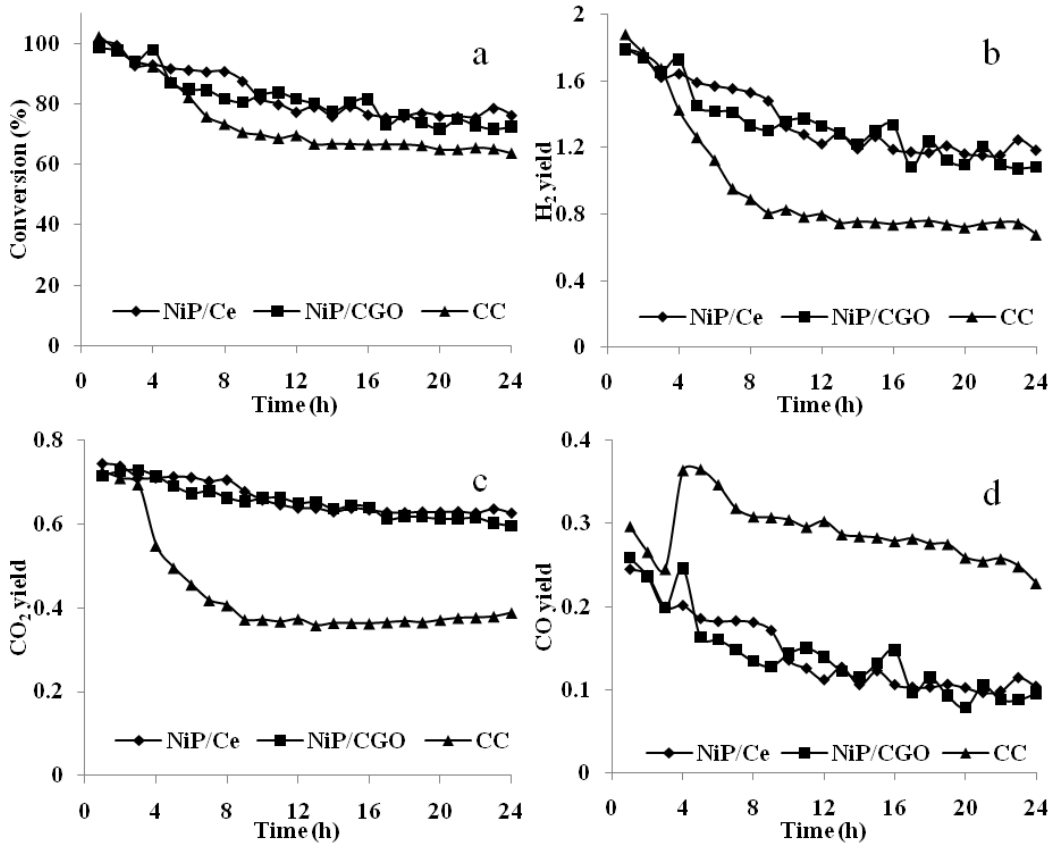

Figure 4. 10 ATR conversion of a fuel comprising of *n*-dodecane, 10 wt% naphthalene and 100 ppm S and product yields *vs.* time on the three catalysts (F_{fuel}=0.02 ml min^{-1}, O_2/C=0.5, H_2O/C=3, 750 °C, and GHSV=10 000 hr^{-1})

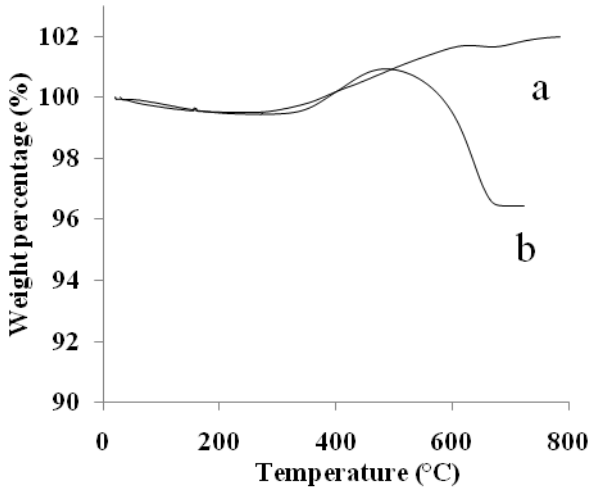

Figure 4. 11 TGA profiles of (a) used NiP/Ce and (b) used CC

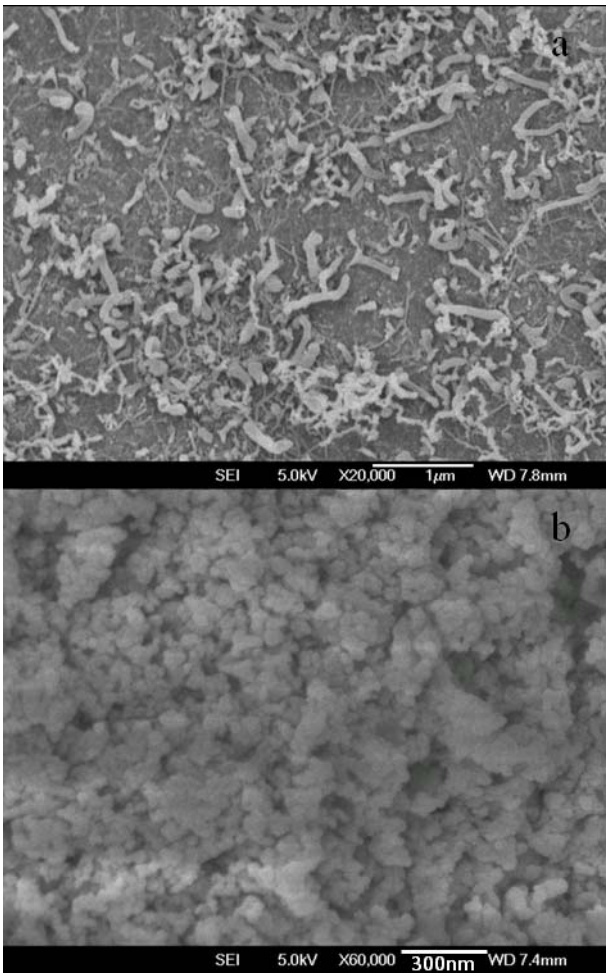

Figure 4. 12 FE-SEM images: (a) the top layer of the used NiP/CGO, and (b) the lower layer of the used NiP/CGO

The nickel phosphide has been found to be immune of coking due to the decrease in reducibility of Ni atom as well as its special role on inducing the generation of Ce^{3+} ions in the support under reducing atmosphere. Moreover, CGO contains a lower concentration of surface Ce^{3+} ions than Ce. This subtle difference in composition however lead to nontrivial impact on the ATR of *n*-dodecane-based surrogate fuel as reported above. Although the Ce supported Ni_xP_y displayed just slightly better performance than the CGO supported Ni_xP_y through a 24h ATR of the surrogate fuel, the former catalyst presented totally no coking while the latter one started growing cokes. Regarding the sole deactivating effect of thiophene on the ATR catalysts, inclusion of 100 ppm thiophene alone in *n*-dodecane caused drops of

fuel conversion by ca. 20% in the two NiP catalytic systems but by 30% in the CC system. According to XPS characterization of the spent catalysts, on which no sulfur species could be identified, we are therefore inclined to deem that sulfur poisoning effect actually promoted coking extent on the catalysts.

4.4 Conclusions

The nickel phosphide clusters dispersed on ceria or Gd-doped ceria were developed to catalyze the ATR of a surrogate diesel comprising of *n*-dodecane, naphthalene (10 wt%) and thiophene (100 ppm S). A commercial steam reforming (SR) catalyst was adopted for benchmarking the conversion of fuel and its selectivity to hydrogen and C-1 products. The reaction mechanism of the ATR of liquid hydrocarbons has been concluded by many researches: i) thermal cracking and combustion, which produce H_2, C (coke), CO_2, steam and C1-C4 hydrocarbons; ii) partial oxidation (POX) and SR of C1-C4; and (iii) steam shift reactions of C and CO with H_2O to produce CO_2 and H_2, and reforming of CO_2 by C to produce CO. Hence the conversion of fuel primarily depends on step (i) and removal of coke, while the selectivity to hydrogen also depends on step (iii). Compared to the commercial SR catalyst, both NiP/Ce and NiP/CGO demonstrate superior coke and sulfur tolerance because their nickel reactive sites possess less affinity with sulfur and also more importantly the Ce^{3+} ions generated at the surface of the support during ATR process assist with step (iii) that cleans coke from the nickel reactive site. As a result, these two supported NiP catalysts offer higher fuel conversions and hydrogen selectivity than the benchmark when the fuel contains naphthalene and thiophene as well. Furthermore, 10 mol% Gd(III) doping in the ceria support of NiP suppresses generation of Ce^{3+} ions in the ceria lattice, which in turn retard step (iii) reactions.

The Ce^{3+} ions generated from the reduction of the precursors of the two supported NiP catalysts were checked by H_2-TPR, and the existence of Ce^{3+} ions in the two catalysts were confirmed by XPS spectroscopy analysis. The extent of coking in the used catalysts in question was examined by both thermogravimetric (TGA) analysis and electron micrographic (FE-SEM) image.

CHAPTER 5

NI/$CE_{1-X}M_X$ CATALYST GENERATED FROM METALLO-ORGANIC NETWORK FOR AUTOTHERMAL REFORMING OF LIQUID FUEL

5.1 Introduction

Oxide-supported Ni catalysts are commonly used in hydrocarbon rreforming that produces hydrogen or syngas because of the high reactivity and low cost of nickel. The pristine Ni catalyst is prone to coking, adsorption of sulphur and sintering, which cause swift loss of catalytic activity. Many investigations have been carried out to pursue stable catalytic activity of the supported-Ni catalyst system. Modifying Ni lattice by doping it with a small amount of noble metals has been an effective solution since it prevents carbon deposition on the nickel catalytic site [27, 210, 211]. Alternatively, tuning the metal-support interactions stands for another approach to boost the performance stability of the catalyst since the interactions could adjust Lewis acidity of the supported Ni sites and hence the adsorption behaviours of reactive species. The metal-support interactions involve several aspects of chemistry, e.g. chemical bonding [212], acid-base equilibrium [213], change in particle sizes [214] and morphology [215] of the supported nickel grains. The impregnation method is normally used to prepare the supported catalyst. It focuses on the composition and surface pore structures [216, 217]. Contrary to this traditional method, the precursor approach by which catalytic Ni sites are generated from degradation of a solid solution upon its exposing to a reducing atmosphere at elevated temperatures

advances the metal catalyst preparation method, such as the perovskites whose B-site contains nickel: $(La_{0.5}Sr_{0.5})_2FeNiO_{6-\delta}$ [218], $LaNi_xM_{1-x}O_{3-\delta}$ [219]. As the Ni catalytic site is formed from the decomposition or partial decomposition of a solid solution, the size and chemical environments of the catalytic site would be significantly different from those implemented by the impregnation method.

In this work we continued with using the precursor strategy to prepare the supported-Ni catalyst. Instead of the perovskite precursor, a metallo-organic network (MON), composed of glycine-citrate ligand pair and metal ions of Ni^{2+}, Ce^{4+} and La^{3+} (and/or Gd^{3+}), was synthesized as precursor. The coordination network formed assures homogeneous distribution of the metal ions. Hence the respective metal oxides generated from pyrolysis of the coordination network can mix to a substantially thorough extent. Overwhelming interfacial contact amid these individual oxides is to significantly impact the formation of the binary composite, composed of NiO and the fluorite $Ce_{1-(x+y)}La_xGd_y$, in the calcination step after pyrolysis. To validate such structural impact, the same composite sample but prepared by the impregnation method, NiO/$Ce_{1-x}La_x$_Im, was used as control. As expected, the impregnation method renders the NiO phase higher reducibility than those formed from the MON precursor. Besides the precursor method, the La_2O_3 component played the key role in toughening reducibility of NiO. The five catalysts prepared by the MON method were examined in the autothermal reforming (ATR) [72, 220] of a surrogate diesel fuel, composed of *n*-dodecane, 10 wt% naphthalene and 100 ppm sulphur (from thiophene). Catalytic ATR of liquid hydrocarbon produces reformates in which hydrogen is the principal component. It is therefore a solution to hydrogen storage for powering hydrogen fed fuel cells. Catalytic reforming liquid fuels, the coking, sulphur adsorption and sintering problems become far more severe than

reforming natural gas because of the presence of heavy hydrocarbons, aromatics and organosulfurs [110, 221, 222]. Therefore, exploration of durable diesel-fuel reforming catalysts possessing desired catalytic activity is timely for the applications of the portable auxiliary power unit (APU) [223].

5.2 Experimental

5.2.1 Materials

Cerium nitrate hexahydrate (Sigma Aldrich, >98%), gadolinium nitrate hexahydrate (Sigma Aldrich, >98%), lanthanum nitrate hexahydrate (Sigma Aldrich, >98%), nickel nitrate hexahydrate (Sigma Aldrich, >98%), glycine (Sigma Aldrich, >99%), citric acid (Sigma Aldrich, >99%), ethylene glycol (Merck, >98%), *n*-dodecane (Sigma Aldrich, >99%), thiophene (Merck, >99%), and naphthalene (Sigma Aldrich, >99%) were all used as received. A nickel-based SR commercial catalyst (Alfa Aesar, HiFUEL^{TM} R-110) was used as benchmark.

5.2.2 Preparation of the ceria (or doped-ceria) supported Ni catalysts

The catalysts were prepared by Pechini method utilizing MON as template [205]. All chemicals used were AR grade. In a typical preparation, an aqueous solution of the nitrate salts of the three metals (Ni^{2+}, Ce^{3+} and La^{3+}/Gd^{3+}) with the designated stoichiometry was prepared. After that, glycine and citric acid were introduced into the solution, in which the molar ratio of the metal ions to all the functional groups (-NH_2 and –COOH) was 0.154, the mass ratio of citric acid to glycine was 0.129, and the concentration was about 20 wt.%. The solution was then mixed with 0.8 portion of ethylene glycol by volume. The formulated solution was thickened on a hot plate at

200 °C under stirring. This step resulted in a MON in the end of evaporation. The MON was then subjected to pyrolyzing at 400 °C for 2 h and calcined at 600 °C for another 2 h to remove carbon residues and to allow for the growth of crystal phase in an oxide mixture of the above metals. Pellets of the resultant powder were prepared by moulding, crushed and sieved into 0.5~1 mm granules for packing a catalytic bed. By the impregnation method, an appropriate amount of $Ni(NO_3)\cdot 6H_2O$ was dissolved in 100 ml DI water, then a certain amount of the (pristine or doped) ceria powder prepared by the Pechini method described above was added into this solution. After stirring at room temperature for 2 h, the mixture was stirred at 60 °C overnight to obtain a dry powder. The powder was calcined in air at 600 °C for 3 h to obtain a ceria supported NiO powder and then 0.5~1 mm granules were made. The symbol, $NiO/Ce_{1-(x+y)}Gd_yLa_x$, is used to label the catalyst precursor $NiO/Ce_{1-(x+y)}La_xGd_yO_{2-}$ prepared for simplicity, where composition of ceria is labelled by mole ratios, i.e the subscripts. The Ni(0) loading in all the catalysts prepared in the study was 15 wt%, or the stoichiometric ratios of Ni(0) and $Ce_{0.9}La_{0.1}$, for example, are about 0.43 and 1 respectively in the catalyst precursor $NiO/ Ce_{0.9}La_{0.1}$. The spent catalysts were denoted as $Ni/Ce_{1-(x+y)}Gd_yLa_x$ after reaction since Ni phase was totally reduced to Ni(0) during reaction.

Besides the in-house prepared catalysts, a nickel-based steam reforming (SR) commercial catalyst (Alfa Aesar, HiFUEL^{TM} R-110, Ni loading: 15-40 wt% denoted by CC) was adopted as control. Another catalyst was also prepared by the impregnation method as a reference. An appropriate amount of $Ni(NO_3)\cdot 6H_2O$ was dissolved in 50 ml DI water, then the support powder was added into this solution. After stirring under room temperature for about 3 hrs, the mixture was heated at 60 °C overnight under stirring to evaporate water. The obtained solid was calcined in air at

600 °C for 3 hrs to obtain an oxide powder which is denoted as NiO/$Ce_{0.9}La_{0.1}$_Im. The Ni loading in this reference catalyst was about the same as the others.

5.2.3 Catalyst characterization

The crystalline structures of catalysts were determined by X-ray diffractometry (XRD, SHIMADZU XRD-6000, Cu Kα radiation) using a scanning rate of 5 ° min^{-1}. The temperature-programmed reduction (TPR) was conducted on a physicochemical absorber (Quantachrome Autosorb-1 instrument)using a sample of 50 mg and a gas (5% H_2 in N_2) flow rate of 80 mL min^{-1}. The heating rate was set at 10 °C min^{-1}. The images of the nano-scaled Ni clusters were obtained from a transmission electron microscope (TEM, JEOL JEM-2100F).

5.2.4 Experimental setup and reaction conditions

About 1g catalyst (0.5-1 mm particles) was packed between two plugs of quartz wool in the centre of a quartz tube reactor (1.2 cm o.d., 1 cm i.d. and 40 cm long). The micro plug flow reactor (PFR) was then placed in a thermostat-controlled vertical tube furnace. The air and nitrogen mixture into the reactor was metered by a mass flow controller (Alicat). The fuel and water streams were regulated respectively by ISO-2000 isocratic pumps and sent to combine with the synthetic air (O_2/N_2) stream. The tri-component (air, fuel, and water) stream was then led to a mixer to carry out vaporization and then sent to the PFR. The temperature of the mixer was set at 250 °C and a dry run in the absence of catalyst indicated that the fuel was not pyrolyzed in the mixer. The optimal reforming conditions comprising of the following parameters: fuel-supply rate = 0.02 ml min^{-1}, oxygen and steam supply rates: O_2/C=0.5 and H_2O/C=3, reforming temperature 750 °C, and GHSV=10, 000 h^{-1}.

Specifically, the PFR loaded with catalyst was heated to 750 °C under a N_2 flow, which was then switched to a flow of super heated steam passing through the mixer with the aim of fixing particle packing of catalyst bed. The PFR was held under this condition for 1 h before the fuel was directed to the reactor. The outlet stream was connected to Shimadzu GC after passing a cold trap to knock out condensable components if any. The performance of the catalyst was assessed by fuel conversion, distribution of product gases and their yields, which were computed using the following equations where nitrogen in synthetic air was used as internal standard:

$$\text{Conversion} = \frac{F_{total}(y_{CO} + y_{CO_2} + y_{CH_4})}{F_C \text{ in fuel}} \qquad (5.1)$$

$$\text{Yield} = \frac{F_{total} y_p}{F_p \text{ in fuel}} \qquad (5.2)$$

$$F_{total} = \frac{F_{N_2} \text{ in feed}}{y_{N_2}} \qquad (5.3)$$

where F stands for molar flow rate in mol s^{-1} and y the mole fraction of a component p (subscript) in the gas outlet stream. Theoretically, the conversion should be determined from the amount of dodecane at the exit of the reactor with respect to that at the entry of reactor. However, the fuel conversion is determined using Eq. 1 due to the limitation of analyzing the trace amounts of gaseous hydrocarbons such as methane and ethylene as well as the difficulty of quantifying a small amount of fuel trapped in the water condensation process [28]. The surrogate fuel containing 90 wt % *n*-dodecane, 10 wt% naphthalene and 100 ppm S was formulated to test the coke and sulfur tolerance of the catalysts.

5.3 Results and discussion

5.3.1 The surface activity of La_2O_3 in the doped ceria and its affinity with NiO

Regarding the doped ceria support, $Ce_{1-(x+y)}Gd_yLa_x$, where x = y = 0 or x = 0.1, y = 0 or x = 0, y = 0.1, the surface properties of it, i.e. surface area and surface concentration of dopant (Table 1), was affected by the type of dopant and its extent (x and y values). Doping ceria lattice with the same amount of Gd^{3+} or La^{3+} ions brings about different specific surface areas. The surface area undergoes decreasing with the increase in La^{3+} dopant. In addition, the analysis of surface composition by XPS shows that the surface atomic concentration of La^{3+} is greater than its stoichiometric ratio in the bulk. The same phenomenon however is not found in the Gd-doped ceria. It can be presumed that La^{3+} ions concentrate along the boundaries of ceria grains and hence block numerous gaps between grains due to the La_2O_3 links across the boundaries. This surface-active trait of La_2O_3 in a specific ceramic composite has been previously found [224]. Hence, the surface enrichment of La_2O_3 causes reduction of surface area. Furthermore, when the MON precursor contains Ni^{2+} ions together with the other metal ions for the ceria support, the resulting oxide mixtures (Fig. 1) all consist of NiO and fluorite-like ceria phases [94, 225]. The presence of NiO phase further reduces the surface area of the ceria (Table 1). This suggests that the NiO phase achieve large dispersions on the ceria supports owing to the precursor effect of MON. For instance, compared to NiO/$Ce_{0.9}La_{0.1}$_Im made by the impregnation method, NiO/$Ce_{0.9}La_{0.1}$ showed a lower specific surface, which can be attributed to the nucleation of both NiO and ceria, which took place proximately and simultaneously when both initially split from the same network. In contrast to this, by

the impregnation method, the formation of NiO on $Ce_{0.9}La_{0.1}$ caused a relatively smaller decrease in the porous structure the pristine support possessed. It can be envisaged that an immense interfacial contact between the embryos of NiO and $Ce_{0.9}La_{0.1}$ retarded the evolution of micro-pores inside the ceria due to fast sintering of the NiO phase during the post-synthesis calcination step [226]

Moreover, a test was designed to check if La_2O_3 reacts with NiO at the calcination temperature used. In this test, a MON containing Ni^{2+} and La^{3+} ions with stoichiometric ratios of 0.9 and 0.05 was synthesized. After pyrolysis and calcinations, a minor phase (as marked in Fig. 2a) other than La_2O_3 emerged in the calcination product, in which the NiO remained as the major phase. This particular minor phase must be an interfacial reaction product composed of NiO and La_2O_3 due to immense interfacial contact between these two oxides nuclei as aforementioned. But no such a minor phase appeared if both oxides were prepared separately and then calcined together or if La_2O_3 was replaced by Gd_2O_3 using the MON method. It is clear that the preparation history and the nature of La^{3+} ion lead to formation of the interfacial phase. Furthermore, to understand whether the La_2O_3-NiO minor phase impacts the Ni phase generated through reduction, the oxide as presented in Fig. 2a was reduced by H_2. The reduction produced both La_2O_3 and Ni phases (Fig. 2b), indicating that the La_2O_3 was released from the minor phase while NiO was reduced to Ni. Appealingly, the Ni generated from the reduction displayed the two characteristic diffraction peaks at slightly lower 2θ angles than those generated from the pristine NiO. This expansion of inter-planar spacing can be attributed to the retaining of a trace amount of La^{3+} ions in the Ni lattice when it was formed, where the charge can be balanced by surface oxide anions. The resultant doping structure stabilizes small Ni nanoparticles and

enhances their reforming catalytic activity, which will be described in the following section.

Table 5. 1 BET specific surface area of various samples and surface composition of supports

Sample	BET surface area (m^2/g)	Surface molar ratio of doping element
Ce	88	/
$Ce_{0.9}Gd_{0.1}$	90	0.12
$Ce_{0.9}La_{0.1}$	63	0.18
$Ce_{0.8}La_{0.2}$	35	0.31
NiO/Ce	49	/
NiO/$Ce_{0.9}Gd_{0.1}$	45	/
NiO/$Ce_{0.9}La_{0.1}$	34	/
NiO/$Ce_{0.9}La_{0.1}$_Im	61	/
NiO/$Ce_{0.8}Gd_{0.1}La_{0.1}$	38	/
NiO/$Ce_{0.8}La_{0.2}$	26	/

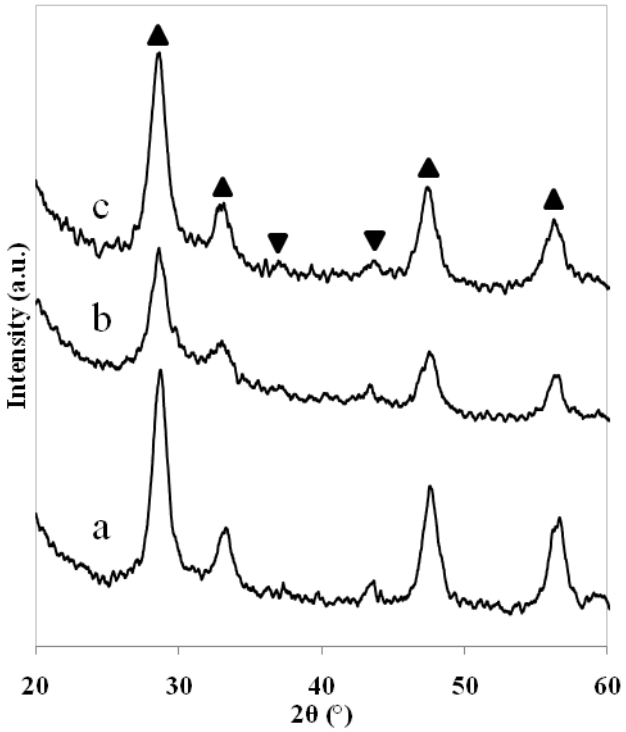

Figure 5. 1 XRD patterns of fresh (a) NiO/Ce, (b) NiO/$Ce_{0.9}Gd_{0.1}$ and (c) NiO/ $Ce_{0.9}La_{0.1}$ catalysts (▲: CeO_2; ▼: NiO)

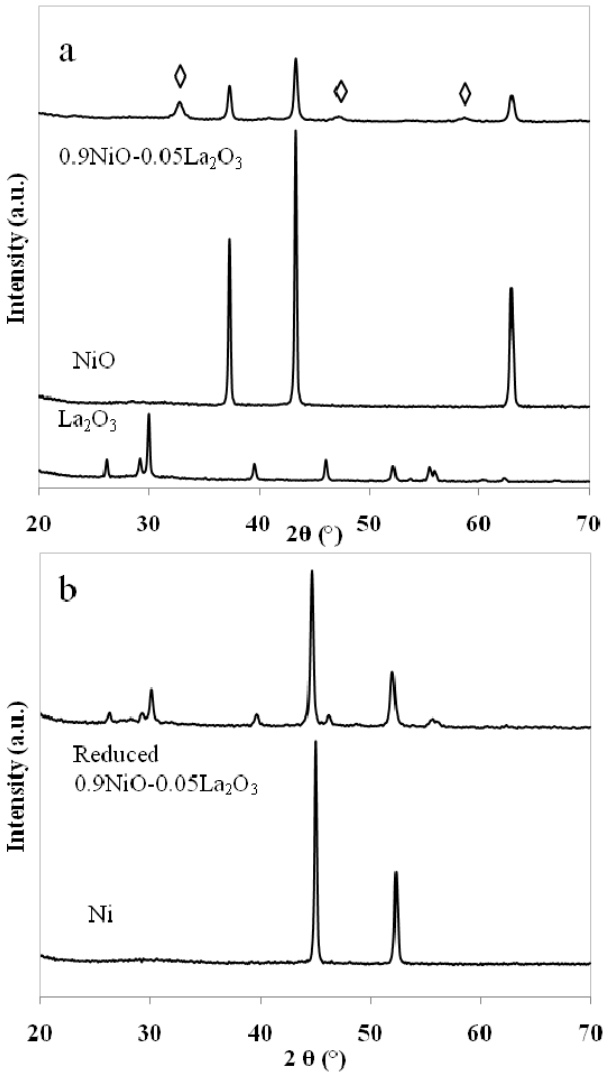

Figure 5. 2 XRD patterns of (a) the calcined oxide mixture of NiO and La_2O_3 made from a MON; (b) the reduced oxides

In the above examination of the interfacial reaction between La_2O_3 and NiO, CeO_2 was not included with the aim of observing the derived minor phase from XRD. It is understandable that forming solid solution of $Ce_{1-x}La_x$ would reduce tendency of the interfacial reaction between La_2O_3 and NiO, whereas the initialmixing to a huge extent between La_2O_3 and NiO nuclei right after pyrolysis of MON could still be a factor in contribution to the diffusion of La^{3+} into NiO. To prove this viewpoint, the reducibility of NiO in both NiO/$Ce_{0.9}La_{0.1}$ and NiO/$Ce_{0.9}La_{0.1}$_Im was measured using TPR analysis (Fig. 3a). Three reduction peaks appear on the TPR diagrams of both pre-catalysts: the two lower-temperature peaks are generated from the reduction of

NiO crystallite. The first peak reflects those of individual NiO crystallites, thoroughly exposed to the reducing atmosphere, on the $Ce_{0.9}La_{0.1}$ support, while the second broad peak represents those that are embedded in the matrix of support. The last very weak peak at about 700 °C is known to be due to the reduction of CeO_2 [226]. The comparison shows that the second TPR peak of NiO/$Ce_{0.9}La_{0.1}$ was well extended beyond 400 °C in contrast to that of its counterpart prepared by the impregnation method. This is consistent with the previous scrutiny showing that the impregnation preparation resulted in no interfacial phase of NiO-La_2O_3. Hence it is rational to propose that the presence of La^{3+} in the NiO crystallites repressed their reducibility. In principle, a trace amount of La^{3+} (r =117 pm) in the fcc Ni(0) (r = 124 pm) lattice could increase Lewis acidity of the Ni crystallites, which in turn enhances catalytic thermal cracking of hydrocarbons. In contrast to this, the reducibility of NiO was not adjourned if the support was $Ce_{0.9}Gd_{0.1}$ instead (Fig. 3b) as previously noticed that Gd_2O_3 in the doped ceria support lacks affinity with NiO despite being derived from the same MON.

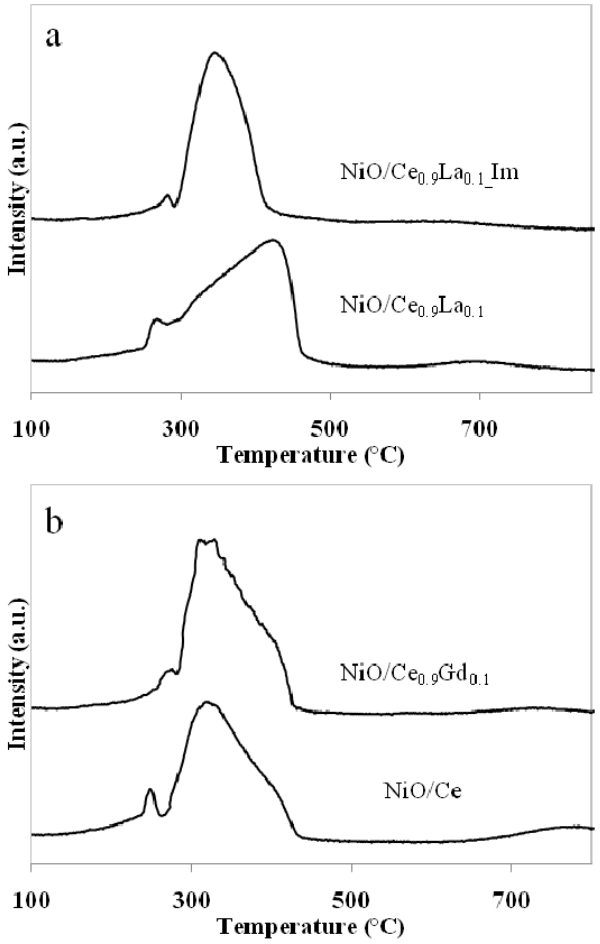

Figure 5. 3 TPR profiles of (a) NiO/$Ce_{0.9}La_{0.1}$_Im and NiO/$Ce_{0.9}La_{0.1}$ oxide composites; (b) NiO/Ce and NiO/$Ce_{0.9}Gd_{0.1}$ oxide composites

5.3.2 The role of La_2O_3 in augmenting the ATR catalytic activity of Ni/$Ce_{0.9}La_{0.1}$

All catalysts were evaluated in ATR of the surrogate fuel, which is composed of *n*-dodecane, 10 wt% naphthalene and 100 ppm S. Figure 5.4 shows the conversions and product yields for the catalysts including a commercial catalyst (denoted as CC). It can be seen that all catalysts underwent deactivation due to the presence of aromatic and sulfur. After 24 h reaction, the conversion of Ni/Ce catalyst dropped to below 80%. When doped with 10% Gd, the catalyst showed a worse performance whereas the fuel conversion dropped to about 60% in 24 h. However, when 10% La was

introduced into the Ni/Ce catalyst, its activity was markedly enhanced and the fuel conversion maintained above 90% in 24h reaction. Among these four catalysts, the CC catalyst exhibited worst performance, which indicate a poorest resistance to aromatic and sulfur poisoning. The trend of hydrogen yields change is similar to that of fuel conversions, except for CC that its hydrogen yield is much lower than the others. This difference can be explained by the change of CO_2 and CO yields. While the CO_2 and CO yields of the other three catalysts followed similar trends as the conversion and hydrogen yield, that of CC had a tremendous change. The CO_2 yield decreased a lot while the CO yield increased. This indicates that the reaction path of this catalyst has changed while that of the ceria or doped ceria supported catalysts maintained almost unchanged. The performance of these three ceria or doped ceria supported catalysts is in good agreement with the TPR results. The addition of La could obviously enhance the interaction between Ni and the support.

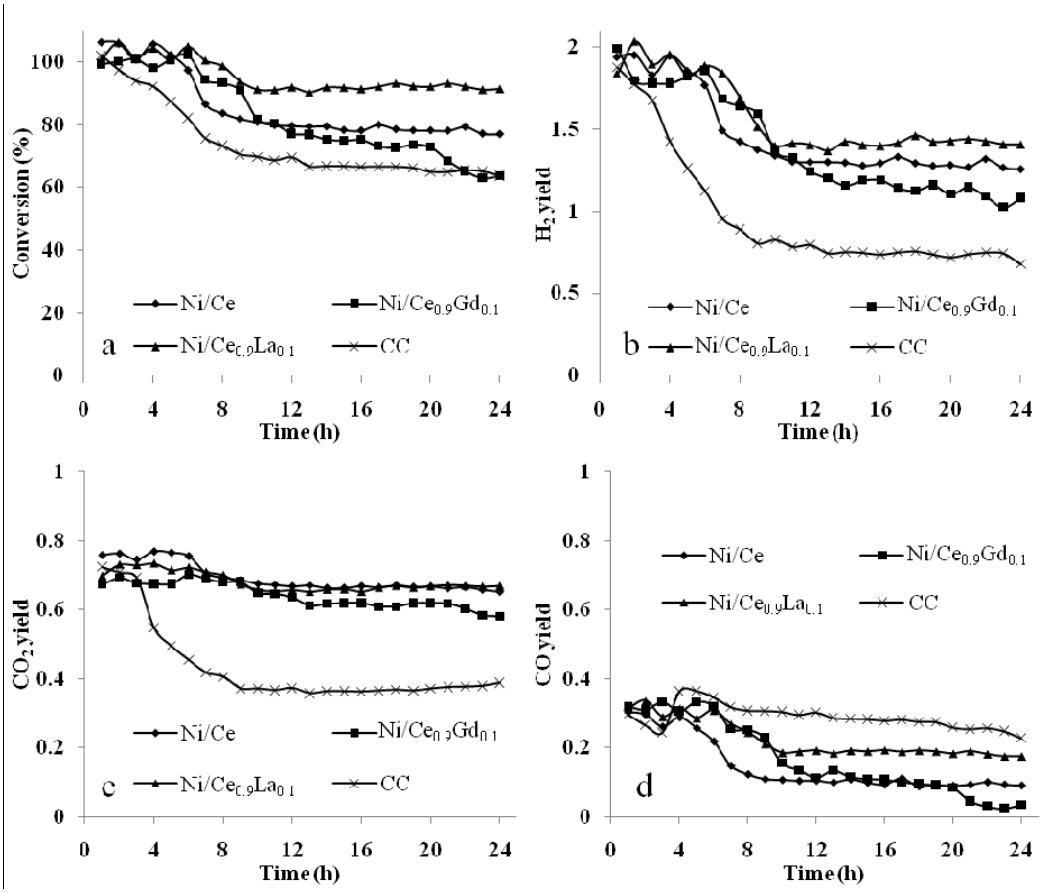

Figure 5. 4 ATR conversions and product yields vs. time on the feed comprising of *n*-dodecane, 10 wt% naphthalene and 100ppm S over various catalysts (F_{fuel}=0.02 ml min^{-1}, O_2/C=0.5, H_2O/C=3, 750 °C, GHSV=10 000 hr^{-1})

The XRD patterns of the spent catalysts are shown in Figure 5.5. All peaks of ceria lattice became sharper after reaction, which indicates sintering of the support due to higher reaction temperature. However, the $Ni/Ce_{0.9}La_{0.1}$ catalyst showed broader peaks than the other two. This could suggest a decreased crystal size of ceria after La doping. Also, these peaks clearly shifted to smaller angles. The reduced reflection angles could indicate an increased lattice parameter which may make it easier for the Ni atoms to enter the lattice, thus enhancing the interaction between Ni and the support. Signs of Ni crystalline structure could be seen after reaction. It can be seen that the peak width of Ni in La doped catalyst is broader than that in the others. The Gd doped catalyst shows sharpest peak of Ni. Figure 5.6 shows the TEM images of the spent catalysts. It can be clearly seen that the $Ni/Ce_{0.9}Gd_{0.1}$ catalyst shows

largest Ni particle size while the Ni/$Ce_{0.9}La_{0.1}$ catalyst shows the smallest compared with others. This result is in good agreement with the XRD patterns.

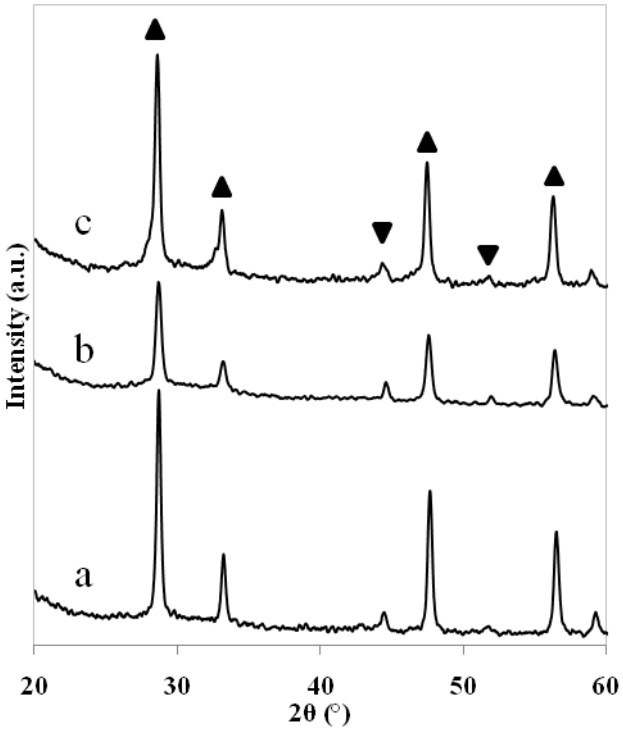

Figure 5. 5 XRD patterns of spent (a) Ni/Ce, (b) Ni/$Ce_{0.9}Gd_{0.1}$ and (c) Ni/$Ce_{0.9}La_{0.1}$ catalysts (▲: CeO_2; ▼: Ni)

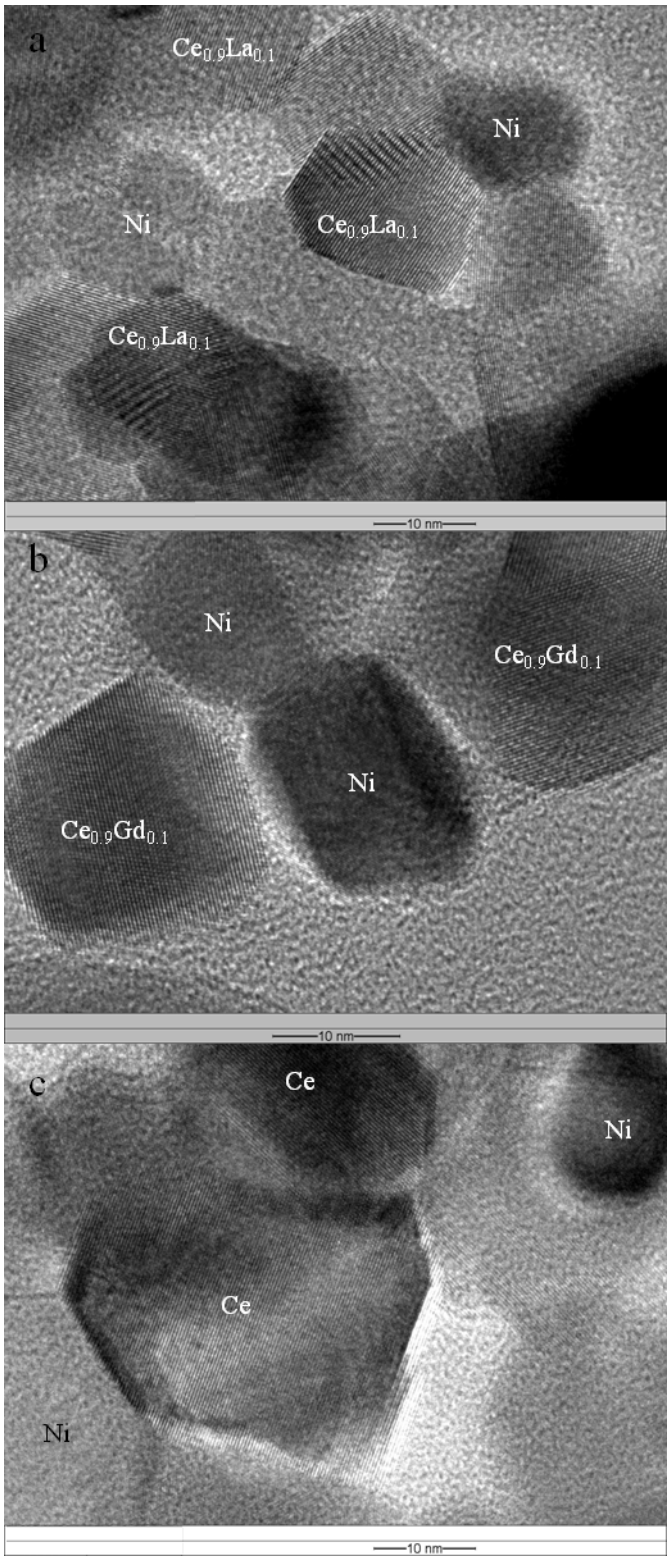

Figure 5. 6 TEM images of spent a) Ni/$Ce_{0.9}La_{0.1}$, (b) Ni/$Ce_{0.9}Gd_{0.1}$ and (c) Ni/Ce catalysts

5.3.3 Diversifying and enhancing the doping structure of $Ce_{1-(x+y)}Gd_yLa_x$ – the effect on the reforming catalysis

The above results could clearly be seen that addition of 10% La onto the Ni/Ce catalyst could largely enhance its activity. Therefore, the effect of a higher doping level onto the Ni/Ce catalyst was investigated. In the following section, the two catalysts, Ni/$Ce_{0.8}La_{0.2}$ and Ni/$Ce_{0.8}Gd_{0.1}La_{0.1}$, with 20% doping level are studied in ATR of the surrogate fuel.

The BET specific surface area of the fresh catalysts is summarized in Table 5.1. It can be seen that the 20% La doping level resulted a lower surface area than the 10% doped one, indicating a stronger promotional effect of La in enhancing the dispersion of nickel content. The specific surface area of Ni/$Ce_{0.8}Gd_{0.1}La_{0.1}$ is similar to that of Ni/$Ce_{0.9}La_{0.1}$, indicating the poor dispersion effect of Gd as suggested in above section. Figure 5.7 shows the XRD patterns of the fresh catalysts. Compared to 10% doping level, peak broadening effect is more obvious in catalysts with 20% doping level. This broadening effect can be seen for both ceria and NiO. Also, the peaks for ceria are less clearly resolved for these two 20% doped catalysts. This could indicate the poorer crystallization of the catalysts with higher doping level. Figure 5.8 shows the TPR profiles of the fresh catalysts. It can be seen that both doped catalysts showed similar profiles regarding both reduction temperature and peak shape. The small peak at around 250 °C disappeared for both doped catalysts, while the reduction peak for bulk NiO is centred at around 400 °C. The peak for Ni/Ce catalyst has a steep ascending slope and a mild descending slope, while the shape for the reduction peak of both doped catalysts has an obtuse shape instead of a sharp one. This could indicate that most NiO molecules in these two catalysts are more difficult to be

reduced than that of the others. It should also be noted that the peak for ceria reduction centred at around 784 °C for the Ni/Ce catalyst totally disappeared for the doped catalysts. The disappearance of this peak is a sign of reduced reducibility of the ceria support.

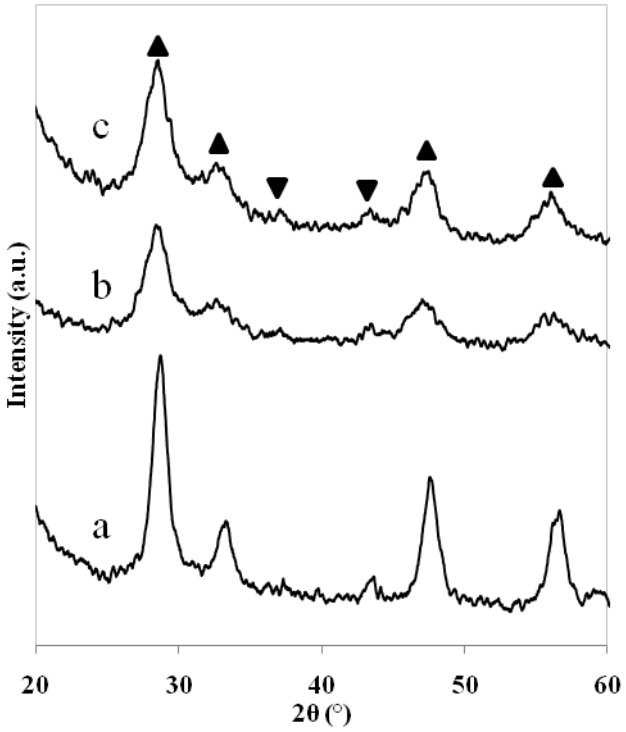

Figure 5. 7 XRD patterns of fresh (a) Ni/Ce, (b) Ni/$Ce_{0.8}Gd_{0.1}La_{0.1}$ and (c) Ni/Ce0.8La0.2 catalysts (▲: CeO_2; ▼: NiO)

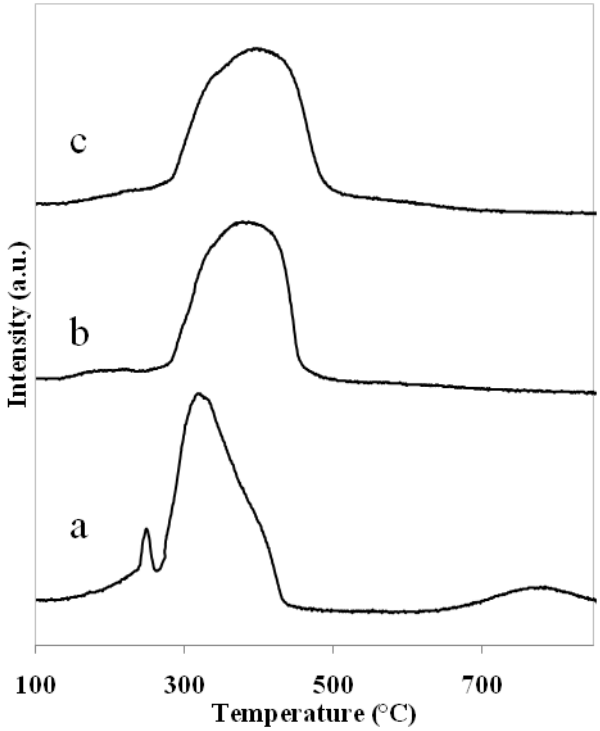

Figure 5. 8 TPR profiles of fresh (a) Ni/Ce, (b) Ni/$Ce_{0.8}Gd_{0.1}La_{0.1}$ and (c) Ni/$Ce_{0.8}La_{0.2}$ catalysts

The catalysts were also evaluated in ATR of the surrogate fuel, where the conversions and product yields are shown in Figure 5.8. It can be seen that both doped catalysts show higher fuel conversion than the Ni/Ce catalyst in 24 h. These two doped catalysts started to deactivate after reacted for about 8 h. The Ni/$Ce_{0.8}La_{0.2}$ catalyst started showing higher fuel conversion than the Ni/$Ce_{0.8}Gd_{0.1}La_{0.1}$ catalyst after reacted for 12 h and maintained till the end of test. However, the hydrogen yields of these two catalysts showed contrarily performance. The hydrogen yield of Ni/$Ce_{0.8}La_{0.2}$ catalyst was comparable with that of the other catalyst in the first 12 h reaction; after that, it showed lower hydrogen yield although its fuel conversion was higher than the other catalyst. By comparing the CO_2 and CO yields, it can be found that the Ni/$Ce_{0.8}La_{0.2}$ catalyst had a lower CO_2 yield and a higher CO yield than the Ni/$Ce_{0.8}Gd_{0.1}La_{0.1}$ catalyst in the second 12 h reaction. This may indicate that the Ni/$Ce_{0.8}Gd_{0.1}La_{0.1}$ catalyst experienced a higher extent of water-gas-shift (WGS)

reaction than the Ni/$Ce_{0.8}La_{0.2}$ catalyst, which would probably resulted a higher hydrogen yield regardless its slightly lower fuel conversion. Also, the hydrogen yield of the Ni/$Ce_{0.8}La_{0.2}$ catalyst dropped close to that of the Ni/Ce catalyst in the second half test period while that of the Ni/$Ce_{0.8}Gd_{0.1}La_{0.1}$ catalyst kept higher hydrogen yield till the end of test. Thus it can be suggested that higher La doping level is not favourable for hydrogen production. But proper La doping level could facilitate hydrogen production even though another unfavourable oxide (Gd) was added in.

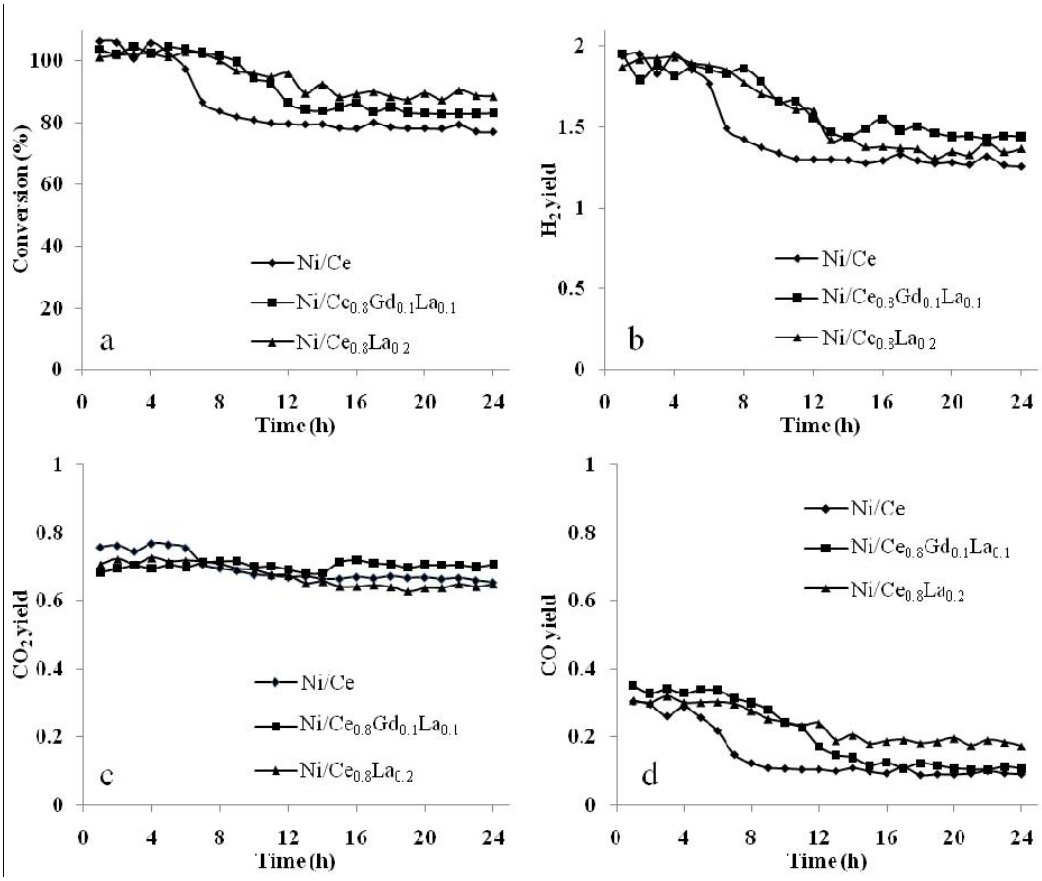

Figure 5. 9 ATR conversions and product yields vs. time on the feed comprising of *n*-dodecane, 10 wt% naphthalene and 100ppm S over various catalysts (F_{fuel}=0.02 ml min^{-1}, O_2/C=0.5, H_2O/C=3, 750 °C, GHSV=10 000 hr^{-1})

Figure 5.10 shows the XRD patterns of the spent catalysts. The peaks of ceria lattice were all sharpened after use due to calcination under higher reaction temperature. The peak width also increased for these two doped catalysts. The shifting of reflection angles to lower region can be more clearly seen after reaction for these

two 20% doped catalysts. This would indicate increased lattice parameter of ceria after doping. The higher reaction temperature (750 °C compared to the calcination temperature of 600 °C) should have furthered the crystallization of the support and strengthened its interaction between Ni sites. This strengthened interaction could probably be induced by incorporating of Ni into the ceria lattice, which was facilitated by the increased lattice parameter after doping. This would probably make the reduction of Ni sites more difficult as demonstrated by the TPR results. It can also be seen that the peak for Ni in both doped catalysts is quite wide and faintness, indicating the higher difficulty in reducing the Ni sites. The TEM images of these four spent catalysts are shown in Figure 5.11. It can be seen that both the Ni/Ce0.8La0.2 and Ni/$Ce_{0.8}Gd_{0.1}La_{0.1}$ catalysts showed smaller ceria particle size than the Ni/Ce catalyst, which is in good agreement with the XRD patterns. The 20% La doped catalyst showed smallest Ni particle size than the others, indicating better Ni dispersion. This is also consistent with the BET results.

In general, La doping on the Ni/Ce catalyst could promote the catalyst activity by enhancing the interaction between Ni sites and the support. The vacancies generated by doping could also facilitate the conduction of oxygen species which would help cleaning the adsorbed carbon species [120]. However, when the doping level exceeds the critical value, the stronger metal-support interaction would inhibit the activity by preventing the reduction of Ni sites. Moreover, higher doping level would sacrifice the reducibility of ceria. This could also be related to the interaction between the nickel species and the ceria support. When the catalyst was doped by La, more vacancies would be generated and the interaction between the nickel species and ceria support would be strengthened. The strengthened interaction would probably indicate partly incorporation of nickel into the ceria lattice. This can be demonstrated

in Figure 5.9 where the peak for nickel phase became very faintness with higher doping level. This incorporation of nickel into ceria lattice could have occupied the vacancies generated by doping of La, thus the oxygen mobility in support could have been reduced and thus restrained the hydrogen production.

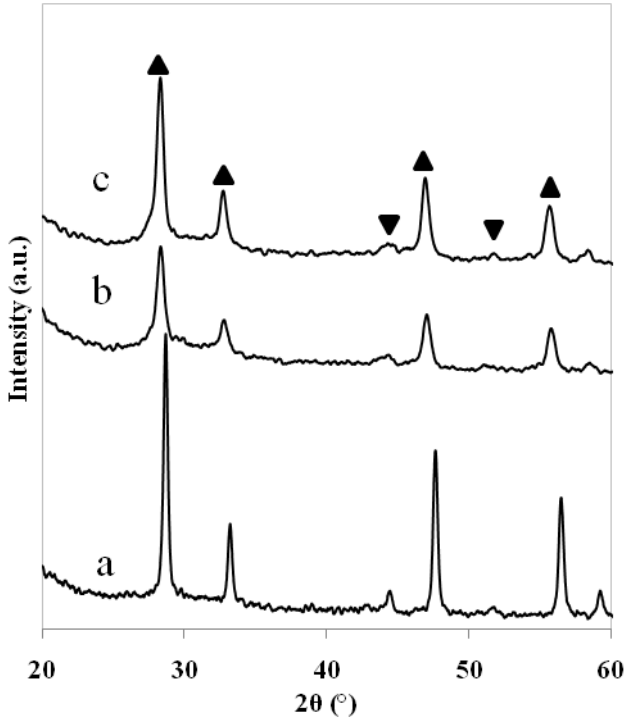

Figure 5. 10 XRD patterns of spent (a) Ni/Ce, (b) Ni/$Ce_{0.8}Gd_{0.1}La_{0.1}$ and (c) Ni/$Ce_{0.8}La_{0.2}$ catalysts (▲: CeO_2; ▼: Ni)

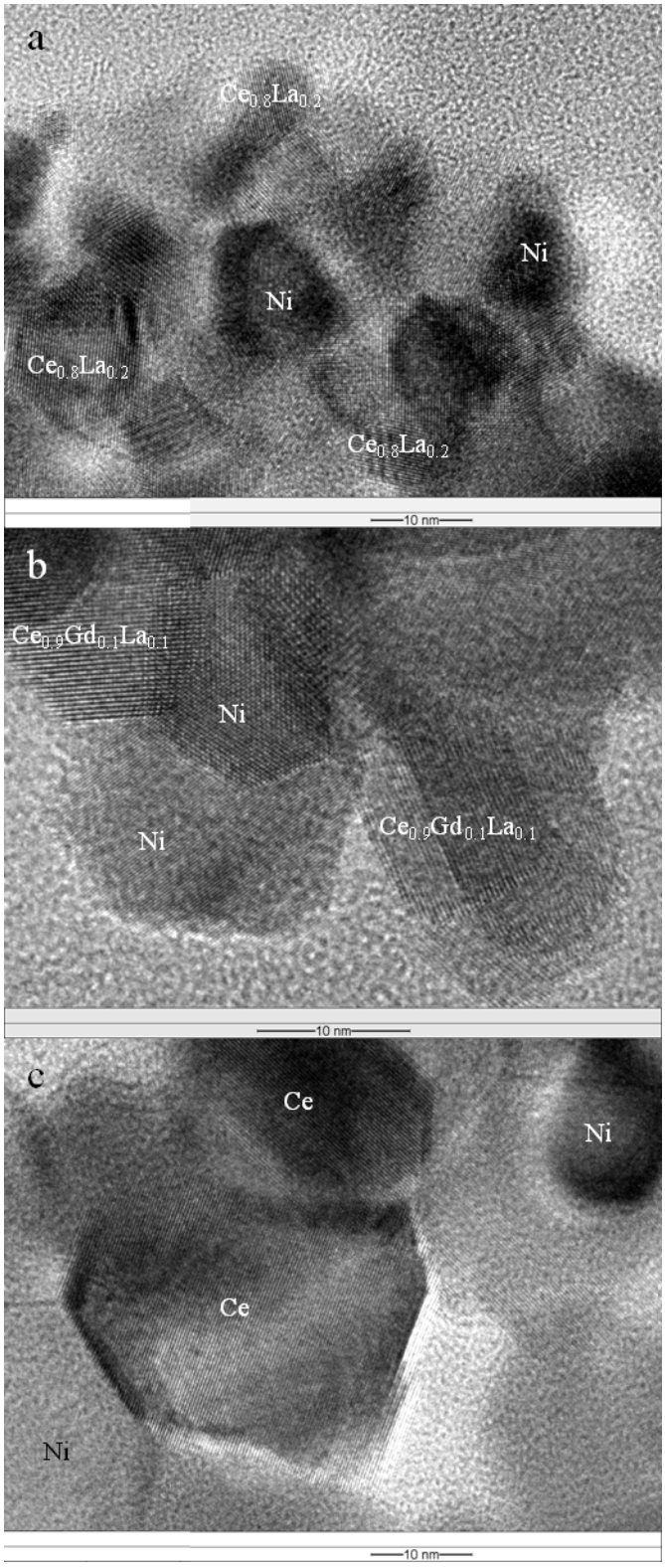

Figure 5. 11 TEM images of spent a) Ni/$Ce_{0.8}La_{0.2}$, (b) Ni/$Ce_{0.8}Gd_{0.1}La_{0.1}$ and (c) Ni/Ce catalysts

5.4 Conclusions

This investigation started with a preparation of ceria-supported nickel oxide composite by using metallo-organic network (MON) as a special template, where the metal ions of interest are mixed like in a solution. This template permits the thorough mixing of these two types of metal oxide (NiO and ceria) when their respective nuclei are generated from the pyrolysis of MON. As aresult, the interface between the two oxides is fundamentally different from those achieved by the conventional impregnation technique in terms of reactivity between different oxides. In the targeted oxide composites, i.e. the pre-catalysts, we introduced either Gd^{3+} or La^{3+} into fluorite CeO_2 lattice to examine their respective effect on the resulting catalyst, which was used to catalyse the autothermal reforming (ATR) of a surrogate fuel composed of *n*-dodecane, 10 wt.% naphthalene and 100 ppm sulphur in a micro-fixed bed reactor. We found through the structural analysis and ATR evaluation that only La^{3+} but not Gd^{3+} works as an effective dopant in this catalyst system. Lanthanum ion plays two roles in the formation of catalyst from MON: it dopes NiO in a trace dose besides ceria in almost stoichiometric amount intended, and it behaves like a surfactant, occupying the surface of ceria. These two roles can be integrated only by the MON method. It was found that 10% La-doping, i.e. $Ni/Ce_{0.9}La_{0.1}$ catalyst, greatly enhanced the fuel conversion (>90%) and hydrogen production (yield > 1.5) relative to the undoped counterpart, e.g. Ni/Ce, over a 24 h assessment. The downloaded catalysts were examined and showed that the La- doped catalyst contained the smallest Ni crystallites and nil coke deposit. Contrary to the control Ni/Ce, the water-shift reaction (WSR) catalytic activity of $Ni/Ce_{0.9}La_{0.1}$ is slightly weakened due to doping. An increase in the doping dose of La to 20% was unhelpful to the catalytic reactivity and H_2 yield, suggesting due to over coverage of La_2O_3 on the ceria support because

this blocks WSR sites. In short, the main finding of this work lies in clarification of the role of La^{3+} in the doped-ceria-supported Ni catalyst system.

CHAPTER 6

NICKEL BORATE AS A PRECURSOR OF HIGHLY REACTIVE NICKEL SPECIES AND BORON OXIDE CO-CATALYST FOR AUTOTHERMAL REFORMING OF HEAVY HYDROCARBONS

6.1 Introduction

Advancing Ni-based catalyst for reforming hydrocarbons has still been an intense research direction because of low cost and high reactivity of Ni. The existing problem lies in vulnerability of the Ni catalytic site, i.e. Ni(0) atoms with low coordination number, to carbon deposition and sulfur poisoning. As elaborated in the previous chapters, chemical modifications on the metal oxide support and on the Ni composition and structure are the two existing strategies. In this chapter, the research focused on modifying the Ni catalytic site. Most of the progresses in developing this strategy have been relying formation of Ni alloy with a selected metal. The representative examples are highlighted as follows. Modifying Ni by noble metals was of interest and effective but a lack of economic incentive is the major concern [27, 210, 211]. Regarding the use of non-precise metals to form ally with Ni, Chen et al. studied the Cu-Ni/SiO_2 catalyzed ethanol steam reforming and found that the Cu-enrich catalysts had formed an alloy structure with a Ni-enriched surface, which made the catalyst to show high conversion and stability against particle sintering [227]. Wang et al. also reported another supported alloy catalyst, which is Ni-Fe/Al_2O_3 catalyst, for steam reforming of tar [119] as a result of surface enrichment of Fe on

the Fe-Ni alloy. Quincoces and co-workers reported a Ni/Al_2O_3 catalyst modified by Mo for CO_2 reforming of methane and found that a low amount of Mo could sensibly increase the resistance to sulphur and led to less carbon deposition [201].

In contrast to these existing designs, we pursued an alternative design by which highly reactive Ni(0) species were released from a thermally very stable compound under the reforming conditions while the rest moiety of the compound left functions as stabilizer to prevent the catalytically reactive Ni(0) species from sintering or deactivating by coke deposition and sulphur adsorption. The compound was nickel borate ($Ni_3(BO_3)_2$). Furthermore, the composition of ceria support showed a clear effect on the reforming performance of the nickel borate. Meticulous structural characterizations of this Ni-based catalyst system and the assessment of its catalytic performance have been carried out. Same as the previous chapters, ATR of the surrogate liquid fuel comprising of *n*-dodecane, 10 wt% naphthalene and 100 ppm S was conducted. Besides, doped ceria was used as the support material and the interaction between the active component and support material was also investigated to explore this catalyst system.

6.2 Experimental

6.2.1 Materials

Cerium nitrate hexahydrate (Sigma Aldrich, >98%), gadolinium nitrate hexahydrate (Sigma Aldrich, >98%), yttrium nitrate hexahydrate (Sigma Aldrich, >98%), nickel nitrate hexahydrate (Sigma Aldrich, >98%), glycine (Sigma Aldrich, >99%), citric acid (Sigma Aldrich, >99%), ethylene glycol (Merck, >98%), sodium borohydride (Merck, >98%), *n*-dodecane (Sigma Aldrich, >99%), thiophene

(Merck, >99%), and naphthalene (Sigma Aldrich, >99%) were all used as received. A nickel-based SR commercial catalyst (Alfa Aesar, HiFUEL^{TM} R-110) was used as benchmark.

6.2.2 Catalyst preparation via precipitation method

The nickel borate catalysts used in this work were prepared by precipitation method. All chemicals used here were AR grade. Ceria or doped-ceria which were prepared by Pechini method [205] were used as support material. Beside ceria, gadolinium doped ceria (CGO) or yttrium doped ceria (CYO) were also used as support material. The doping level for CGO and CYO was both 10% by molar. Firstly, an aqueous solution containing various metal nitrate salts ($Ce(NO)_3 \cdot 6H_2O$, $Gd(NO)_3 \cdot 6H_2O$ or $Y(NO)_3 \cdot 6H_2O$) was prepared by stoichiometry. After that, glycine and citric acid were added, in which the molar ratio of metal ions to all the functional groups (-NH_2 and –COOH) was maintained at 0.154 and the ratio of citric acid to glycine by mass was 0.129. The concentration of the solutes was approximately 20 % by mass. The resulting aqueous solution was then mixed with 0.8 portion of ethylene glycol by volume. The mixture was thickened on a hot plate at 200 °C under stirring and a gel was obtained in the end of evaporation. The gel was then subjected to pyrolyzing at 400 °C for 2 h and calcined at 600 °C for another 2 h to remove carbon residues and to allow for the growth of crystal phase. After this, about 2 g of as-prepared oxide powders was added in about 100 mL $Ni(NO_3)_2 \cdot H_2O$ solution (0.07 M). This mixture was stirred for about 1 h to ensure a uniform dispersion and complete wetting of the oxide powders. Then a 0.21 M $NaBH_4$ solution (100 mL) was added into the above mixture drop wisely under stirring. The reaction was accomplished by mixing the two solutions and stirred overnight at room temperature. The precipitant

was separated by filtration and washed with de-ionized water and ethanol. Then it was dried in vacuum oven under 60 °C. The resulting catalyst powder was pressed into pellets and then crushed and sieved into 0.5-1 mm particles for use. These nickel borate catalysts were named as NiBO/Ce, NiBO/CGO and NiBO/CYO. The nickel content in these catalysts was about 15%. The nickel borate powder without support was also prepared for analysis.

Beside these nickel borate catalysts, another catalyst was also prepared by impregnation method as a reference. An appropriate amount of $Ni(NO_3)\cdot 6H_2O$ was dissolved in 100 ml DI water, then a certain amount of the support powder (CYO) prepared using the Pechini method described above was added into this solution. After stirring at room temperature for 2 h, the mixture was heated at 60 °C overnight under stirring to evaporate water. The obtained solid was calcined in air at 600 °C for 3 h for complete pyrolyzing of nickel nitrate. It was then molded and crushed down to granules (0.5-1 mm) for use. This catalyst was named as Ni/CYO. The nickel loading of this catalyst was also about 15%.

6.2.3 Catalyst characterization

The crystalline structures of catalysts were determined by X-ray diffractometry (XRD, SHIMADZU XRD-6000, Cu Kα radiation) using a scanning rate of 5 ° min^{-1}. The morphologies of the different catalysts were observed and recorded on a field-emission scanning electron spectroscope instrument (JEOL, JSM-6700F). The temperature-programmed reduction (TPR) was conducted on a physicochemical absorber (Quantachrome Autosorb-1 instrument)using a sample of 50 mg and a gas (5% H_2 in N_2) flow rate of 80 mL min^{-1}. The heating rate was set at 10 °C min^{-1}. The oxidation states of Ni, B and Ce in the NiP/Ce and Ni/Ce catalysts

were characterized on an instrument of X-ray photoelectron spectroscopy (XPS, Kratos Axis HiS System) equipped with Al *Kα* X-ray source (1486.6 eV) and the take-off angle of 90° with pass energy of 40 eV. C1s (284.6 eV) was used as the internal reference to calibrate the spectra obtained.

6.2.4 Experimental setup and reaction conditions

Approximately 1g catalyst (0.5-1 mm particles) was packed between two plugs of quartz wool in the centre of a quartz tube reactor (1.2 cm o.d., 1 cm i.d. and 40 cm long). The micro plug flow reactor (PFR) was then placed in a thermostat-controlled vertical tube furnace. The synthetic air (O_2/N_2) and nitrogen mixture was metered into the reactor by a mass flow controller (Alicat). The fuel (*n*-dodecane) and water streams were regulated respectively by ISO-2000 isocratic pumps and sent to combine with the synthetic air stream. The feed stream (air, fuel, and water) was led to a mixer to carry out vaporization and then to the PFR. The temperature of the mixer was set at 250 °C and a dry run in the absence of catalyst indicated that the fuel was not pyrolyzed in the mixer. The optimal reforming conditions comprising of the following parameters: fuel-supply rate = 0.02 ml min^{-1}, oxygen and steam supply rates: $O_2/C=0.5$ and $H_2O/C=3$, to reforming temperature 750 °C, and GHSV = 10,000 h^{-1}. Specifically, the PFR loaded with catalyst was heated to 750 °C under a N_2 flow and was then switched to a flow of super heated steam passing through the mixer with the aim of stabilizing the flow and packing of catalyst bed. The PFR was held under this condition for 1 h before the fuel was directed to the reactor. The outlet stream was connected to Shimadzu GC after passing a cold trap to knock out condensable components if any. After reaction, the inlet stream was switched to nitrogen to protect the catalyst under N_2 until the PFR was cooled down to room temperature. The

performance of the catalyst was assessed by fuel conversion, distribution of product gases and their yields, which were computed using the following equations where nitrogen in the synthetic air was used as internal standard:

$$\text{Conversion} = \frac{F_{total}(y_{CO} + y_{CO_2} + y_{CH_4})}{F_C \text{ in fuel}} \qquad (6.1)$$

$$\text{Yield} = \frac{F_{total} y_p}{F_p \text{ in fuel}} \qquad (6.2)$$

$$F_{total} = \frac{F_{N_2} \text{ in feed}}{y_{N_2}} \qquad (6.3)$$

where F stands for molar flow rate in mol s^{-1} and y the mole fraction of a component p (subscript) in the gas outlet stream. Theoretically, the conversion should be determined from the amount of dodecane at the exit of the reactor with respect to that at the entry of reactor. However, the fuel conversion is determined using Eq. 1 due to the limitation of analyzing the trace amounts of gaseous hydrocarbons such as methane and ethylene as well as the difficulty of quantifying a small amount of fuel trapped in the water condensation process [28]. The surrogate fuel containing 90 wt % *n*-dodecane, 10 wt% naphthalene and 100ppm S was formulated to test the coke and sulfur tolerance of the catalysts.

6.3 Results and discussion

6.3.1 Catalyst characterization

6.3.1.1 Characterization of the unsupported nickel borate powder

Figure 6.1 shows the XRD patterns of the fresh and calcined (750 °C for 2h) un-supported nickel borate powders. The fresh sample showed two broad peaks centred at 34.0 ° and 60.12° respectively. It is obvious that the fresh powder was poorly crystallized. Nevertheless, the calcined sample showed an orthorhombic XRD pattern as reported in literature [228]. In this literature, the authors defined the structure of nickel borate as $Ni_3(BO_3)_2$. In order to identify the structure, the fresh and calcined nickel borate powders were characterized by XPS. Figure 6.2 shows the Ni 2*p* and B 1*s* XPS spectra of the fresh and calcined nickel borate powders. Since the binding energy of both Ni and B did not shift after calcination, the XPS spectra could be taken as a representative to analyze the surface electronic state of nickel borate. The Ni 2p spectra showed a characteristic binding energy around 855.6 eV which could be ascribed to Ni^{2+} species [146, 210]. On the other hand, the peak around 191.7 eV was assigned to B^{3+} species[229]. It should be noted that this binding energy is lower than that of B in B_2O_3 (192.9 eV [230]). Hence, it could be speculated that Ni donated partial electrons to B, making Ni electron-deficient and B electron-enriched.

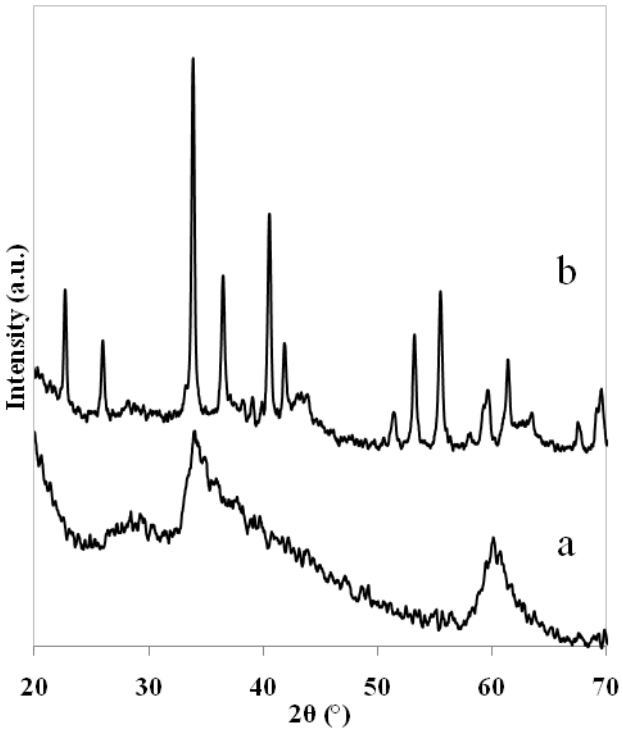

Figure 6. 1 XRD patterns of (a) fresh unsupported $Ni_3(BO_3)_2$ powder, (b) calcined unsupported $Ni_3(BO_3)_2$ powder

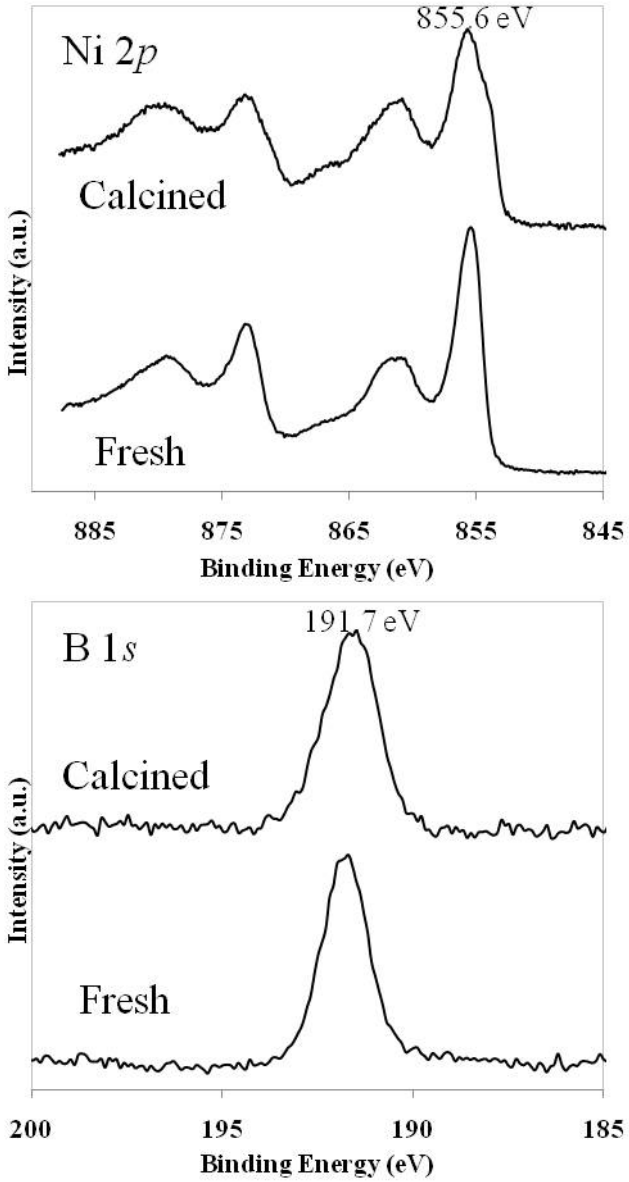

Figure 6. 2 The Ni 2*p* and B 1*s* XPS spectra of fresh and calcined $Ni_3(BO_3)_2$ powder

6.3.1.2 Structure characterization of the nickel borate catalysts

Table 6.1 summarizes the BET specific surface area of the supports and fresh catalysts. It can be seen that addition of Gd and Y onto ceria both increased its surface area. The reason could be that addition of second metal could reduce the domain size of ceria. After deposition of nickel borate, the surface area of all catalysts increased. This result would suggest that nickel borate possesses many active sites which could

preferably adsorb nitrogen molecules. And the amorphous structure of the fresh nickel borate could be porous and thus trap more nitrogen molecules. The NiBO/CGO catalyst exhibited lower surface area compared with others. For the other two nickel borate catalysts, their surface area increased twice over. This could be ascribed to the CGO support as it exhibits a lower energy surface agglomerating of nickel borate nodules. On the other hand, nickel borate has a better distribution on ceria and Y doped ceria. The surface morphologies of the fresh nickel borate catalysts were characterized by FE-SEM and the results are shown in Figure 6.3. It could be clearly seen that nickel borate clusters in NiBO/CYO catalyst had a more uniformly distributed size compared with the other two. However, nickel borate in the NiBO/CGO catalyst showed aggregated clusters. Thus it is consistent with the results obtained from BET analysis. For the Ni/CYO catalyst, its surface area decreased after deposition of nickel. This is due to the promotional effect of Ni sites behaved as centres for sintering during the calcination step [226].

Table 6. 1 BET specific surface area of the supports and fresh catalysts

Sample	BET surface area (m^2/g)
CeO_2	46
$Ce_{0.9}Gd_{0.1}O_x$ (CGO)	75
$Ce_{0.9}Y_{0.1}O_x$ (CYO)	58
NiBO/Ce	115
NiBO/CGO	96
NiBO/CYO	127
Ni/CYO	39

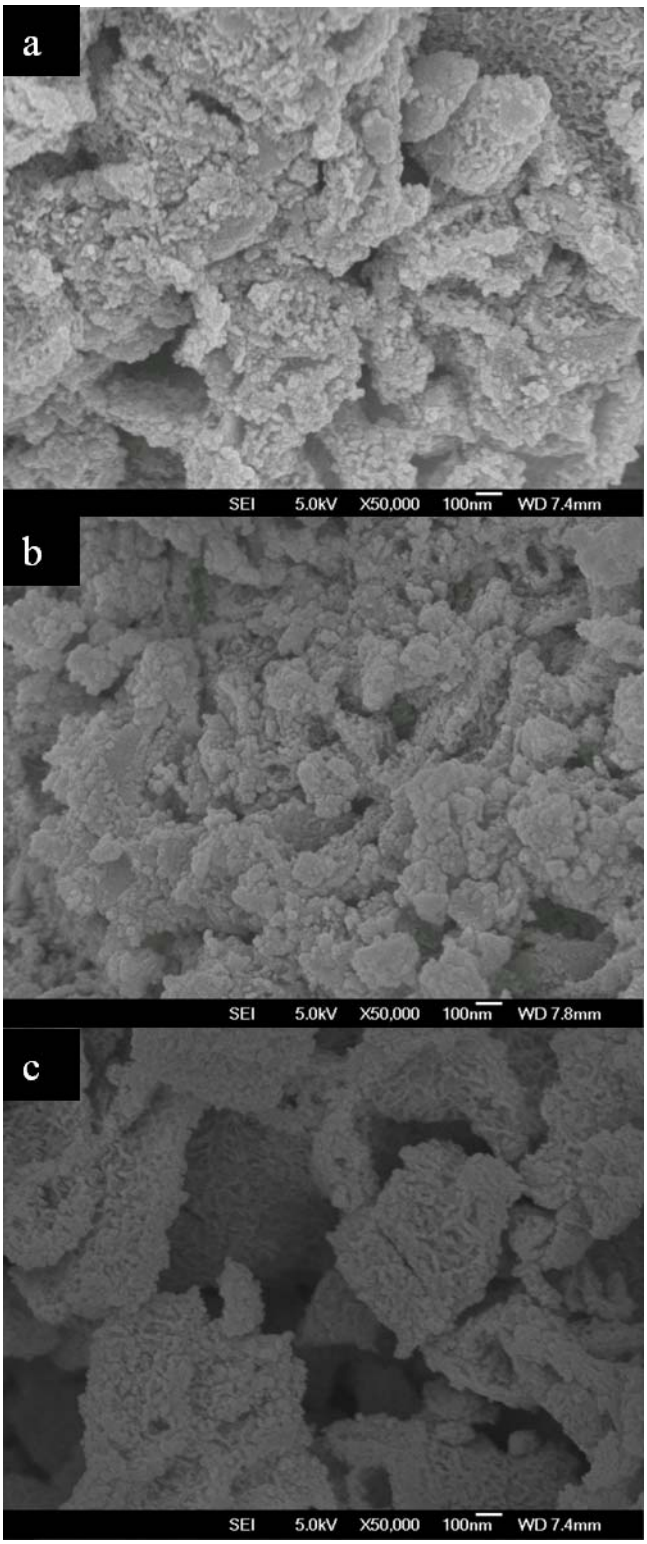

Figure 6. 3 FE-SEM images of the fresh (a) NiBO/Ce, (b) NiBO/CGO and (c) NiBO/CYO catalysts

Figure 6.4 shows the XRD patterns of the four fresh catalysts. The nickel borate catalysts did not undergo any calcination after preparation. Thus the XRD patterns of these three catalysts showed peaks solely for the supports. These XRD patterns revealed that the ceria supports possessed a fluorite-like structure (with 2θ = 28.6°, 33.1°, 47.5° and 56.4°) [94, 225]. A slight broadening effect of the XRD reflections could be seen for the doped samples. This could indicate the decrease in crystalline size, which may explain the increase in surface area of the doped supports. Also, the peaks of the NiBO/CGO catalyst slightly shifted to lower angles. This may indicate the increase in lattice parameter and demonstrate the incorporation of relatively larger Gd^{3+} ions into the ceria lattice. Nickel in the impregnated catalyst which was obtained after calcination was in oxidation state (NiO). The XRD peaks at about 37.1 ° and 43.4 ° are characteristic for Ni in NiO [231]. Figure 5.5 shows the XPS spectra of Ni and B in the fresh nickel borate catalysts. It can be seen that they show exactly the same peaks of Ni and B as that in the unsupported nickel borate powder.

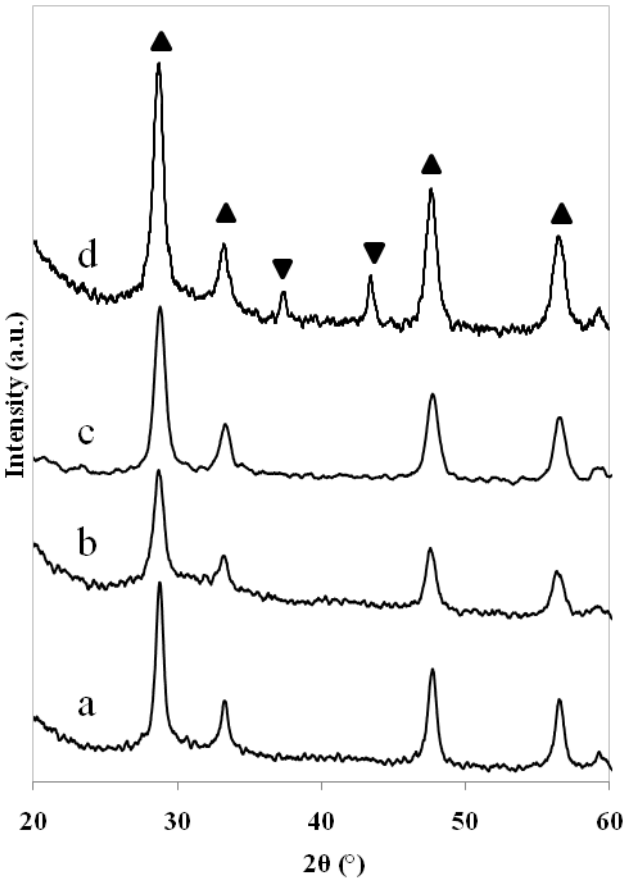

Figure 6. 4 XRD patterns of the fresh (a) NiBO/Ce, (b) NiBO/CGO, (c) NiBO/CYO and (d) Ni/CYO catalysts (▲: CeO_2; ▼: NiO)

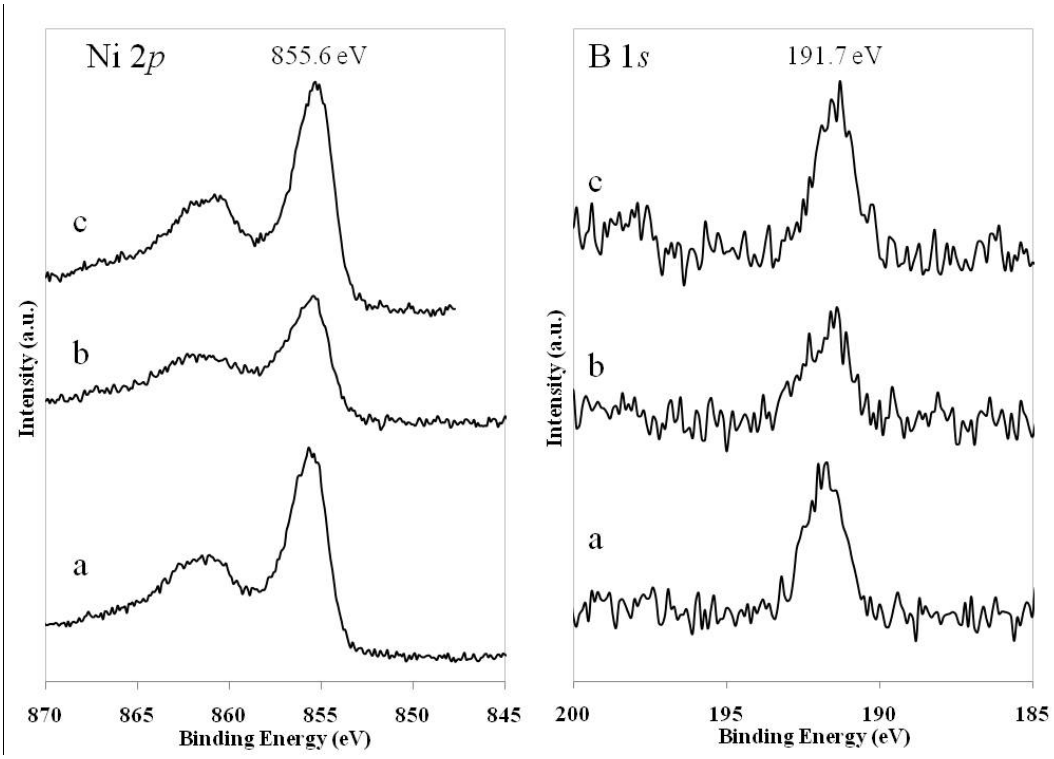

Figure 6. 5 The Ni 2*p* and B 1*s* XPS spectra of the fresh (a) NiBO/Ce, (b) NiBO/CGO and (c) NiBO/CYO catalysts

6.3.1.3 H_2-TPR of the fresh catalysts

Figure 6.6 shows the TPR profiles of the fresh catalysts. While the nickel borate catalysts showed multiple peaks, the Ni/CYO catalyst just exhibited two peaks. The small peak centred at 265 °C can be attributed to the reduction of surface NiO which was loosely bonded. The broad peak which centred at about 347 °C can be attributed to the reduction of bulk NiO which has a stronger interaction with the support [232]. As for the nickel borate catalysts, they showed broad reduction peaks for Ni species and also peaks for ceria reduction. The NiBO/Ce catalyst showed one sharp peak centred at 306 °C followed by a small shoulder peak centred at 338 °C and a broad shoulder peak centred at 383 °C; while the NiBO/CGO catalyst showed one sharp peak centred at 331 °C followed by a small shoulder peak centred at 344 °C and a broad shoulder peak centred at 415 °C. Moreover, the NiBO/CYO catalyst exhibited a sharp peak centred at 307 °C followed by a broad shoulder peak centred at 365 °C.

The sharp reduction peak could be attributed to the surface nickel borate which is loosely bonded, while the followed broad shoulder peak could be attributed to reduction of bulk nickel borate. Thus the intensity of this sharp peak could represent the dispersion of nickel borate. According to the TPR profiles, the NiBO/CGO catalyst showed weaker peak of the surface layer. This could demonstrate the result obtained in BET analysis that it had a lower specific surface area than the other two nickel borate. Beside the reduction peak of Ni, these three nickel borate catalysts also showed two peaks for reduction of ceria. The NiBO/Ce catalyst showed a stronger peak centred at 545 °C and a weak peak centred at 722 °C; while the NiBO/CGO catalyst showed a stronger peak centred at 531 °C and a weak peak centred at 705 °C. Moreover, the NiBO/CYO catalyst exhibited a stronger peak centred at 517 °C and a weak peak centred at 700 °C. The first reduction peak could be attributed to reduction of surface ceria which is loosely bonded, and the second reduction peak could be attributed to the reduction of bulk ceria [110]. It can be seen that the NiBO/CYO catalyst showed lowest ceria reduction temperature, which may indicate that ceria in this catalyst will be more easily to be reduced. It is known that oxygen transferred from ceria to react with molecules (such as CO, CH_4 and other reducing species adsorbed on the metal sites) is very essential in the ceria supported catalysts. Thus a higher reducibility of ceria could enhance the storage and transportation of oxygen in the catalyst.

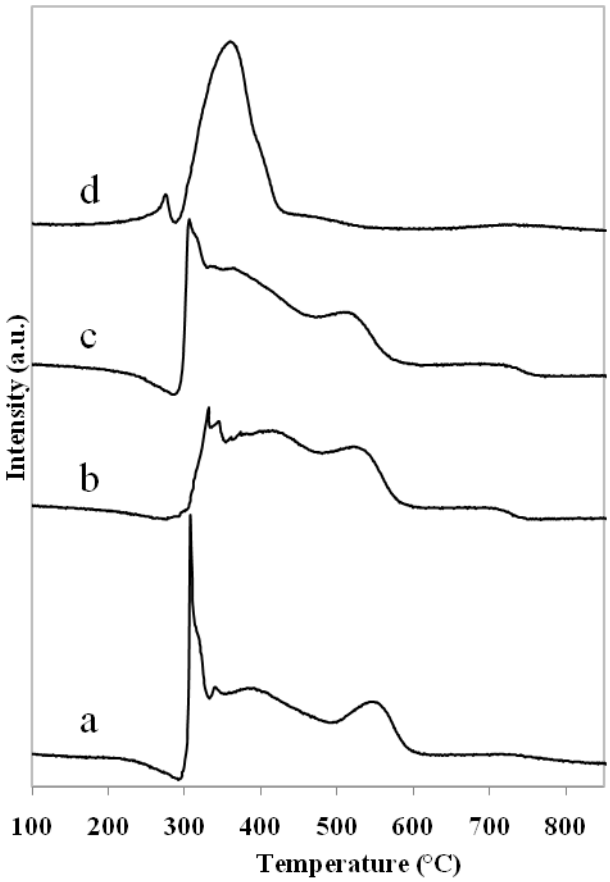

Figure 6. 6 TPR profiles of the fresh (a) NiBO/Ce, (b) NiBO/CGO, (c) NiBO/CYO and (d) Ni/CYO catalysts

6.3.2 Reaction studies

All catalysts were evaluated in ATR of the surrogate fuel, which is composed of *n*-dodecane, 10 wt% naphthalene and 100 ppm S. Figure 6.7 shows the conversions and product yields for the four catalysts. It can be seen that all catalysts maintained a high conversion around 100% in the first few hours. After that, all catalysts underwent deactivation to different extents. The CGO supported nickel borate catalyst showed worst performance and the conversion dropped to above 70% in 24 h test. However, the other two nickel borate catalysts maintained a conversion above 90% in the 24 h test. Especially the CYO supported nickel borate catalyst kept a conversion above 95% in the 24 h performance test. On the other hand, the Ni/CYO catalyst

prepared by impregnation method exhibited a much worse performance than the NiBO/CYO catalyst. Its fuel conversion quickly dropped to below 80% within 10 h but basically maintained in the following period. With respect to the hydrogen yield, its trend basically followed that of the conversion change. The NiBO/CYO catalyst maintained a hydrogen conversion around 1.5 in 24 h reaction. It should be noted that although the conversions of the NiBO/Ce and NiBO/CYO catalysts started to show difference after 12 h reaction, the difference between their hydrogen yields showed up after just 7 h reaction. It can be seen that the carbon monoxide of these two catalysts are close to each other throughout the test. The carbon dioxide yields of these two catalysts also showed difference after 7 h reaction. Thus the difference of the conversions between these two catalysts from 7 h to 12 h test was mainly due to the different methane yields which are not shown here. This could indicate that the NiBO/Ce catalyst started deactivation earlier than the NiBO/CYO catalyst.

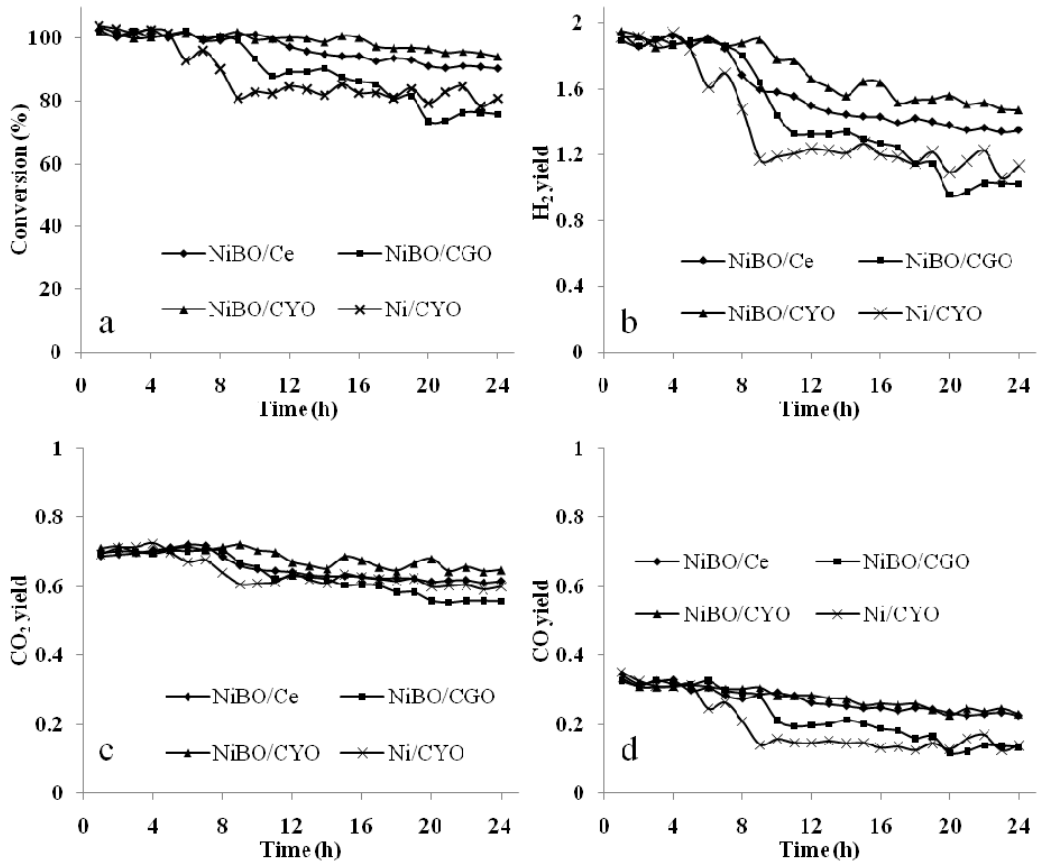

Figure 6. 7 ATR conversions and product yields vs. time on the feed comprising of *n*-dodecane, 10 wt% naphthalene and 100ppm S over various catalysts (F_{fuel}=0.02 ml min^{-1}, O_2/C=0.5, H_2O/C=3, 750 °C, GHSV=10 000 hr^{-1})

6.3.3 XRD characterization of the spent catalysts

The XRD patterns of the spent catalysts are shown in Figure 6.8. All peaks of ceria lattice became sharper after reaction, which indicates sintering of the support. A broadening effect of the XRD reflections for ceria could also be seen for the doped samples. However, these catalysts showed different XRD reflections for nickel species. Nickel in the Ni/CYO catalyst was completely reduced to Ni^0, showing characteristic peaks at 44.6 ° and 52.0 ° [233]. All the three nickel borate catalysts showed a peak at 22.9 ° which can be attributed to crystalline nickel borate. It can also be seen that the NiBO/CYO showed strongest peak intensity for nickel borate in these three catalysts. On the other hand, the NiBO/CYO catalyst showed very feeble

peak for Ni^0 which could almost be regarded as the baseline noise. Nevertheless, the NiBO/CGO catalyst showed clear characteristic peak for Ni^0 at 44.6 ° and 52.0 °. As for the NiBO/Ce catalyst, it showed both peaks for Ni^0 and Ni in NiO. This could be due to the oxidation of reduced Ni^0 species. The above results could indicate that the nickel species basically existed as nickel borate in the NiBO/CYO catalyst after reaction. However, nickel species in the other two catalysts underwent decomposition to different extent and mostly existed as Ni metal or nickel oxide after reaction.

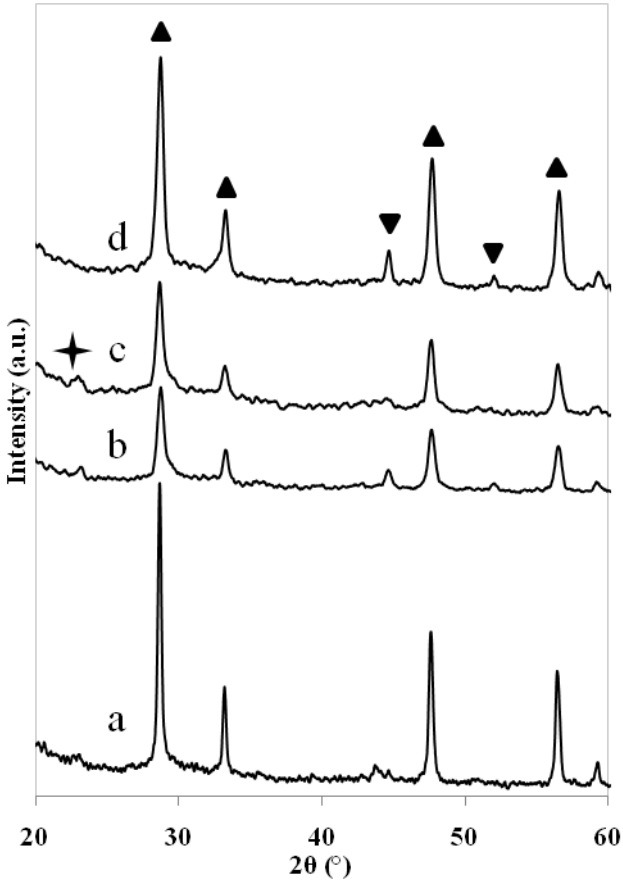

Figure 6. 8 XRD patterns of the spent (a) NiBO/Ce, (b) NiBO/CGO, (c) NiBO/CYO and (d) Ni/CYO catalysts (▲: CeO_2; ▼: Ni; +: $Ni_3(BO_3)_2$)

6.3.4 XPS characterization of the spent catalysts

The spent nickel borate catalysts were also characterized by XPS. Figure 6.9 shows the Ni 2*p* and B 1*s* XPS spectra of the spent catalysts. All three catalysts showed a peak around 191.2 eV which can be attributed to B^{3+} species. It can be seen this peak slightly shifted about 0.5 eV to lower binding energy. This would suggest that boron attracted more electrons from nickel during the reaction. As for the Ni 2p spectra, these three catalysts showed very different oxidation states. The NiBO/CGO catalyst showed a strong peak around 852.7 eV which is characteristic for Ni^0 while that peak for Ni^{2+} species became quite weak [136]. This would suggest that most nickel in this catalyst was reduced to zero valent state. The NiBO/Ce catalyst showed comparable peaks of Ni^{2+} species and Ni^0 around 856.0 eV and 852.7 eV respectively. A very small peak which can be attributed to Ni in NiO could also be seen between these two peaks. As for the NiBO/CYO catalyst, it showed very strong peak around 856.0 eV for Ni^{2+} species in nickel borate and a very tiny peak around 852.7 eV for Ni^0. This result is quite consistent with that of the XRD analysis, which indicated the existence of nickel borate structure after reaction. It should also be noted the peak for Ni^{2+} species slightly shifted to higher binding energy compared with the fresh catalysts, which could be corresponded to the boron spectra which slightly shifted to lower binding energy. Thus it could be suggested that there is a strong interaction between nickel and boron in borate group. Although nickel has an affinity to carbon and sulphur species, this interaction possibly made nickel to be occupied in advance and consequently lowered the probability of carbon and sulphur adsorption, which consequently depressed the catalyst deactivation. Another possible reason could be that carbon or sulphur species, which are electron-donating agents, would preferably adsorb on boron species since boron carries a higher positive charge compared with

nickel. As suggested by the TPR profiles which revealed the reducibility of nickel borate, it should be speculated that nickel borate was firstly reduced to Ni^0 and B_2O_3 under the reducing atmosphere. Ni^0 served as the active component under the protection of B_2O_3. But somehow Ni^0 was re-oxidized to nickel borate after reaction as a result of its highly dispersion which made it unstable as nickel metal. The NiBO/Ce and NiBO/CGO catalysts showed worse performance due to the poorer dispersion of nickel and only part of them could be re-oxidized after reaction. Especially for the Ni/CGO catalyst, it showed worst performance due to its largest extent of nickel borate decomposition.

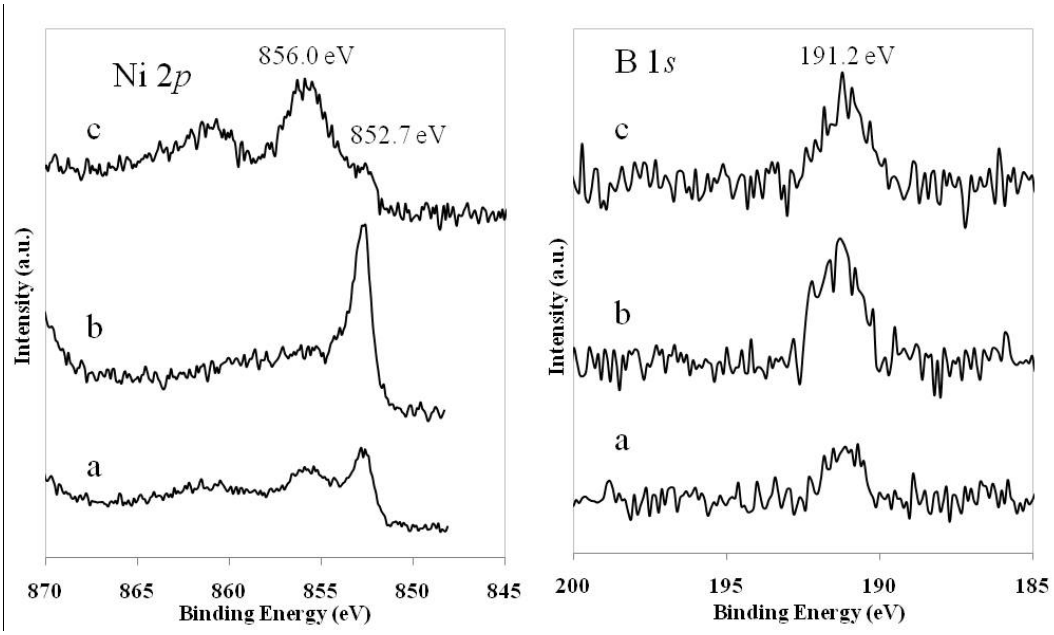

Figure 6. 9 The Ni 2*p* and B 1*s* XPS spectra of the spent (a) NiBO/Ce, (b) NiBO/CGO and (c) NiBO/CYO catalysts

The Ce 3*d* XPS spectra of the four spent catalysts were also studied and the results are shown in Figure 6.10. It can be seen that the XPS spectra for Ni/CYO catalyst before and after use were almost the same, where all the present peaks are characteristic for Ce^{4+} ions [234]. However, one characteristic peak for Ce^{4+} ions at 888.2 eV of the nickel borate catalysts became feeble after use and tended to shift to

lower binding energy. This is a clear sign of the generation of Ce^{3+} ions. This result is consistent with that obtained from the TPR analysis that ceria is easier to be reduced in the nickel borate catalysts. Thus it is reasonable to speculate that nickel borate could facilitate the reduction of ceria. This ceria reduction induced by supported active metal usually happens on supported noble metal catalysts. Our previous study demonstrated that nickel phosphide could also induce such phenomenon. However, in this work nickel borate was also found to be able to induce ceria reduction. This enhanced reducibility could probably help to remove the surface carbon species by increasing the amount of oxygen species. As shown in the FE-SEM results, the NiBO/CYO catalyst had a better nickel borate distribution compared with the other two catalysts. This would mean that the interface area between nickel borate and the support in the NiBO/CYO catalyst was also higher than the others. Thus it could be speculated that more oxygen species could be transferred to the nickel borate active sites and help to maintain a higher activity. Since this ceria reduction could only be induced by nickel borate but not nickel metal, the stability of nickel borate is very essential. This viewpoint could also be supported by the above performance results.

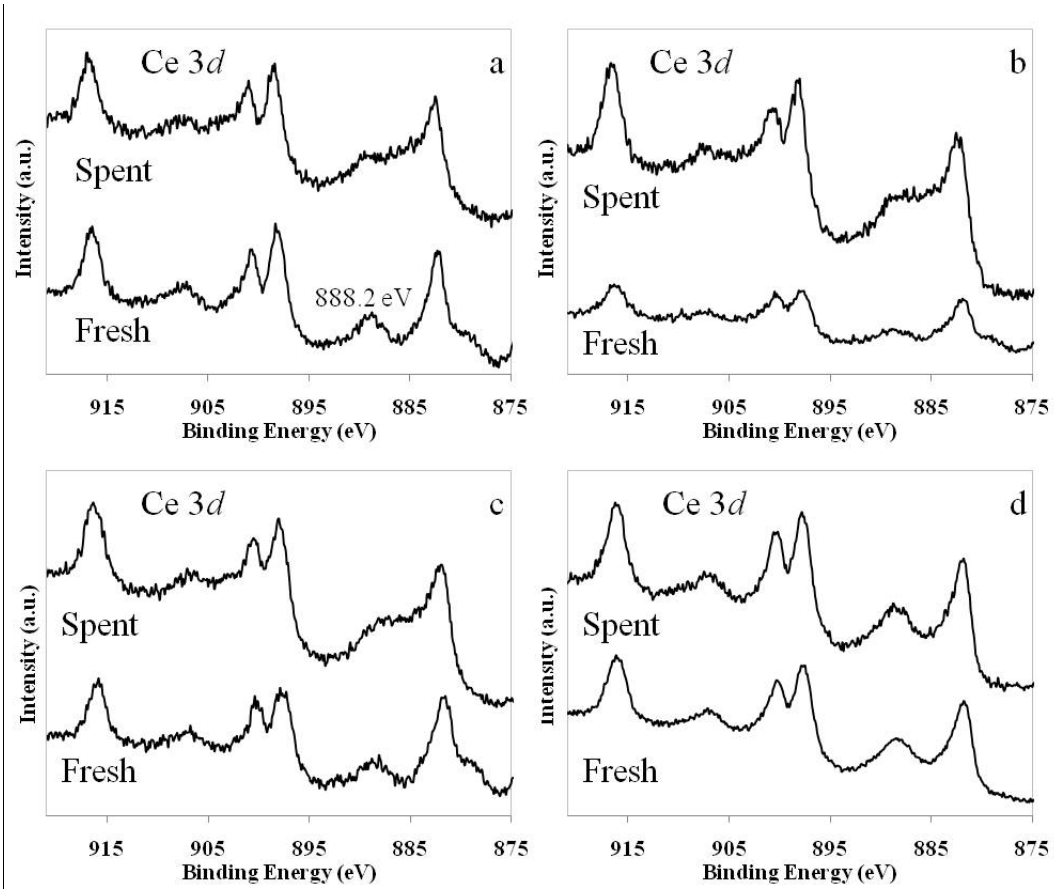

Figure 6. 10 The Ce 3*d* XPS spectra of the spent (a) NiBO/Ce, (b) NiBO/CGO, (c) NiBO/CYO and (d) Ni/CYO catalysts

6.3.5 Prolonged activity test of the NiBO/CYO catalyst

The above studies revealed that the NiBO/CYO catalyst showed good performance in ATR of this surrogate fuel in 24 h period. However, it can be seen that the conversion still kept decreasing in the 24 h testing though the rate was slow. Thus a prolonged activity test of NiBO/CYO catalyst in ATR of this surrogate fuel was carried out to study its stability. Moreover, another stability test for ATR of surrogate fuel without 100 ppm S using the same catalyst was also done in order to study the effect of sulphur on the catalyst.

Figure 6.11 shows the conversions and product yields of the NiBO/CYO catalyst in ATR of different fuels. It can be seen that the NiBO/CYO catalyst

maintained a high conversion (>95%) in the first 36 h reaction at the present of sulphur. However, a rapid conversion drop occurred in the following period. The conversion dropped to about 70% after 48 h reaction. On the other hand, the fuel conversion in the absence of sulphur maintained close to 100% in the first 40 h reaction. Then it slightly decreased to around 95% after 48 h reaction. Thus it is obvious that sulphur in the surrogate fuel was the primary component that caused catalyst deactivation. As for the hydrogen yields, the difference between these two trials is much larger than that expected from the difference of fuel conversions. Although the fuel conversion at the present of sulphur in the first 36 h reaction was just slightly lower than that without sulphur, its hydrogen yield is much lower than the other trial. It is apparent that sulphur severely suppressed the production of hydrogen. It should be noted that although the fuel conversion kept above 95% in the 48 h reaction at the absence of sulphur, its hydrogen yield still decreased a lot in the second half the testing period. This could suggest that catalyst also underwent deactivation to some extent even when only naphthalene was present. It's just the effect was less severe than sulphur. The comparison of carbon dioxide and carbon monoxide yields also showed a higher value for the fuel without sulphur. According to the above results, it can be seen that sulphur poisoning played a more important role in the deactivation of NiBO/CYO catalyst.

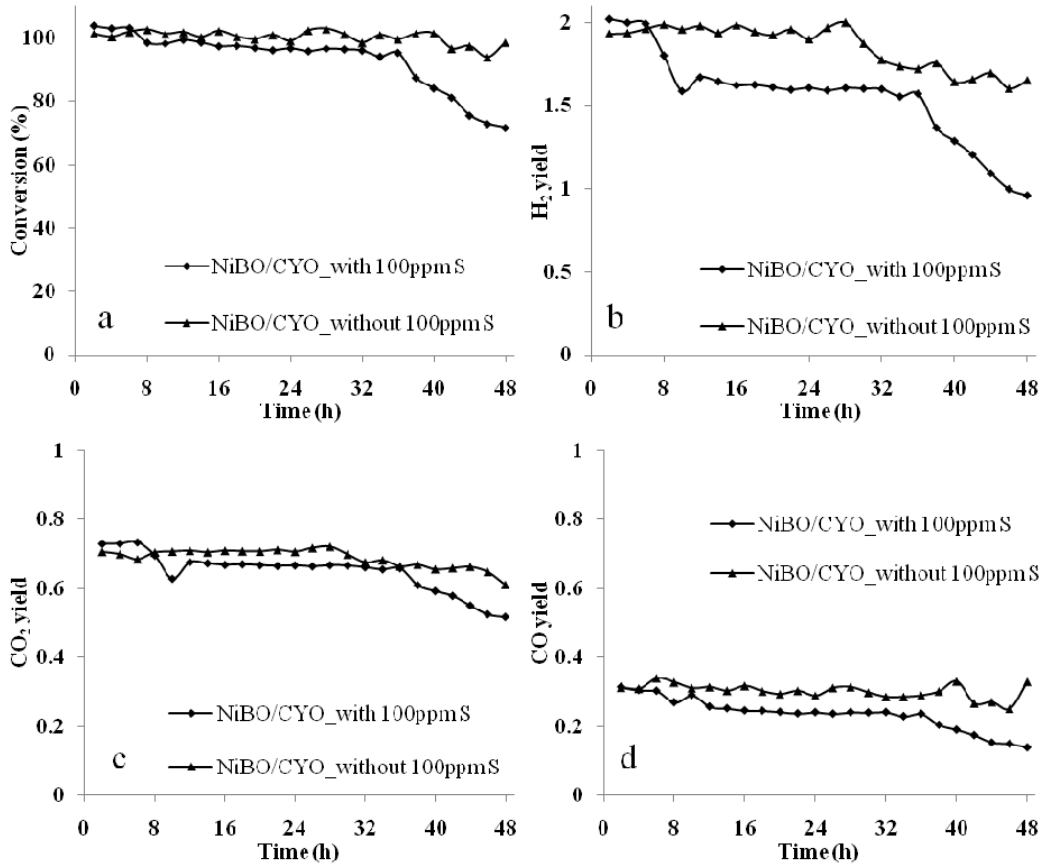

Figure 6. 11 ATR conversions and product yields vs. time for the NiBO/CYO catalysts in fuel with and without 100ppm S (F_{fuel}=0.02 ml min^{-1}, O_2/C=0.5, H_2O/C=3, 750 °C, GHSV=10 000 hr^{-1})

6.3.6 Characterization of the catalysts after prolonged activity test

The catalysts spent in ATR of those two fuels were firstly characterized by XRD and the results are shown in Figure 6.12. Both the catalysts showed characteristic peak for crystalline nickel borate at 22.9 °. This peak is stronger for the catalyst used in the fuel without sulphur, indicating a higher amount of nickel borate remained in the catalyst after reaction. The NiBO/CYO catalyst spent in ATR of fuel with sulphur strong and sharp peaks at 44.6 ° and 52.0 ° which are characteristic for Ni^0. On the other hand, the catalyst spent in ATR of fuel without sulphur showed wide and faint peaks for Ni^0. This result would suggest that nickel species in the catalyst underwent different extent of sintering under a prolonged test period which

changed its dispersion. Consequently more nickel will exist as Ni^0 in the spent catalyst while only part of them could be re-oxidized to nickel borate. It is also obvious that sulphur has a more vital effect on the catalyst. The XRD peak for Ni^0 is much wider for the sulphur free fuel, indicating a much smaller crystalline size. Therefore, although the Ni^0 particles were not small enough to be re-oxidized, they still possess a much higher dispersion for the sulphur free fuel.

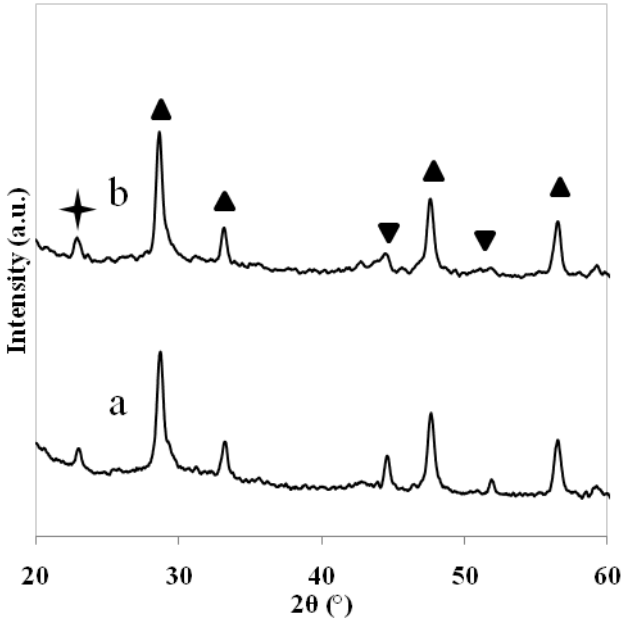

Figure 6. 12 XRD patterns of the spent NiBO/CYO catalysts in ATR of fuel (a) with 100ppm S, (b) without 100ppm S (▲: CeO_2; ▼: Ni; +: $Ni_3(BO_3)_2$)

These two spent catalysts were also characterized by XPS. Figure 6.13 shows the Ni2*p* and B1*s* XPS spectra of the spent catalysts. It can be seen that both catalysts showed a peak around 191.3 eV which can be attributed to B^{3+} species. Similar to above results, it also slightly shifted to lower binding energy. As for the Ni species, the catalyst spent in fuel with sulphur showed a strong peak around 852.7 eV which is characteristic for Ni^0 and a very weak peak for Ni^{2+} species. These results are quite consistent with the XRD patterns. This would suggest that nickel in this catalyst was almost completely reduced to Ni^0. This result could probably explain the deactivation

of the catalyst. On the other hand, the catalyst spent in fuel without sulphur showed a stronger peak around 856.0 eV for Ni^{2+} species and s smaller peak around 852.7 eV for Ni^0. This could indicate the smaller degree of nickel borate decomposition in this catalyst, which is consistent with the partial activity loss of the catalyst. The above results could confirm the claim that the dispersion of nickel species plays a key role in the catalytic performance.

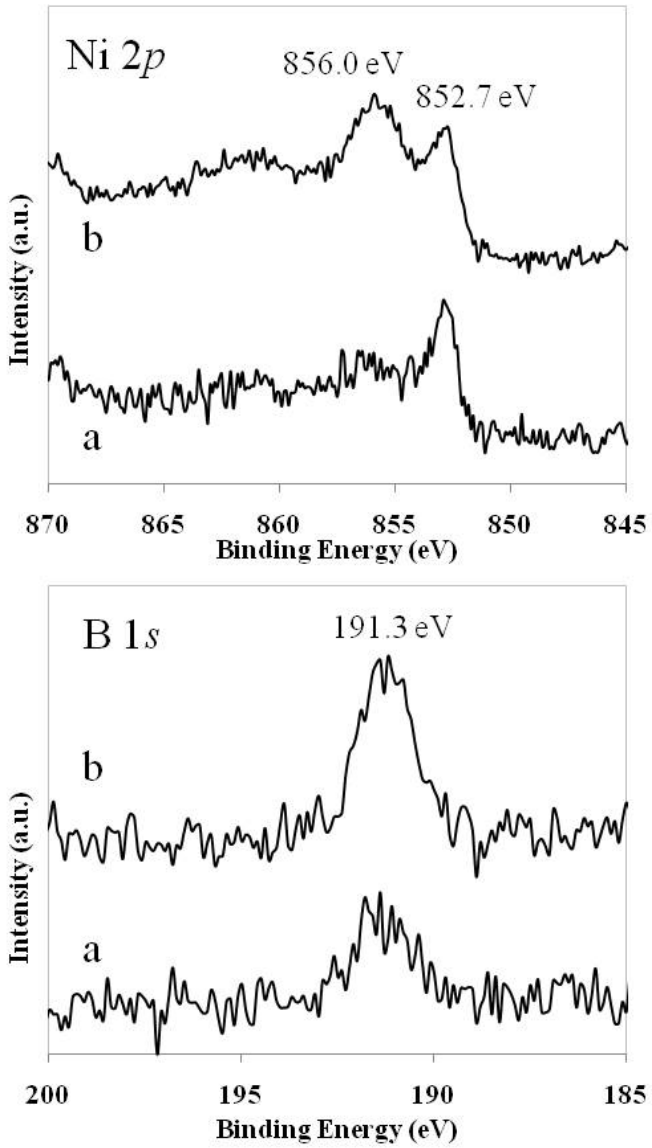

Figure 6. 13 The Ni 2*p* and B 1*s* XPS spectra of the spent NiBO/CYO catalysts in ATR of fuel (a) with 100ppm S, (b) without 100ppm S

Also shown in Figure 6.14 are the Ce 3*d* XPS spectra of the spent catalysts. Similar to above results, one characteristic peak for Ce^{4+} ions at 888.2 eV of the spent nickel borate catalysts became feeble after use and tended to shift to lower binding energy. This is a clear sign of the generation of Ce^{3+} ions. This effect is more obvious for the catalyst spent in fuel without sulphur that a new peak is likely to form around 885.9 eV which is characteristic for Ce^{3+} ions. This could further demonstrate that nickel borate induced this ceria reduction since more nickel borate in this catalyst was restored than the other.

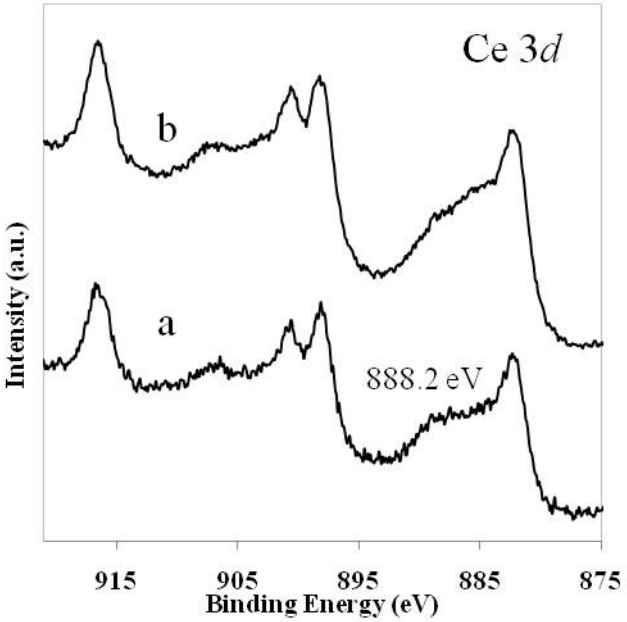

Figure 6. 14 The Ce 3*d* XPS spectra of the spent NiBO/CYO catalysts in ATR of fuel (a) with 100ppm S, (b) without 100ppm S

It can be seen that the dispersion of nickel species was very essential to the performance of the catalyst. It seems that sulphur has more vital effect on the catalyst deactivation. The reason could be that sulphur would preferably attack boron in boron oxide since it bears higher positive charge. It was reported that B could serve as sponge for S and also neutralize the electron donating agent S^{2-} [235]. Thus B^{3+} in the boron oxide would be more intended to adsorb sulphur. Although this would protect

nickel from being attacked, it could interrupt the interaction between nickel and boron and consequently leave the nickel particles to be alone and unprotected. In the initial stage (a shorter reaction time like less than 24 h), this adsorption of sulphur on boron species could be removed by the oxygen species transferred from the support material. However, sulphur compound goes through the catalyst bed at a constant rate while the transportation rate of oxygen species would decrease. This is due to the sintering of both nickel species and ceria support which would result a reduced interface area and thus a decreased oxygen species transportation rate. Therefore, as time goes on, the removing rate of adsorbed sulphur by the transferred oxygen species would decrease and sulphur would accumulate on boron species. And this will finally result isolation of boron species from Ni. As long as Ni is exposed to the reaction atmosphere, it will be quickly attacked by carbon and sulphur and cause catalyst deactivation. The interaction between Ni and boron could be proved by the XPS results. The unsupported nickel borate powder was reduced in a 5% H_2/He flow and the XPS analysis showed that this compound was completely reduce to Ni metal and B_2O_3. This could be demonstrated by the XPS results where boron exhibited a characteristic peak around 193.8 eV for B^{3+}. However, it can be seen that boron in the spent catalyst showed a peak around 191.3 eV which is lower than that in B_2O_3, indicating a higher electron density which is probably a result of Ni-boron interaction. Once this interaction was interrupted, Ni will undergo sintering and deactivation. And the coverage of boron species by sulphur would also prevent its combination with Ni. The most possible reason for this could possibly be attributed to the oxygen species transferred from the ceria support which helped to keep the surface clean and protect this interaction between Ni and boron. Nevertheless, ceria reduction could be solely induced by Ni-boron complex but not Ni metal itself as proved in previous section.

Thus a perfect redox cycling formed between these two components: Ni-boron complex helped to induce ceria reduction and enhanced the transportation of oxygen species; this enhanced transportation of oxygen species helped Ni-boron complex to maintain their interaction and resist carbon and sulphur adsorption. Actually there is one point which is interesting that Ni-boron complex served as active component in this catalyst. Usually boron was reported to exist as boride to promote the active metals in catalysts used for methane steam reforming [51], Fisher-Tropsch reaction [235] or sulfolene hydrogenation [173], etc. Compared with boride compound, the boron oxide has a stronger interaction with nickel. The high positive charge of boron on boron oxide would also make it more attractive to carbon or sulphur and avoid blocking nickel sites. Moreover, the relatively large boron oxide groups could possibly impede larger molecules like sulphur species from adsorption to nickel sites. What more important is that this Ni-boron complex could induce ceria reduction which has never been reported before.

6.4 Conclusions

Ceria supported nickel borate catalysts were studied in ATR of surrogate fuel composing of *n*-dodecane, 10 wt% naphthalene and 100 ppm S. Three types of supports, ceria, Gd doped ceria (CGO) and Y doped ceria (CYO, both 10 mol% doping) were studied. The results revealed that the CYO supported nickel borate catalyst showed best performance of the three catalysts in 24 h reaction study. Another reference Ni catalyst prepared by impregnation method using CYO as support was also tested and showed much poorer performance that the CYO supported nickel borate catalyst. The XRD and XPS analysis revealed relation between the amount of reserved nickel borate after reaction and the catalytic

performance of the catalysts. The CYO supported nickel borate catalyst showed almost no Ni metal in 24 h reaction study while the other two showed existence of Ni metal in different extent. The different amount of reserved nickel borate could probably stands for different levels of nickel dispersion, which is related to the activity of the catalysts. However, the prolonged activity test of the CYO supported nickel borated catalyst showed fast deactivation after 40 h reaction. Meanwhile, this catalyst evaluated in the surrogate fuel without sulphur showed good performance in 48 h reaction study. Similarly, different amount of reserved nickel borate was found in these two catalysts where the present of sulphur resulted a complete catalyst deactivation. The mechanism behind this result could be attributed to the redox cycling between Ni-boron complex and the doped-ceria support. Ni-boron complex helped to induce ceria reduction and enhanced the transportation of oxygen species; this enhanced transportation of oxygen species helped Ni-boron complex to protect their interaction and resist carbon and sulphur adsorption. However, this balance could be upset due to sintering of both ceria support and Ni-boron complex which would result decreased oxygen species transportation. Finally the interaction between Ni and boron would be interrupted and cause severe catalyst deactivation.

CHAPTER 7

CONCLUSIONS AND RECOMMENDATIONS

7.1 Conclusions

Due to the low cost and high activity of Ni metal, it is of great interest as the catalyst used in catalytic autothermal reforming process for the production of hydrogen, a promising alternative fuel in the future. However, development of a catalytically active and stable reforming catalyst represents the challenging issue to this reaction system because of the presence of heavy and branched aliphatic hydrocarbons, aromatics and organosulfur compounds in the liquid hydrocarbon fuels. These ingredients bring about carbon deposition and sulphur poisoning on catalytic sites that all ruin the performance of catalyst. This project studies ceria supported Ni-based catalysts for ATR of liquid hydrocarbons. On the basis of this recent progress, three types of ceria or doped ceria-supported nickel-based catalysts were prepared and evaluated in the ATR of proxy fuel in this thesis. The design of these catalysts was based on the deactivation mechanism of nickel catalysts as described before. Basically two types of designing principles were considered: one is to modify the Ni active sites by the addition of a second component; the other is the adoption of ceria or doped-ceria as the support material. For the first principle, nickel phosphide and nickel borate were selected to be the active components in the catalysts. The use of ceria or doped ceria as support of Ni has alleviated the deactivation trend due to the oxygen conducting trait of the doped ceria.

1) The first catalytic system is ceria-supported nickel phosphide (Ni_xP_y), which was firstly prepared by electroless nickel deposition of nickel-phosphorous

alloy grains on particles of a commercial ceria. The NiP was then in-situ formed from the alloy in the initial stage of ATR. The ENP process is a good way to prepare highly well mixed nickel-phosphorous alloy as mentioned before. Thus it was used in this work to prepare the nickel phosphide catalyst. The commercial ceria used in this part was very dense probably because it was calcined under very high temperature. Thus it possessed a very low specific surface area as well as a relatively smooth surface morphology as observed from the FESEM images. In order to enhance its specific surface area and the roughness of its surface, it was pre-treated by precipitation of ceria o its surface prior to the ENP process. The BET analysis and FESEM images showed that this pretreatment process effectively enhanced its specific surface area and also its surface roughness. This effect of pretreatment could also be seen during the sensitization-activation step of the ENP process. Good adhesive of palladium nuclei was observed after the pre-treatment process.

The catalyst was used to reform pure *n*-octane and the surrogate gasoline fuel composed of *n*-octane and naphthalene (6 wt%). A commercial Ni-based steam reforming catalyst and a ceria supported nickel catalyst prepared by traditional impregnation method were used as benchmark. The reaction conditions such as temperature, oxygen-to-carbon ratio, and steam-to-carbon ratio were optimized first. These three catalysts all showed superior catalytic performance in ATR of pure *n*-octane, and the fuel conversion for the commercial catalyst was even slightly higher than the other two. However, the FESEM images revealed that carbon whiskers could only be seen on the catalyst prepared by impregnation method. When the surrogate gasoline fuel was used as the feed, these three catalysts also showed good but similar catalytic performance. This time, the FESEM images showed that carbon whiskers could be seen on both the catalyst prepared by impregnation method and the

commercial catalyst while the nickel phosphide catalyst exhibited nil coking extent after reforming the surrogate fuel.

The NiP crystallites were characterized by XRD and the charge distribution of its Ni-P bond was examined by XPS. The XRD results demonstrated the existence of nickel phosphide in the catalyst, which may indicate that it served as the active component in the catalyst. The XPS analysis revealed that the Ni carries slightly higher negative charge than the Ni^0 as usually observed while P carries slightly lower positive charge than P^0. This would prove the modification effect of the alloying element to the Ni metal. The increased electron density of Ni would probably lower down it affinity to the carbon atoms, which will effectively prevent the polymerization of atomic carbon. The XPS investigation also divulged the presence of Ce^{3+} species in the ceria support on which the NiP crystallites were distributed, indicating that the support contained oxygen vacancies. This ceria reduction could also be demonstrated by the TPO analysis where the profile of the spent nickel phosphide catalyst showed a strong peak at around 900 °C which can be attributed to the oxidation of Ce^{3+} species. It should also be noted that this ceria reduction after reaction could only be seen for this nickel phosphide catalyst. The catalyst prepared by the impregnation method did not show any peak for the Ce^{3+} species in the XPS spectra. According to the above results, it is believed that these two subtle structural differences could be proposed to provide the nickel phosphide catalyst with resistance to carbon deposition.

The above NiP catalyst was modified by using in-house made ceria, which was synthesised by the Pechini method and hence possessed a higher surface area than the commercial one. Thus the nickel phosphide loading on this catalyst was also

enhanced. Beside ceria, the Gd-doped ceria was also prepared as support. A surrogate diesel fuel, comprising of *n*-dodecane, 10 wt% naphthalene and 100 ppm S (from thiophene) was formulated for examining the ATR catalytic performance of the above two catalysts, NiP/Ce and NiP/CGO. The commercial catalyst was also used a benchmark here. The reaction studies showed that these three catalysts showed good performance in the ATR of pure *n*-dodecane. However, when the surrogate diesel fuel was used as the feed, all catalysts showed deactivation along time. Among them, the commercial catalyst showed worst performance while the Ni/Ce catalyst showed slightly better performance than the Ni/CGO catalyst.

The TGA analysis showed that no carbon was deposited on the NiP/Ce catalyst while the commercial catalyst contained about 5 wt% deposited carbon. As for the NiP/CGO catalyst, the FESEM images revealed a severely carbon deposited top layer of the catalyst bed and a carbon free lower layer catalyst bed. These results could indicate that the NiP/Ce had a good carbon resistance compared with others. The XPS analysis of these two nickel phosphide catalysts revealed the reduction of ceria for both catalysts. However, the NiP/Ce catalyst showed a much stronger and clearer characteristic peaks for Ce^{3+} species than the NiP/CGO catalyst. This could indicate that the reducibility of ceria in these two catalysts was different. The TPR profiles also demonstrated this point. Thus it could be suggested that it is this difference in ceria reducibility that resulted different carbon resistance of these two catalysts. It is obvious that doping ceria by 10 mol% Gd noticeably repressed the Ce^{3+} concentration in the support. The Ce^{3+} ions present at the surface of catalyst support act to sustain water-gas shift reaction as well as to enhance the stability of catalytic reactivity. It should be noted that the enhanced reducibility of ceria is usually induced by the noble metals as reported. But here the nickel phosphide also had such effect.

2) The second catalytic system was developed using the following strategy: from homogeneous metallo-organic gel to a biphasic oxide mixture where the phase separation and formation of the two metal oxides ($La_xCe_{1-x}O_{2-\delta}$ and NiO) took place simultaneously. As mentioned above, the Pechini method could ensure a very high extent of compositional uniformity in a multicomponent metal oxide. This is because the distributional uniformity of the metal ions in the hydrogel precursor is very close to that in the homogeneous aqueous solution. As a result, the minor NiO phase was extremely uniformly distributed in the dominant phase $La_xCe_{1-x}O_{2-\delta}$ and the Ni^0 particles generated from the reduction of NiO were closely imbedded in the $La_xCe_{1-x}O_{2-\delta}$ phase. The Ni^0 particles thus prepared have complete different chemical environments from those made by impregnation method. The $Ni/La_xCe_{1-x}O_{2-\delta}$ catalysts were used to operate ATR of the surrogate diesel fuel, comprising of *n*-dodecane, 10 wt% naphthalene and 100 ppm S (thiophene). The output showed that doping the support $La_xCe_{1-x}O_{2-\delta}$ with 10% La ($x = 0.1$) remarkably enhanced the catalytic activity. An increase in La^{3+} doping to 20% resulted in a slight reduction in the fuel conversion but an apparent loss of the hydrogen yield. The La-doping effect is three-fold on the basis of the structural analysis of X-ray diffraction (XRD), transmission electron microscopy (TEM), and temperature programmed reduction (TPR): the miniaturization of Ni^0 crystallite, the decrease in domain sizes of ceria, and the stimulation of oxygen vacancies in the support.

3) The third catalytic system combined doping the ceria support by Y and hybridizing the Ni catalyst by boron species with the aim of improving resilience of the catalyst against deactivation effects. This catalyst was prepared by precipitation of nickel borate ($Ni_3(BO_3)_2$) on the doped-ceria support synthesised by Pechini method. The freshly prepared nickel borate has an amorphous structure, but will convert to

crystalline structure under high temperature calcination. The resulting catalyst was examined in ATR of the surrogate diesel fuel same as above. Beside Y doped ceria, ceria and Gd-doped ceria were also used as the support materials for comparison. An Y^{3+} doped ceria supported nickel catalyst prepared by impregnation method were used as benchmarks.

These four catalysts showed quite different performance in the reaction study. The Gd-doped ceria supported nickel borate catalyst showed the worst performance of the four while the Y-doped ceria supported nickel borate catalyst showed best performance in 24 h test (fuel conversion>95%). The XRD and XPS analysis revealed different structures of the nickel borate catalysts after reactions. It was found that nickel borate underwent different extent of decomposition in these three catalysts. Nickel borate in the Gd-doped ceria supported catalyst almost completely decomposed to Ni metal and boron oxide, while the nickel borate in the Y-doped ceria supported catalyst only underwent slight extent of decomposition. These characterizations could indicate that Ni-boron complex served as the catalytically active component and was responsible to the high activity. The catalytic activity of Ni-boron complex was even higher than that of the Ni metal as can be seen from the reaction studies. The XPS analysis also revealed that nickel borate induced generation of Ce^{3+} ions in the ceria support, which cannot be seen in the catalyst prepared by impregnation method. However, the extension of activity assessment duration showed a fast drop in performance after 40h for the Y-doped ceria supported nickel borate catalyst. On the other hand, if the fuel only consisted of *n*-dodecane and 10 wt% naphthalene, the catalyst still retained high activity in the test up to 50 h. The XPS and XRD analyses revealed the cause for the loss of catalytic activity when the fuel contained sulphur: degradation of nickel borate to Ni^0. On the contrary, nickel borate

basically survived after reaction in the absence of sulphur in the fuel. It is clear that the boron species of the catalyst was etched by sulphur through certain mechanism and hence the Ni^0 left alone became susceptible to coking and sulphur adsorption. The mechanism behind this result could be attributed to the redox cycling between nickel borate and the doped-ceria support. Nickel borate helped to induce ceria reduction and enhanced the transportation of oxygen species; this enhanced transportation of oxygen species helped to protect the interaction between Ni and boron and also resist carbon and sulphur adsorption. However, this balance could be upset due to sintering of both ceria support and nickel borate which would result decreased oxygen species transportation.

7.2 Suggestions of the future work

On the basis of the above results of this study, the following recommendations are considered relevant to the future research on the development of stable catalysts for catalytic reforming of liquid hydrocarbon fuels and also improving the fuel processing:

1) Employing nano sized ceria as the support material. As can be seen from the results of this thesis work, ceria played an essential role in promoting the resistance to carbon deposition and sulphur poisoning of the reforming catalysts. The promotion effect of ceria arises from its oxygen storage capacity and oxygen conduction ability. Thus the interfacial area between the ceria support and the supported active metal could remarkably influence the catalyst performance. A stronger interaction between the support and the active metal would for sure enhance the oxygen transportation to the catalyst surface, thus could facilitate the catalysts

resistance to deactivation. Therefore, it is necessary to prepare the ceria support in nano size and maybe also in different shape.

2) Stabilizing the crystalline nickel borate catalyst. The nickel borate catalyst showed superior catalytic performance in ATR of the surrogate fuel in certain time period. However, it may undergo decomposition after longer time exposing to the sulphur containing fuel. Thus it would be meaningful to stabilize the nickel borate catalyst to maintain its high activity. The possible approach could be calcining the fresh catalyst under a temperature higher than the reaction temperature. After this treatment, it is possible that it will not decompose and persist a longer time. But this approach should be better to conducted using nano sized doped-ceria as the support material. This is because calcination under a higher temperature will result higher degree of sintering and thus a loss of partial activity. Thus if the specific area of the fresh catalyst is high enough, which also means that the dispersion of the active sites is good enough, the left activity after calcination could still be good enough for use.

3) Improve the fuel processing technology. In this work, the liquid fuel was delivered to the reactor using a HPLC pump and an evaporator. For hydrocarbon fuels with lower boiling temperature, this method has no problem in fuel delivery. However, when heavier fuel is employed, it may undergo pyrolysis in the evaporator and deposit carbon in it. This may result the loss of fuel as well as the blocking of the evaporator. In order to solve this problem, it is better to use an intense nozzle in front of the reactor. In this case, the liquid fuel will be sprayed in to tiny droplet with high speed going into the reactor. These high speed droplets will be quickly vaporized at the inlet section of the catalyst bed then go through the catalyst bed. This method could be considered as the best way to process those heavy fuels in laboratory study.

Literature Cited

[1] S Sa,H Silva,L Brandao,JM Sousa, A Mendes, Catalysts for methanol steam reforming--A review, Appl. Catal., B, 99 (2010) 43-57.

[2] D Ashok S, Hydrogen production by reforming of liquid hydrocarbons in a membrane reactor for portable power generation-Model simulations, J. Power Sources, 180 (2008) 516-529.

[3] DG Loffler,K Taylor, D Mason, A light hydrocarbon fuel processor producing high-purity hydrogen, J. Power Sources, 117 (2003) 84-91.

[4] S Ahmed, M Krumpelt, Hydrogen from hydrocarbon fuels for fuel cells, Int. J. Hydrogen Energy, 26 (2001) 291-301.

[5] Y Choi, HG Stenger, Fuel cell grade hydrogen from methanol on a commercial $Cu/ZnO/Al_2O_3$ catalyst, Appl. Catal., B, 38 (2002) 259-269.

[6] DL Hoang,SH Chan, OL Ding, Hydrogen production for fuel cells by autothermal reforming of methane over sulfide nickel catalyst on a gamma alumina support, J. Power Sources, 159 (2006) 1248-1257.

[7] J Sun,X Qiu,F Wu,W Zhu,W Wang, S Hao, Hydrogen from steam reforming of ethanol in low and middle temperature range for fuel cell application, Int. J. Hydrogen Energy, 29 (2004) 1075-1081.

[8] JJ Strohm,J Zheng, C Song, Low-temperature steam reforming of jet fuel in the absence and presence of sulfur over Rh and Rh-Ni catalysts for fuel cells, J. Catal., 238 (2006) 309-320.

[9] I Kang,J Bae, G Bae, Performance comparison of autothermal reforming for liquid hydrocarbons, gasoline and diesel for fuel cell applications, J. Power Sources, 163 (2006) 538-546.

[10] M Rezaei,F Meshkani,AB Ravandi,B Nematollahi,A Ranjbar,N Hadian, Z Mosayebi, Autothermal reforming of methane over Ni catalysts supported on nanocrystalline MgO with high surface area and plated-like shape, Int. J. Hydrogen Energy, 36 (2011) 11712-11717.

[11] J Rostrup-Nielsen, DL Trimm, Mechanisms of carbon formation on nickel-containing catalysts, J. Catal., 48 (1977) 155-165.

[12] CH Bartholomew,PK Agrawal,JR Katzer,HP D.D. Eley, BW Paul, Sulfur Poisoning of Metals, in: Adv. Catal., Academic Press, 1982, pp. 135-242.

[13] JAC Dias, JM Assaf, Autothermal reforming of methane over Ni/r-Al_2O_3 promoted with Pd: The effect of the Pd source in activity, temperature profile of reactor and in ignition, Appl. Catal., A, 334 (2008) 243-250.

[14] S Yoon,I Kang, J Bae, Suppression of ethylene-induced carbon deposition in diesel autothermal reforming, Int. J. Hydrogen Energy, 34 (2009) 1844-1851.

[15] S Araki,N Hino,T Mori, S Hikazudani, Durability of a Ni based monolithic catalyst in the autothermal reforming of biogas, Int. J. Hydrogen Energy, 34 (2009) 4727-4734.

[16] AB Shigarov,VV Kireenkov,VA Kuzmin,NA Kuzin, VA Kirillov, Autothermal reforming of diesel fuel in a structured porous metal catalyst: Both kinetically and transport controlled reaction, Catal. Today, 144 (2009) 341-349.

[17] A Qi,S Wang,G Fu, D Wu, Autothermal reforming of *n*-octane on Ru-based catalysts, Appl. Catal., A, 293 (2005) 71-82.

[18] BJ Dreyer,IC Lee,JJ Krummenacher, LD Schmidt, Autothermal steam reforming of higher hydrocarbons: *n*-Decane, *n*-hexadecane, and JP-8, Appl. Catal., A, 307 (2006) 184-194.

[19] A Qi,S Wang,C Ni, D Wu, Autothermal reforming of gasoline on Rh-based monolithic catalysts, Int. J. Hydrogen Energy, 32 (2007) 981-991.

[20] PK Cheekatamarla, AM Lane, Catalytic autothermal reforming of diesel fuel for hydrogen generation in fuel cells: I. Activity tests and sulfur poisoning, J. Power Sources, 152 (2005) 256-263.

[21] N Laosiripojana, S Assabumrungrat, Methane steam reforming over Ni/Ce-ZrO_2 catalyst: Influences of Ce-ZrO_2 support on reactivity, resistance toward carbon formation, and intrinsic reaction kinetics, Appl. Catal., A, 290 (2005) 200-211.

[22] MH Halabi,MHJM de Croon,J van der Schaaf,PD Cobden, JC Schouten, Low temperature catalytic methane steam reforming over ceria-zirconia supported rhodium, Appl. Catal., A, 389 (2010) 68-79.

[23] K Hou, R Hughes, The kinetics of methane steam reforming over a Ni/a-Al_2O_3 catalyst, Chem. Eng. J. (Lausanne), 82 (2001) 311-328.

[24] DL Trimm, Catalysts for the control of coking during steam reforming, Catal. Today, 49 (1999) 3-10.

[25] Q Ming,T Healey,L Allen, P Irving, Steam reforming of hydrocarbon fuels, Catal. Today, 77 (2002) 51-64.

[26] C Fauteux-Lefebvre,N Abatzoglou,J Blanchard, F Gitzhofer, Steam reforming of liquid hydrocarbons over a nickel-alumina spinel catalyst, J. Power Sources, 195 (2010) 3275-3283.

[27] VS Guggilla,J Akyurtlu,A Akyurtlu, I Blankson, Steam Reforming of *n*-Dodecane over Ru-Ni-Based Catalysts, Ind. Eng. Chem. Res., 49 (2010) 8164-8173.

[28] I Kang, J Bae, Autothermal reforming study of diesel for fuel cell application, J. Power Sources, 159 (2006) 1283-1290.

[29] T Zhu, M Flytzani-Stephanopoulos, Catalytic partial oxidation of methane to synthesis gas over Ni-CeO_2, Appl. Catal., A, 208 (2001) 403-417.

[30] SC Tsang,JB Claridge, MLH Green, Recent advances in the conversion of methane to synthesis gas, Catal. Today, 23 (1995) 3-15.

[31] APE York,T Xiao, MLH Green, Brief Overview of the Partial Oxidation of Methane to Synthesis Gas, Top. Catal., 22 (2003) 345-358.

[32] WJM Vermeiren,E Blomsma, PA Jacobs, Catalytic and thermodynamic approach of the oxyreforming reaction of methane, Catal. Today, 13 (1992) 427-436.

[33] D Dissanayake,MP Rosynek,KCC Kharas, JH Lunsford, Partial oxidation of methane to carbon monoxide and hydrogen over a Ni/Al_2O_3 catalyst, J. Catal., 132 (1991) 117-127.

[34] PM Torniainen,X Chu, LD Schmidt, Comparison of monolith-supported metals for the direct oxidation of methane to syngas, J. Catal., 146 (1994) 1-10.

[35] DA Hickman, LD Schmidt, Production of Syngas by Direct Catalytic Oxidation of Methane, Science, 259 (1993) 343-346.

[36] SA Larrondo,A Kodjaian,I Fabregas,MG Zimicz,DG Lamas,BE Walsoe de Reca, NE Amadeo, Methane partial oxidation using Ni/$Ce_{0.9}Zr_{0.1}O_2$ catalysts, Int. J. Hydrogen Energy, 33 (2008) 3607-3613.

[37] Y Chen,W Zhou,Z Shao, N Xu, Nickel catalyst prepared via glycine nitrate process for partial oxidation of methane to syngas, Catal Commun, 9 (2008) 1418-1425.

[38] AF Lucredio,G Jerkiewickz, EM Assaf, Nickel catalysts promoted with cerium and lanthanum to reduce carbon formation in partial oxidation of methane reactions, Appl. Catal., A, 333 (2007) 90-95.

[39] AB Stambouli, E Traversa, Solid oxide fuel cells (SOFCs): a review of an environmentally clean and efficient source of energy, Renewable and Sustainable Energy Reviews, 6 (2002) 433-455.

[40] MW Smith,DA Berry,D Shekhawat,DJ Haynes, JJ Spivey, Partial oxidation of liquid hydrocarbons in the presence of oxygen-conducting supports: Effect of catalyst layer deposition, Fuel, 89 (2010) 1193-1201.

[41] D Dissanayake,MP Rosynek, JH Lunsford, Are the equilibrium concentrations of carbon monoxide and hydrogen exceeded during the oxidation of methane over a nickel/ytterbium oxide catalyst?, The Journal of Physical Chemistry, 97 (1993) 3644-3646.

[42] R Subramanian,GJ Panuccio,JJ Krummenacher,IC Lee, LD Schmidt, Catalytic partial oxidation of higher hydrocarbons: reactivities and selectivities of mixtures, Chem. Eng. Sci., 59 (2004) 5501-5507.

[43] M Hartmann,L Maier,HD Minh, O Deutschmann, Catalytic partial oxidation of iso-octane over rhodium catalysts: An experimental, modeling, and simulation study, Combust. Flame, 157 (2010) 1771-1782.

[44] M Hartmann,L Maier, O Deutschmann, Hydrogen production by catalytic partial oxidation of iso-octane at varying flow rate and fuel/oxygen ratio: From detailed kinetics to reactor behavior, Appl. Catal., A, 391 (2011) 144-152.

[45] M Nilsson,K Jansson,P Jozsa, LJ Pettersson, Catalytic properties of Pd supported on $ZnO/ZnAl_2O_4/Al_2O_3$ mixtures in dimethyl ether autothermal reforming, Appl. Catal., B, 86 (2009) 18-26.

[46] JC Escritori,SC Dantas,RR Soares, CE Hori, Methane autothermal reforming on nickel-ceria-zirconia based catalysts, Catal Commun, 10 (2009) 1090-1094.

[47] SS Lim,HJ Lee,DJ Moon,JH Kim,NC Park,JS Shin, YC Kim, Autothermal reforming of propane over Ce modified Ni/$LaAlO_3$ perovskite-type catalysts, Chem. Eng. J. (Lausanne), 152 (2009) 220-226.

[48] K Sato,K Nagaoka,H Nishiguchi, Y Takita, *n*-C_4H_{10} autothermal reforming over MgO-supported base metal catalysts, Int. J. Hydrogen Energy, 34 (2009) 333-342.

[49] JR Rostrup-Nielsen, Sulfur-passivated nickel catalysts for carbon-free steam reforming of methane, J. Catal., 85 (1984) 31-43.

[50] T-J Huang, M-C Huang, Effect of Ni content on hydrogen production via steam reforming of methane over Ni/GDC catalysts, Chem. Eng. J. (Lausanne), 145 (2008) 149-153.

[51] J Xu,L Chen,KF Tan,A Borgna, M Saeys, Effect of boron on the stability of Ni catalysts during steam methane reforming, J. Catal., 261 (2009) 158-165.

[52] T-J Huang,H-J Lin, T-C Yu, A Comparison of Oxygen-vacancy Effect on Activity Behaviors of Carbon Dioxide and Steam Reforming of Methane over Supported Nickel Catalysts, Catalysis Letters, 105 (2005) 239-247.

[53] Y Matsumura, T Nakamori, Steam reforming of methane over nickel catalysts at low reaction temperature, Appl. Catal., A, 258 (2004) 107-114.

[54] B Yildiz, MS Kazimi, Efficiency of hydrogen production systems using alternative nuclear energy technologies, Int. J. Hydrogen Energy, 31 (2006) 77-92.

[55] HG Düsterwald,J Günnewig, P Radtke, DRIVE – The Future of Automotive Power: Fuel Cells Perspective, Fuel Cells, 7 (2007) 183-189.

[56] JA Ritter, AD Ebner, State-of-the-Art Adsorption and Membrane Separation Processes for Hydrogen Production in the Chemical and Petrochemical Industries, Sep. Sci. Technol., 42 (2007) 1123-1193.

[57] DA Morgenstern, JP Fornango, Low-Temperature Reforming of Ethanol over Copper-Plated Raney Nickel: A New Route to Sustainable Hydrogen for Transportation, Energy Fuels, 19 (2005) 1708-1716.

[58] F Frusteri,S Freni,V Chiodo,L Spadaro,O Di Blasi,G Bonura, S Cavallaro, Steam reforming of bio-ethanol on alkali-doped Ni/MgO catalysts: hydrogen production for MC fuel cell, Appl. Catal., A, 270 (2004) 1-7.

[59] F Soyal-BaltacIoglu,AE Aksoylu, ZI Onsan, Steam reforming of ethanol over Pt-Ni Catalysts, Catal. Today, 138 (2008) 183-186.

[60] Y Chen,Z Shao, N Xu, Ethanol Steam Reforming over Pt Catalysts Supported on $Ce_xZr_{1-x}O_2$ Prepared via a Glycine Nitrate Process, Energy Fuels, 22 (2008) 1873-1879.

[61] GA Deluga,JR Salge,LD Schmidt, XE Verykios, Renewable hydrogen from ethanol by autothermal reforming, Science, 303 (2004) 993+.

[62] J Kugai,V Subramani,C Song,MH Engelhard, Y-H Chin, Effects of nanocrystalline CeO_2 supports on the properties and performance of Ni-Rh bimetallic catalyst for oxidative steam reforming of ethanol, J. Catal., 238 (2006) 430-440.

[63] S Adhikari,S Fernando, A Haryanto, A Comparative Thermodynamic and Experimental Analysis on Hydrogen Production by Steam Reforming of Glycerin, Energy Fuels, 21 (2007) 2306-2310.

[64] S Cavallaro, Ethanol Steam Reforming on Rh/Al_2O_3 Catalysts, Energy Fuels, 14 (2000) 1195-1199.

[65] Y Chen,H Xu,Y Wang, G Xiong, Hydrogen production from the steam reforming of liquid hydrocarbons in membrane reactor, Catal. Today, 118 (2006) 136-143.

[66] J Kugai,S Velu, C Song, Low-temperature reforming of ethanol over CeO_2-supported Ni-Rh bimetallic catalysts for hydrogen production, Catalysis Letters, 101 (2005) 255-264.

[67] PD Vaidya, AE Rodrigues, Insight into steam reforming of ethanol to produce hydrogen for fuel cells, Chem. Eng. J. (Lausanne), 117 (2006) 39-49.

[68] A Haryanto,S Fernando,N Murali, S Adhikari, Current Status of Hydrogen Production Techniques by Steam Reforming of Ethanol: A Review, Energy Fuels, 19 (2005) 2098-2106.

[69] MH Youn,JG Seo,S Park,DR Park,JC Jung,P Kim, IK Song, Hydrogen production by auto-thermal reforming of ethanol over Ni-Ti-Zr metal oxide catalysts, Renewable Energy, 34 (2009) 731-735.

[70] S Cavallaro, S Freni, Ethanol steam reforming in a molten carbonate fuel cell. A preliminary kinetic investigation, Int. J. Hydrogen Energy, 21 (1996) 465-469.

[71] S Cavallaro,V Chiodo,S Freni,N Mondello, F Frusteri, Performance of Rh/Al_2O_3 catalyst in the steam reforming of ethanol: H_2 production for MCFC, Appl. Catal., A, 249 (2003) 119-128.

[72] NB Klinghoffer,F Barrai, MJ Castaldi, Autothermal reforming of JP8 on a Pt/Rh catalyst: Catalyst durability studies and effects of sulfur, J. Power Sources, 196 (2011) 6374-6381.

[73] J Boon,E van Dijk,S de Munck, R van den Brink, Steam reforming of commercial ultra-low sulphur diesel, J. Power Sources, 196 (2011) 5928-5935.

[74] PK Cheekatamarla, WJ Thomson, Poisoning effect of thiophene on the catalytic activity of molybdenum carbide during tri-methyl pentane reforming for hydrogen generation, Appl. Catal., A, 287 (2005) 176-182.

[75] Y Sone,H Kishida,M Kobayashi, T Watanabe, A study of carbon deposition on fuel cell power plants - morphology of deposited carbon and catalytic metal in carbon deposition reactions on stainless steel, J. Power Sources, 86 (2000) 334-339.

[76] B Lenz, T Aicher, Catalytic autothermal reforming of Jet fuel, J. Power Sources, 149 (2005) 44-52.

[77] M Krumpelt,TR Krause,JD Carter,JP Kopasz, S Ahmed, Fuel processing for fuel cell systems in transportation and portable power applications, Catal. Today, 77 (2002) 3-16.

[78] M Harada,K Takanabe,J Kubota,K Domen,T Goto,K Akiyama, Y Inoue, Hydrogen production by autothermal reforming of kerosene over $MgAlO_x$-supported Rh catalysts, Appl. Catal., A, 371 (2009) 173-178.

[79] K Lehnert, P Claus, Influence of Pt particle size and support type on the aqueous-phase reforming of glycerol, Catal Commun, 9 (2008) 2543-2546.

[80] SM de Lima,AM Silva,UM Graham,G Jacobs,BH Davis,LV Mattos, FB Noronha, Ethanol decomposition and steam reforming of ethanol over $CeZrO_2$ and $Pt/CeZrO_2$ catalyst: Reaction mechanism and deactivation, Appl. Catal., A, 352 (2009) 95-113.

[81] RK Kaila,A Gutierrez,R Slioor,M Kemell,M Leskel, AOI Krause, Zirconia-supported bimetallic RhPt catalysts: Characterization and testing in autothermal reforming of simulated gasoline, Appl. Catal., B, 84 (2008) 223-232.

[82] A Tanksale,JN Beltramini,JA Dumesic, GQ Lu, Effect of Pt and Pd promoter on Ni supported catalysts--A TPR/TPO/TPD and microcalorimetry study, J. Catal., 258 (2008) 366-377.

[83] SL Lakhapatri, MA Abraham, Deactivation due to sulfur poisoning and carbon deposition on Rh-Ni/Al2O3 catalyst during steam reforming of sulfur-doped n-hexadecane, Applied Catalysis A: General, In Press, Accepted Manuscript.

[84] A Bampenrat,V Meeyoo,B Kitiyanan,P Rangsunvigit, T Rirksomboon, Naphthalene Steam Reforming over Mn-doped CeO2-ZrO2 Supported Nickel Catalysts, Appl. Catal., A, In Press, Accepted Manuscript.

[85] A Nandini,KK Pant, SC Dhingra, Kinetic study of the catalytic carbon dioxide reforming of methane to synthesis gas over Ni-K/CeO2-Al2O3 catalyst, Appl. Catal., A, 308 (2006) 119-127.

[86] J-H Kim,DJ Suh,T-J Park, K-L Kim, Effect of metal particle size on coking during CO_2 reforming of CH_4 over Ni-alumina aerogel catalysts, Appl. Catal., A, 197 (2000) 191-200.

[87] C Wang,T Wang,L Ma,Y Gao, C Wu, Steam reforming of biomass raw fuel gas over NiO-MgO solid solution cordierite monolith catalyst, Energy Conversion and Management, 51 446-451.

[88] MH Youn,JG Seo,S Park,JC Jung,DR Park, IK Song, Hydrogen production by auto-thermal reforming of ethanol over Ni catalysts supported on ZrO2: Effect of preparation method of ZrO2 support, Int. J. Hydrogen Energy, 33 (2008) 7457-7463.

[89] DL King,JJ Strohm,X Wang,H-S Roh,C Wang,Y-H Chin,Y Wang,Y Lin,R Rozmiarek, P Singh, Effect of nickel microstructure on methane steam-reforming activity of Ni-YSZ cermet anode catalyst, J. Catal., 258 (2008) 356-365.

[90] JDA Bellido, EM Assaf, Effect of the Y2O3-ZrO2 support composition on nickel catalyst evaluated in dry reforming of methane, Appl. Catal., A, 352 (2009) 179-187.

[91] S Corthals,J Van Nederkassel,J Geboers,H De Winne,J Van Noyen,B Moens,B Sels, P Jacobs, Influence of composition of MgAl2O4 supported NiCeO2ZrO2 catalysts on coke formation and catalyst stability for dry reforming of methane, Catal. Today, 138 (2008) 28-32.

[92] K Omata,Y Endo,H Ishii,A Masuda, M Yamada, Effective additives of Ni/-Al2O3 catalyst at low methane conversion of oxidative reforming for syngas formation, Appl. Catal., A, 351 (2008) 54-58.

[93] LPR Profeti,EA Ticianelli, EM Assaf, Production of hydrogen via steam reforming of biofuels on Ni/CeO_2-Al_2O_3 catalysts promoted by noble metals, Int. J. Hydrogen Energy, 34 (2009) 5049-5060.

[94] H Borchert,Y Borchert,VV Kaichev,IP Prosvirin,GM Alikina,AI Lukashevich,VI Zaikovskii,EM Moroz,EA Paukshtis,VI Bukhtiyarov, VA Sadykov, Nanostructured, Gd-Doped Ceria Promoted by Pt or Pd: Investigation of the Electronic and Surface Structures and Relations to Chemical Properties, J. Phys. Chem. B, 109 (2005) 20077-20086.

[95] A Shotipruk,S Assabumrungrat,P Pavasant, N Laosiripojana, Reactivity of CeO_2 and Ce-ZrO_2 toward steam reforming of palm fatty acid distilled (PFAD) with co-fed oxygen and hydrogen, Chem. Eng. Sci., 64 (2009) 459-466.

[96] GCd Araujo,SMd Lima,JM Assaf,MA Pena,JLG Fierro, M do Carmo Rangel, Catalytic evaluation of perovskite-type oxide LaNi1-xRuxO3 in methane dry reforming, Catal. Today, 133-135 129-135.

[97] Y Nabae,I Yamanaka,M Hatano, K Otsuka, Mechanism of Suppression of Carbon Deposition on the Pd-Ni/Ce(Sm)O_2-La(Sr)CrO_3 Anode in Dry CH_4 Fuel, J. Phys. Chem. C, 112 (2008) 10308-10315.

[98] K Leszek, Carbon deposition in Pd/CeO_2 catalyst: TEM study, Catal. Today, 50 (1999) 237-245.

[99] JG McCarty, H Wise, Hydrogenation of surface carbon on alumina-supported nickel, J. Catal., 57 (1979) 406-416.

[100] DL Trimm, The Formation and Removal of Coke from Nickel Catalyst, Catalysis Reviews, 16 (1977) 155-189.

[101] JA Rodriguez, J Hrbek, Interaction of Sulfur with Well-Defined Metal and Oxide Surfaces: Unraveling the Mysteries behind Catalyst Poisoning and Desulfurization, Accounts of Chemical Research, 32 (1999) 719-728.

[102] A-M Azad,MJ Duran,AK McCoy, MA Abraham, Development of ceria-supported sulfur tolerant nanocatalysts: Pd-based formulations, Appl. Catal., A, 332 (2007) 225-236.

[103] KC Taylor, Nitric Oxide Catalysis in Automotive Exhaust Systems, Catalysis Reviews, 35 (1993) 457-481.

[104] J Rodriguez, D Wayne Goodman, High-pressure catalytic reactions over single-crystal metal surfaces, Surf. Sci. Rep., 14 (1991) 1-107.

[105] JA Rodriguez, The chemical properties of bimetallic surfaces: Importance of ensemble and electronic effects in the adsorption of sulfur and SO_2, Prog. Surf. Sci., 81 (2006) 141-189.

[106] P Marecot,E Paraiso,JM Dumas, J Barbier, Deactivation of nickel catalysts by sulphur compounds: II. Chemisorption of hydrogen sulphide, Appl. Catal., A, 80 (1992) 89-97.

[107] SL Lakhapatri, MA Abraham, Deactivation due to sulfur poisoning and carbon deposition on Rh-Ni/Al_2O_3 catalyst during steam reforming of sulfur-doped *n*-hexadecane, Appl. Catal., A, 364 (2009) 113-121.

[108] CT Campbell, BE Koel, H_2S/Cu(111): A model study of sulfur poisoning of water-gas shift catalysts, Surf. Sci., 183 (1987) 100-112.

[109] PD Szuromi,RD Kelley, TE Madey, Influence of sulfur on methanation over tungsten(110), The Journal of Physical Chemistry, 90 (1986) 6499-6507.

[110] PK Cheekatamarla, AM Lane, Catalytic autothermal reforming of diesel fuel for hydrogen generation in fuel cells: II. Catalyst poisoning and characterization studies, J. Power Sources, 154 (2006) 223-231.

[111] R-N J.R,HB Calvin, BB John, Promotion by Poisoning, in: Stud. Surf. Sci. Catal., Elsevier, 1991, pp. 85-101.

[112] HS Bengaard,JK Norskov,J Sehested,BS Clausen,LP Nielsen,AM Molenbroek, JR Rostrup-Nielsen, Steam Reforming and Graphite Formation on Ni Catalysts, J. Catal., 209 (2002) 365-384.

[113] B Tadeusz, Nickel catalysts for steam reforming of hydrocarbons; size of crystallites and resistance to coking, Applied Catalysis, 4 (1982) 223-231.

[114] KO Christensen,D Chen,R Lodeng, A Holmen, Effect of supports and Ni crystal size on carbon formation and sintering during steam methane reforming, Appl. Catal., A, 314 (2006) 9-22.

[115] S Takenaka,Y Orita,H Umebayashi,H Matsune, M Kishida, High resistance to carbon deposition of silica-coated Ni catalysts in propane stream reforming, Appl. Catal., A, 351 (2008) 189-194.

[116] L Huang,J Xie,R Chen,D Chu,W Chu, AT Hsu, Effect of iron on durability of nickel-based catalysts in auto-thermal reforming of ethanol for hydrogen production, Int. J. Hydrogen Energy, 33 (2008) 7448-7456.

[117] E Nikolla,J Schwank, S Linic, Promotion of the long-term stability of reforming Ni catalysts by surface alloying, J. Catal., 250 (2007) 85-93.

[118] A Carrero,JA Calles, AJ Vizcaino, Effect of Mg and Ca addition on coke deposition over Cu-Ni/SiO_2 catalysts for ethanol steam reforming, Chem. Eng. J. (Lausanne), 163 (2010) 395-402.

[119] L Wang,D Li,M Koike,S Koso,Y Nakagawa,Y Xu, K Tomishige, Catalytic performance and characterization of Ni-Fe catalysts for the steam reforming of tar from biomass pyrolysis to synthesis gas, Appl. Catal., A, 392 (2011) 248-255.

[120] H Song, US Ozkan, Changing the Oxygen Mobility in Co/Ceria Catalysts by Ca Incorporation: Implications for Ethanol Steam Reforming, The Journal of Physical Chemistry A, 114 (2009) 3796-3801.

[121] CMY Yeung,KMK Yu,QJ Fu,D Thompsett,MI Petch, SC Tsang, Engineering Pt in Ceria for a Maximum Metal-Support Interaction in Catalysis, Journal of the American Chemical Society, 127 (2005) 18010-18011.

[122] SJ Skinner, JA Kilner, Oxygen ion conductors, Materials Today, 6 (2003) 30-37.

[123] A Yee,SJ Morrison, H Idriss, A Study of the Reactions of Ethanol on CeO_2 and Pd/CeO_2 by Steady State Reactions, Temperature Programmed Desorption, and In Situ FT-IR, J. Catal., 186 (1999) 279-295.

[124] LV Mattos, FB Noronha, Hydrogen production for fuel cell applications by ethanol partial oxidation on Pt/CeO_2 catalysts: the effect of the reaction conditions and reaction mechanism, J. Catal., 233 (2005) 453-463.

[125] N Laosiripojana, S Assabumrungrat, Catalytic steam reforming of ethanol over high surface area CeO_2: The role of CeO_2 as an internal pre-reforming catalyst, Appl. Catal., B, 66 (2006) 29-39.

[126] W Cai,F Wang,AC Van Veen,H Provendier,C Mirodatos, W Shen, Autothermal reforming of ethanol for hydrogen production over an Rh/CeO_2 catalyst, Catal. Today, 138 (2008) 152-156.

[127] WLS Faria,LC Dieguez, M Schmal, Autothermal reforming of propane for hydrogen production over $Pd/CeO_2/Al_2O_3$ catalysts, Appl. Catal., B, 85 (2008) 77-85.

[128] L Cao,L Pan,C Ni,Z Yuan, S Wang, Autothermal reforming of methane over Rh/Ce0.5Zr0.5O2 catalyst: Effects of the crystal structure of the supports, Fuel Processing Technology, 91 (2010) 306-312.

[129] J Xu,CMY Yeung,J Ni,F Meunier,N Acerbi,M Fowles, SC Tsang, Methane steam reforming for hydrogen production using low water-ratios without carbon formation over ceria coated Ni catalysts, Appl. Catal., A, 345 (2008) 119-127.

[130] N Laosiripojana,W Sutthisripok,P Kim-Lohsoontorn, S Assabumrungrat, Reactivity of Ce-ZrO_2 (doped with La-, Gd-, Nb-, and Sm-) toward partial oxidation of liquefied petroleum gas: Its application for sequential partial oxidation/steam reforming, Int. J. Hydrogen Energy, 35 (2010) 6747-6756.

[131] AM da Silva,KR de Souza,G Jacobs,UM Graham,BH Davis,LV Mattos, FB Noronha, Steam and CO_2 reforming of ethanol over Rh/CeO_2 catalyst, Appl. Catal., B, 102 (2011) 94-109.

[132] W Wang,R Ran, Z Shao, Lithium and lanthanum promoted Ni-Al_2O_3 as an active and highly coking resistant catalyst layer for solid-oxide fuel cells operating on methane, J. Power Sources, 196 (2011) 90-97.

[133] M Sugisawa,K Takanabe,M Harada,J Kubota, K Domen, Effects of La addition to Ni/Al_2O_3 catalysts on rates and carbon deposition during steam reforming of *n*-dodecane, Fuel Processing Technology, 92 (2011) 21-25.

[134] I Gavrielatos,V Drakopoulos, SG Neophytides, Carbon tolerant Ni-Au SOFC electrodes operating under internal steam reforming conditions, J. Catal., 259 (2008) 75-84.

[135] NC Triantafyllopoulos, SG Neophytides, Dissociative adsorption of CH_4 on NiAu/YSZ: The nature of adsorbed carbonaceous species and the inhibition of graphitic C formation, J. Catal., 239 (2006) 187-199.

[136] CKS Choong,Z Zhong,L Huang,Z Wang,TP Ang,A Borgna,J Lin,L Hong, L Chen, Effect of calcium addition on catalytic ethanol steam reforming of Ni/Al_2O_3: I. Catalytic stability, electronic properties and coking mechanism, Appl. Catal., A, 407 (2011) 145-154.

[137] CKS Choong,L Huang,Z Zhong,J Lin,L Hong, L Chen, Effect of calcium addition on catalytic ethanol steam reforming of Ni/Al_2O_3: II. Acidity/basicity, water adsorption and catalytic activity, Appl. Catal., A, 407 (2011) 155-162.

[138] R Mukundan,EL Brosha, FH Garzon, Sulfur Tolerant Anodes for SOFCs, Electrochemical and Solid-State Letters, 7 (2004) A5-A7.

[139] L Aguilar,S Zha,S Li,J Winnick, M Liu, Sulfur-Tolerant Materials for the Hydrogen Sulfide SOFC, Electrochemical and Solid-State Letters, 7 (2004) A324-A326.

[140] WT Owens,NM Rodriguez, RTK Baker, Effect of sulfur on the interaction of nickel with ethylene, Catal. Today, 21 (1994) 3-22.

[141] A Kulprathipanja,GO Alptekin,JL Falconer, JD Way, Pd and Pd-Cu membranes: inhibition of H_2 permeation by H_2S, Journal of Membrane Science, 254 (2005) 49-62.

[142] AC Lausche,JA Schaidle, LT Thompson, Understanding the effects of sulfur on Mo_2C and Pt/Mo_2C catalysts: Methanol steam reforming, Appl. Catal., A, 401 (2011) 29-36.

[143] JA Rodriguez,T Jirsak, S Chaturvedi, Reaction of S_2 and SO_2 with Pd/Rh(111) surfaces: Effects of metal--metal bonding on sulfur poisoning, The Journal of Chemical Physics, 110 (1999) 3138-3147.

[144] JA Rodriguez,T Jirsak,S Chaturvedi, J Hrbek, Surface Chemistry of SO_2 on Sn and Sn/Pt(111) Alloys: Effects of Metal-Metal Bonding on Reactivity toward Sulfur, Journal of the American Chemical Society, 120 (1998) 11149-11157.

[145] I Alstrup, NT Andersen, Statistical models for ensemble control by alloying and poisoning of catalysts: II. Comparisons with Monte Carlo simulations and with experimental results, J. Catal., 104 (1987) 466-479.

[146] JM Mayne,KA Dahlberg,TA Westrich,AR Tadd, JW Schwank, Effect of metal particle size on sulfur tolerance of Ni catalysts during autothermal reforming of isooctane, Appl. Catal., A, 400 (2011) 203-214.

[147] M Rangan,MM Yung, JW Medlin, Experimental and computational investigations of sulfur-resistant bimetallic catalysts for reforming of biomass gasification products, J. Catal., 282 (2011) 249-257.

[148] X Karatzas,K Jansson,A Gonzalez,J Dawody, LJ Pettersson, Autothermal reforming of low-sulfur diesel over bimetallic RhPt supported on Al_2O_3, CeO_2-ZrO_2, SiO_2 and TiO_2, Appl. Catal., B, In Press, Accepted Manuscript (2011).

[149] Q Xue,L Gao, Y Lu, Sulfur-tolerant Pt/Gd_2O_3-CeO_2-Al_2O_3 catalyst for high efficiency H_2 production from autothermal reforming of retail gasoline, Catal. Today, 146 (2009) 103-109.

[150] Y Lu,J Chen,Y Liu,Q Xue, M He, Highly sulfur-tolerant Pt/$Ce_{0.8}Gd_{0.2}O_{1.9}$ catalyst for steam reforming of liquid hydrocarbons in fuel cell applications, J. Catal., 254 (2008) 39-48.

[151] JA Schwarz,C Contescu, A Contescu, Methods for Preparation of Catalytic Materials, Chem. Rev. (Washington, DC, U. S.), 95 (1995) 477-510.

[152] H Song, US Ozkan, The role of impregnation medium on the activity of ceria-supported cobalt catalysts for ethanol steam reforming, Journal of Molecular Catalysis A: Chemical, 318 (2010) 21-29.

[153] PM Pimentel,AE Martinelli,DMdA Melo,AMG Pedrosa,JD Cunha, CNd Silva Junior, Pechini synthesis and microstructure of nickel-doped copper chromites, Materials Research, 8 (2005) 221-224.

[154] SW Tay,L Hong, Z Liu, Interface-sustained magnetic properties displayed by the La_2O_3 - SrO - Co_2O_3 nanocomposite, Journal of Applied Physics, 98 (2005) 124308-124308.

[155] X Yin,L Hong,BH Chen, TM Ko, Modeling the stability of electroless plating bath-diffusion of nickel colloidal particles from the plating frontier, J. Colloid Interface Sci., 262 (2003) 89-96.

[156] F Delaunois,JP Petitjean,P Lienard, M Jacob-Duliere, Autocatalytic electroless nickel-boron plating on light alloys, Surf. Coat. Technol., 124 (2000) 201-209.

[157] Y Chen,M Cao,Q Xu, J Zhu, Electroless nickel plating on silicon carbide nanoparticles, Surf. Coat. Technol., 172 (2003) 90-94.

[158] S Sun,J Liu,C Yan, F Wang, A novel process for electroless nickel plating on anodized magnesium alloy, Applied Surface Science, 254 (2008) 5016-5022.

[159] A Grosjean,M Rezrazi,J Takadoum, P Bercot, Hardness, friction and wear characteristics of nickel-SiC electroless composite deposits, Surf. Coat. Technol., 137 (2001) 92-96.

[160] R Taheri,INA Oguocha, S Yannacopoulos, Effect of heat treatment on age hardening behaviour of electroless nickel-phosphorus coatings, Mater. Sci. Technol., 17 (2001) 278-284.

[161] C-H Chen,B-H Chen, L Hong, Role of Cu^{2+} as an Additive in an Electroless Nickel-Phosphorus Plating System: A Stabilizer or a Codeposit?, Chem. Mater., 18 (2006) 2959-2968.

[162] D Baudrand, J Bengston, Electroless plating processes: Developing technologies for electroless nickel, palladium, and gold, Metal Finishing, 93 (1995) 55-57.

[163] GO Mallory, JB Hajdu, Electroless Plating - Fundamentals and Applications, in, William Andrew Publishing/Noyes, 1990.

[164] BH Chen,L Hong,Y Ma, TM Ko, Effects of Surfactants in an Electroless Nickel-Plating Bath on the Properties of Ni-P Alloy Deposits, Ind. Eng. Chem. Res., 41 (2002) 2668-2678.

[165] JEAM Meerakker, On the mechanism of electroless plating. II. One mechanism for different reductants, J. Appl. Electrochem., 11 (1981) 395-400.

[166] LM Abrantes, JP Correia, On the Mechanism of Electroless Ni-P Plating, Journal of The Electrochemical Society, 141 (1994) 2356-2360.

[167] BJ Hwang, SH Lin, Reaction Mechanism of Electroless Deposition: Observations of Morphology Evolution during Nucleation and Growth Via Tapping Mode AFM, Journal of The Electrochemical Society, 142 (1995) 3749-3754.

[168] A Malecki, A Micek-Ilnicka, Electroless nickel plating from acid bath, Surf. Coat. Technol., 123 (2000) 72-77.

[169] MC Zhang,ET Kang,KG Neoh, KL Tan, Electroless Plating of Copper and Nickel on Surface-Modified Poly(tetrafluoroethylene) Films, Journal of The Electrochemical Society, 148 (2001) C71-C80.

[170] T Homma,K Naito,M Takai,T Osaka,Y Yamazaki, T Namikawa, Transmission Electron Microscopy Study of Electroless NiP and Cu Films at Initial Deposition Stage, Journal of The Electrochemical Society, 138 (1991) 1269-1274.

[171] M Seita,M Kusaka,H Nawafune, S Mizumoto, Direct metallization using Ni-Co alloy on surface modified polyimide film, American Electroplaters and Surface Finishers Society, Orlando, FL, ETATS-UNIS, 1999.

[172] Z-J Wu,S-H Ge,M-H Zhang,W Li,S-C Mu, K-Y Tao, Controlled Synthesis of Supported Nickel Boride Catalyst Using Electroless Plating, The Journal of Physical Chemistry C, 111 (2007) 8587-8593.

[173] Z Wu,M Zhang,S Ge,Z Zhang,W Li, K Tao, Synthesis and characterization of a porous amorphous Ni-B catalyst on titania by silver-catalyzed electroless plating, J. Mater. Chem., 15 (2005) 4928-4933.

[174] Z Wu,J Chen,Q Di, M Zhang, Size-controlled synthesis of a supported Ni nanoparticle catalyst for selective hydrogenation of p-nitrophenol to p-aminophenol, Catal Commun, (2011).

[175] HB Hassan, ZA Hamid, Electroless Ni-B supported on carbon for direct alcohol fuel cell applications, Int. J. Hydrogen Energy, 36 (2011) 849-856.

[176] K Eom,K Cho, H Kwon, Effects of electroless deposition conditions on microstructures of cobalt-phosphorous catalysts and their hydrogen generation properties in alkaline sodium borohydride solution, J. Power Sources, 180 (2008) 484-490.

[177] X Chen,BD Gould, JW Schwank, *n*-Dodecane reforming over monolith-based Ni catalysts: SEM study of axial carbon distribution profile, Appl. Catal., A, 356 (2009) 137-147.

[178] JR Rostrup-Nielsen,J Sehested,GWR J.J. Spivey, BH Davis, Whisker carbon revisited, in: Stud. Surf. Sci. Catal., Elsevier, 2001, pp. 1-12.

[179] X Chen,AR Tadd, JW Schwank, Carbon deposited on Ni/CeZrO isooctane autothermal reforming catalysts, J. Catal., 251 (2007) 374-387.

[180] LSF Feio,CE Hori,LV Mattos,D Zanchet,FB Noronha, JMC Bueno, Partial oxidation and autothermal reforming of methane on Pd/CeO2-Al2O3 catalysts, Appl. Catal., A, 348 (2008) 183-192.

[181] MC Alvarez-Galvan,RM Navarro,F Rosa,Y Briceno,F Gordillo Alvarez, JLG Fierro, Performance of La,Ce-modified alumina-supported Pt and Ni catalysts for the oxidative reforming of diesel hydrocarbons, Int. J. Hydrogen Energy, 33 (2008) 652-663.

[182] Q Xue,L Gao, Y Lu, Sulfur-tolerant Pt/Gd2O3-CeO2-Al2O3 catalyst for high efficiency H2 production from autothermal reforming of retail gasoline, Catalysis Today, In Press, Corrected Proof.

[183] X Liu,J Chen, J Zhang, Hydrodechlorination of Chlorobenzene over Silica-Supported Nickel Phosphide Catalysts, Ind. Eng. Chem. Res., 47 (2008) 5362-5368.

[184] K Wang,L Hong, Z-L Liu, Investigation into the Roles of Sulfur-Containing Amino Acids in Electroless Nickel Plating Bath, Ind. Eng. Chem. Res., 47 (2008) 6517-6524.

[185] Y Li,X Wang,C Xie, C Song, Influence of ceria and nickel addition to alumina-supported Rh catalyst for propane steam reforming at low temperatures, Appl. Catal., A, 357 (2009) 213-222.

[186] K Wang,L Hong, Z-L Liu, Exploring the Water-Soluble Phosphine Ligand as the Environmentally Friendly Stabilizer for Electroless Nickel Plating, Ind. Eng. Chem. Res., 48 (2009) 1727-1734.

[187] KK Kar, D Sathiyamoorthy, Influence of process parameters for coating of nickel-phosphorous on carbon fibers, Journal of Materials Processing Technology, 209 (2009) 3022-3029.

[188] JA Cecilia,A Infantes-Molina,E Rodriguez-Castellon, A Jimenez-Lopez, A novel method for preparing an active nickel phosphide catalyst for HDS of dibenzothiophene, J. Catal., 263 (2009) 4-15.

[189] SJ Sawhill,DC Phillips, ME Bussell, Thiophene hydrodesulfurization over supported nickel phosphide catalysts, J. Catal., 215 (2003) 208-219.

[190] II Abu, KJ Smith, The effect of cobalt addition to bulk MoP and Ni2P catalysts for the hydrodesulfurization of 4,6-dimethyldibenzothiophene, J. Catal., 241 (2006) 356-366.

[191] X Yin,L Hong, B-H Chen, Role of a Pb^{2+} Stabilizer in the Electroless Nickel Plating System: A Theoretical Exploration, The Journal of Physical Chemistry B, 108 (2004) 10919-10929.

[192] X Yu,H Li, J-F Deng, Selective hydrogenation of adiponitrile over a skeletal Ni-P amorphous catalyst (Raney Ni-P) at 1 atm pressure, Appl. Catal., A, 199 (2000) 191-198.

[193] SJ Sawhill,KA Layman,DR Van Wyk,MH Engelhard,C Wang, ME Bussell, Thiophene hydrodesulfurization over nickel phosphide catalysts: effect of the precursor composition and support, J. Catal., 231 (2005) 300-313.

[194] C Korsvik,S Patil,S Seal, WT Self, Superoxide dismutase mimetic properties exhibited by vacancy engineered ceria nanoparticles, Chem. Commun., (2007) 1056-1058.

[195] L Xu,G Guo,D Uy,AE O'Neill,WH Weber,MJ Rokosz, RW McCabe, Cerium phosphate in automotive exhaust catalyst poisoning, Appl. Catal., B, 50 (2004) 113-125.

[196] E Rocchini,M Vicario,J Llorca,C de Leitenburg,G Dolcetti, A Trovarelli, Reduction and Oxygen Storage Behavior of Noble Metals Supported on Silica-Doped Ceria, J. Catal., 211 (2002) 407-421.

[197] F Kreith, Y Goswami, The CRC handbook of mechanical engineering (2nd edition), CRC Press, 2004.

[198] H Wang,Y Liu,L Wang, YN Qin, Study on the carbon deposition in steam reforming of ethanol over Co/CeO_2 catalyst, Chem. Eng. J. (Lausanne), 145 (2008) 25-31.

[199] A Shamsi, Partial oxidation of methane and the effect of sulfur on catalytic activity and selectivity, Catal. Today, 139 (2009) 268-273.

[200] R Yang,C Xing,C Lv,L Shi, N Tsubaki, Promotional effect of La_2O_3 and CeO_2 on $Ni/g\text{-}Al_2O_3$ catalysts for CO_2 reforming of CH_4, Appl. Catal., A, 385 (2010) 92-100.

[201] CE Quincoces,SP de Vargas,P Grange, MG Gonzez, Role of Mo in CO_2 reforming of CH_4 over Mo promoted Ni/Al_2O_3 catalysts, Mater. Lett., 56 (2002) 698-704.

[202] YT Kim,JH Um,SH Kim,T-H Lim, H-I Lee, Effect of promoter on Ni/MgO catalyst in C_8H_{18} autothermal reforming in solid oxide fuel cell system, Appl. Catal., A, 384 (2010) 10-17.

[203] CK Cheng,SY Foo, AA Adesina, Glycerol Steam Reforming over Bimetallic $Co\text{-}Ni/Al_2O_3$, Ind. Eng. Chem. Res., 49 (2010) 10804-10817.

[204] L Liu, L Hong, Nickel phosphide catalyst for autothermal reforming of surrogate gasoline fuel, AIChE J., 57 (2011) 3143-3152.

[205] DJ Haynes,A Campos,DA Berry,D Shekhawat,A Roy, JJ Spivey, Catalytic partial oxidation of a diesel surrogate fuel using an Ru-substituted pyrochlore, Catal. Today, 155 (2010) 84-91.

[206] DS Jung,SH Lee,JM Han,HJ Hwang,JH Lee, YC Kang, Microstructure and electrical properties of nano-sized $Ce_{1-x}Gd_xO_2$ ($0 < x < 0.2$) particles prepared by spray pyrolysis, J. Ceram. Soc. Jpn., 116 (2008) 969-974.

[207] X Zheng,S Yuan,Z Tian,S Yin,J He,K Liu, L Liu, Nickel/Nickel Phosphide Core-shell Structured Nanoparticles: Synthesis, Chemical, and Magnetic Architecture, Chem. Mater., 21 (2009) 4839-4845.

[208] BD Gould,X Chen, JW Schwank, Dodecane reforming over nickel-based monolith catalysts, J. Catal., 250 (2007) 209-221.

[209] D Xia,Y Tian,G Zhu,Y Xiang,L Luo, TTS Huang, Theoretical and Experimental Studies on the Thermal Cracking of Tetrahydrothiophene, Energy Fuels, 21 (2006) 1-6.

[210] M Ocsachoque,F Pompeo, G Gonzalez, Rh-Ni/CeO_2-Al_2O_3 catalysts for methane dry reforming, Catal. Today, 172 (2011) 226-231.

[211] AF Lucredio,JM Assaf, EM Assaf, Methane conversion reactions on Ni catalysts promoted with Rh: Influence of support, Appl. Catal., A, 400 (2011) 156-165.

[212] JH Kwak,J Hu,D Mei,C-W Yi,DH Kim,CHF Peden,LF Allard, J Szanyi, Coordinatively Unsaturated Al^{3+} Centers as Binding Sites for Active Catalyst Phases of Platinum on r-Al_2O_3, Science, 325 (2009) 1670-1673.

[213] T Setoyama, Acid-Base bifunctional catalysis: An industrial viewpoint, Catal. Today, 116 (2006) 250-262.

[214] C Mattevi,CT Wirth,S Hofmann,R Blume,M Cantoro,C Ducati,C Cepek,A Knop-Gericke,S Milne,C Castellarin-Cudia,S Dolafi,A Goldoni,R Schloegl, J Robertson, In-situ X-ray Photoelectron Spectroscopy Study of Catalyst-Support Interactions and Growth of Carbon Nanotube Forests, The Journal of Physical Chemistry C, 112 (2008) 12207-12213.

[215] N Aldea,B Barz,AC Gluhoi,P Marginean,X Yaning,H Yaning,L Tao, Z Wu, The analysis of the interaction metal-support in Ni catalysts by extended x-ray absorption fine structure and x-ray diffraction using synchrotron radiation, Journal of Optoelectronics and Advanced Materials, 6 (2004) 1287-1296.

[216] SA Selim,HA Hassan,M Abd-El-Khalik, RS Mikhail, The effect of impregnation conditions on the surface structure of silica-supported CuO catalysts, Thermochim. Acta, 45 (1981) 349-360.

[217] R Morales,L Melo,A Llanos, F Zaera, Characterization of bifunctional PtSn/H[Al]ZSM5 catalysts: a comparison between two impregnation strategies, Journal of Molecular Catalysis A: Chemical, 228 (2005) 227-232.

[218] X Yin, L Hong, Partial oxidation of methane to syngas over the catalyst derived from double perovskite $(La_{0.5}Sr_{0.5})_2FeNiO_{6-d}$, Appl. Catal., A, 371 (2009) 153-160.

[219] K Sutthiumporn, S Kawi, Promotional effect of alkaline earth over Ni-La_2O_3 catalyst for CO_2 reforming of CH_4: Role of surface oxygen species on H_2 production and carbon suppression, Int. J. Hydrogen Energy, 36 14435-14446.

[220] S Martin, A Worner, On-board reforming of biodiesel and bioethanol for high temperature PEM fuel cells: Comparison of autothermal reforming and steam reforming, J. Power Sources, 196 (2011) 3163-3171.

[221] DJ Haynes,A Campos,MW Smith,DA Berry,D Shekhawat, JJ Spivey, Reducing the deactivation of Ni-metal during the catalytic partial oxidation of a surrogate diesel fuel mixture, Catal. Today, 154 (2010) 210-216.

[222] JA Villoria,MC Alvarez-Galvan,SM Al-Zahrani,P Palmisano,S Specchia,V Specchia,JLG Fierro, RM Navarro, Oxidative reforming of diesel fuel over LaCoO3 perovskite derived catalysts: Influence of perovskite synthesis method on catalyst properties and performance, Appl. Catal., B, 105 (2011) 276-288.

[223] O Erdinc, M Uzunoglu, Recent trends in PEM fuel cell-powered hybrid systems: Investigation of application areas, design architectures and energy management approaches, Renewable and Sustainable Energy Reviews, 14 (2010) 2874-2884.

[224] SW Tay,L Hong, Z Liu, A study of interface-sustained ferromagnetism in $1/2(1-x)Ln_2O_3$-xSrO/$1/3Co_3O_4$ nano-composite, J. Colloid Interface Sci., 306 (2007) 433-439.

[225] CN Xian,H Li,LQ Chen, JS Lee, Morphological and catalytic stability of mesoporous peony-like ceria, Microporous and Mesoporous Materials, 142 (2011) 202-207.

[226] DH Prasad,HI Ji,HR Kim,JW Son,BK Kim,HW Lee, JH Lee, Effect of nickel nano-particle sintering on methane reforming activity of Ni-CGO cermet anodes for internal steam reforming SOFCs, Appl. Catal., B, 101 (2011) 531-539.

[227] L-C Chen, SD Lin, The ethanol steam reforming over Cu-Ni/SiO2 catalysts: effect of Cu/Ni ratio, Appl. Catal., B, In Press, Accepted Manuscript.

[228] Menaka,SE Lofland,KV Ramanujachary, AK Ganguli, A new low temperature methodology to obtain pure nanocrystalline nickel borate, Journal of Organometallic Chemistry, 695 (2010) 1002-1005.

[229] I Jimenez,DGJ Sutherland,T van Buuren,JA Carlisle,LJ Terminello, FJ Himpsel, Photoemission and x-ray-absorption study of boron carbide and its surface thermal stability, Physical Review B, 57 (1998) 13167.

[230] W-y Wang,Y-q Yang,J-g Bao, H-a Luo, Characterization and catalytic properties of Ni-Mo-B amorphous catalysts for phenol hydrodeoxygenation, Catal Commun, 11 (2009) 100-105.

[231] U Oemar,K Hidajat, S Kawi, Role of catalyst support over PdO-NiO catalysts on catalyst activity and stability for oxy-CO_2 reforming of methane, Appl. Catal., A, 402 (2010) 176-187.

[232] JS Lisboa,LE Terra,PRJ Silva,H Saitovitch, FB Passos, Investigation of Ni/Ce-ZrO_2 catalysts in the autothermal reforming of methane, Fuel Processing Technology, 92 (2011) 2075-2082.

[233] M Liao,W Wang,R Ran, Z Shao, Development of a Ni-$Ce_{0.8}Zr_{0.2}O_2$ catalyst for solid oxide fuel cells operating on ethanol through internal reforming, J. Power Sources, 196 (2011) 6177-6185.

[234] J Krishna Reddy,G Suresh,CH Hymavathi,V Durga Kumari, M Subrahmanyam, Ce (III) species supported zeolites as novel photocatalysts for hydrogen production from water, Catal. Today, 141 (2009) 89-93.

[235] J Li, NJ Coville, Effect of boron on the sulfur poisoning of Co/TiO_2 Fischer-Tropsch catalysts, Appl. Catal., A, 208 (2001) 177-184.

LIST OF PUBLICATIONS

1) Liu Lei, Hong Liang, Interactions between CeO_2 and Ni_xP_y for Enhancing Coking and Sulfur Resistance in Autothermal Reforming of Liquid Hydrocarbons. *Fuel* 96 (2012) 348-354.

2) Liu Lei, Hong Liang, Nickel Phosphide Catalyst for Autothermal Reforming of Surrogate Gasoline Fuel. *AIChE Journal* 57 (2011) 3143-3152.

3) Liu Lei, Hong Liang, $Ni/Ce_{1-x}M_x$ Catalyst Generated from Metallo-organic Network for Autothermal Reforming of Liquid Fuel. To be submitted.

4) Liu Lei, Hong Liang, Nickel borate as a precursor of highly reactive nickel species and boron oxide co-catalyst for autothermal reforming of heavy hydrocarbons. To be submitted.